博士論文

Experimental Study of Tripping Rods Effects on Enhancement of Efficiency of a Vortex-Induced Vibration Based Energy Harvesting System

（トリッピングロッドが渦励振発電システムの効率向上に与える影響に関する実験的研究）

国立大学法人　横浜国立大学大学院

工学府

Luis Antonio Rodrigues Quadrante

（ルイス　アントニオ　ロドリゲス　クァドランテ）

2013 年 11 月

This thesis is submitted to the Faculty of the Graduate School of Yokohama Nation University, in partial fulfillment of the requirements for the degree of Doctor of Engineering. This thesis is entirely my own work and except there otherwise stated describes my own research.

Luis Antonio Rodrigues Quadrante

Acknowledgements

The opportunity to study in Japan at Yokohama National University was a grateful and unforgettable experience. This doctor thesis marks the end of five years of much learning in engineering and also in life. All this knowledge could be acquired due to people who had been part of my life in Japan. Among them, I would to thank and express gratitude to my supervisor Prof. Nishi for the opportunity of continue studying here in Japan after I finished my master course and also for his knowledge, experience and help during the preparation and conduction of all the experiments for this thesis. I would like to thank Prof. Arai for offering his doctor course vacancy for me even knowing that another professor would be my supervisor. Also I would like to thank Prof. Takayama and Prof. Hirakawa for the assistance on the preparation and execution of my experiments in their laboratory. A special thanks to all member of the Marine Environmental Design Laboratory with I shared these three years of my doctor course and also helped during my experiments and discussion of results.

Special thanks to Prof. Hirayama for giving me the opportunity of moving to Japan to do my master course and his recommendation to Prof. Arai and Prof. Nishi to help me continuing with at the doctor course. Also, thanks to Prof. Dr. Kazuo Nishimoto for his recommendation and support allowing me to participate in this graduation program in Japan.

During my stay in Japan I had the opportunity to know many people and make many friends and I also would like to thank Andre, Yugo, Danilo, Kelly, Marcio, Dalton, Felipe, Ramirez, Lillian, Miguel, Julio, Gustavo, Victor, Phan, Thang, Moriguchi, Nishio, Ueno, Ono, Sema and Ikeda for making the life in Japan more enjoyable.

Special thanks to my wife Minako Kato for all her support, stimulate, trust and comprehension in these three years and also to my firstborn Leon Kato Quadrante who brought the most happy moments of my entire life and helped me to overcome the stressful moments of my research with his beautiful smile every time I arrive home. Also to Kato family whom made me feel that I have a family here in Japan too.

Finally I would like to thank my family for support and trust in me all the time, even from the other side of the world.

Contents

List of Figures

List of Tables

Abstract

This doctoral thesis show an experimental study about the enhancement of energy conversion efficiency of a vortex-induced vibrations (VIV) based energy generation system. Firstly, there is a discussion about the recent scenario of energy demand on the world and the necessity of development of renewable energy generation systems in order to reduce the CO_2 emissions from the use of fossil fuels and also reduce the dependency of this kind of fuel because it is a limited source of power.

The generation system used in this study is constituted by a cylinder, which oscillates when submitted to a constant fluid flow, and a leverage system, responsible to transmit the translational motion of the cylinder to the translational motion of a magnetic bar inside a coil, generating electricity. This generation system was already tested previously to this work and achieved a maximum conversion efficiency of 4.5%.

To enhance the system efficiency a pair of tripping rods were attached to the cylinder symmetrically positioned in relation to the stagnation point. Tripping rods also are cylinder, but with much small diameters than the main cylinder. Their attachment changes the flow pattern around the cylinder and can produce since reduction to increase of hydrodynamic forces and amplitude of VIV, according to their angular positions.

The experiments were divided in three cases, starting from the simplest case and adding complexity. The first experiments consisted of a stationary cylinder submitted to a constant flow and was carried out to measure the drag and lift forces acting on the cylinder in function of

tripping rods angular position, which varied from 15^o to 165^o, with a 7.5^o interval. The second set of experiments was conducted with a free-oscillating cylinder without energy generation system. This system had small mass and damping ratios, 6.13 and 0.016 respectively. Tripping rods were positioned at 60^o, 75^o, 105^o and 120^o in order to observe the changes on VIV amplitude imposed by their presence. The third and last set of experiments consisted of free-oscillating cylinder with the generating system attached. This experimental setup had larger mass and damping ratios due de inclusion of the generating system, achieving a mass ratio of 12.34 and an average damping ratio of 0.048.

The stationary cylinder experiments were carried out at constant Reynolds number of 7.48×10^3. It was observed during these experiments that when placing tripping rods at angular positions ranging from 22.5^o to 52.5^o and from 97.5^o to 165^o a reduction of the forces acting on the cylinder occurred, achieving a maximum reduction of 67% on lift and 20% on drag forces. An increase on lift and drag forces was observed when placing tripping rods between 52.5^o and 90^o, achieving a maximum increase of 68% on lift and 40% on drag forces.

On free-oscillating tests without generator, Reynolds number varied from 3.45×10^3 to 2.04×10^4 and the reduced velocity from 2 to 12. When tripping rods were positioned at 60^o and 75^o significant changes occurred, with an monotonically increase of oscillation amplitudes, starting at reduced velocity 7 and continuing until 12, with a maximum amplitude 56% larger than the obtained with the smooth cylinder. When tripping rods were placed behind the cylinder, at 105^o and 120^o, the opposite occurred, and the amplitudes were reduced significantly, achieving an almost complete VIV suppression at 120^o.

Finally, the free-oscillating experiments with the generator showed that even with larger mass and damping ratios the presence of tripping rods can bring lots of benefits for energy generation using VIV, especially when they were placed at 75^{o}. The system efficiency during smooth cylinder tests achieved a maximum of 2.8%, while the efficiency with tripping rods at 75^{o} achieved a maximum of 12.47%, representing a 342% increase. But the increase on efficiency was not the only benefit brought by tripping rods. Their presence also increased the lock-in range and maintained the power generation almost constant at reduced velocities between 6.5 and 8.5, meaning that the system can maintain the generation even with flow speed variations inside this range.

The results showed up that the attachment of tripping rods have a great potential on the improvement of energy harvesting using VIV phenomena. This research covered only a small number of combinations of mass ratio, damping ratio, Reynolds number and diameter of tripping rods in relation to the diameter the main cylinder. It means that further research can be made as an extension of the current work, opening the opportunity for other researchers to investigate manners of increase even more the efficiency of energy conversion.

論文要旨

この博士論文は、渦励振を利用した発電システムのエネルギー変換効率を向上させるための実験的研究について記したものである。最初に、世界におけるエネルギー需要に関する最近の動向、および再生可能エネルギー技術を開発することの必要性について述べる。この必要性は、化石燃料消費に伴う二酸化炭素排出量の削減のため、および、賦存量が限られている資源への依存性を削減するためという目的に起因している。

本研究で用いる発電システムは一本の円柱を有する。この円柱は流れの中に置かれた時に振動する。また、本システムはてこ機構を含み、この機構は円柱の並進運動を、コイル内部における磁石の並進運動に伝達させる役割をもつ。この磁石の運動により電力を発生させる。この発電システムを用いた発電試験は過去に行われており、その際のエネルギー変換効率は最大で 4.5％であった。

発電効率を向上させるために本研究では、小直径の円柱（トリッピングロッド）を２つ、前方よどみ点に関して対称に円柱表面に付加することを試みた。この付加により円柱表面付近における流れを変化させ、円柱に作用する流体力、渦励振の振幅を増大させる効果を期待できる。円柱中心と前方よどみ点とを結ぶ線分と、円柱中心とトリッピングロッド取り付け位置とを結ぶ線分とがなす角度（以下、取り付け角度）によって、この効果に大小が変化することが予想された。

三種類の実験を実施した。一つ目は、円柱を固定した状態で支持し、一定流速の流れの中に置き、円柱に作用する抗力と揚力の計測である。取り付け角度は 15 度から 165 度まで 7.5 度刻みで変化させた。レイノルズ数は 7.48×10^3 である。

二つ目は、円柱をばね支持し、発電機を外した状態での計測である。質量比は 6.13、減衰比は 0.016 である。取り付け角度は 60 度、75 度、105 度、120 度の 4 か所とした。レイノルズ数は 3.45×10^3 から 2.04×10^4 までの領域であり、この領域は換算流速 2 から 12 までの領域に相当する。

三つ目は、円柱をばね支持し、発電機を付けた状態での計測である。質量比は 12.34、減衰比は 0.048 である。

一つ目の固定円柱試験の結果、取り付け角度が 22.5^o から 52.5^o までの領域および 97.5^o から 165^o までの領域のとき、流体力が低下することが示された。トリッピングロッドの付加なしの場合に比べて揚力は最大で 67％、抗力は最大で 20％低下した。取り付け角度が 52.5^o から 90^o までの領域のとき、揚力、抗力ともに増加し、トリッピングロッドの付加なしの場合に比べて揚力は最大で 68%、抗力は最大で 40％増加した。

二つ目の振動円柱試験（発電機なし）では、取り付け角度が 60 度および 75 度のとき、顕著な効果が検出された。換算流速が 7 以上になると振動振幅が単調に増加し、この傾向は換算流速 12 まで続いた。トリッピングロッドなしの場合に比べて振幅が最大で 56％増加した。一方で、トリッピングロッドを円柱後方に付加（取り付け角度 105 度、120 度）したときは、振幅は大幅に減少し、120 度の場合では振動はほぼ完全に消失した。

三つ目の振動円柱試験（発電機あり）では、質量比と減衰比が比較的に大きいにもかかわらず、トリッピングロッドの付加は、エネルギー変換効率の向上をもたらすことが示された。このことは取り付け角度が 75 度の場合に特に顕著であった。付加なしの場合では、変換効率は 2.8%に過ぎなかったのに対して、付加ありの場合では最大で 12.47%（3.42 倍に相当）にまで高まった。また本実験により、トリッピングロッドの付加による効果には、変換効率を向上させるという点だけではなく、自励振動の同期領域を拡大させるという点もあることが見出された。付加ありの場合、換算流速 6.5 から 8.5 までの領域では、発生電力が一定に維持され、このことは流速がこの範囲内で変化しても発生電力が安定に保たれることを意味する。

以上の実験結果から、トリッピングロッドの付加は、渦励振を利用する発電システムのエネルギー変換効率を向上させる効果をもつことが示された。本研究では、質量比、減衰比、レイノルズ数、トリッピングロッドと振動円柱との直径比に関して数個の場合のみ実験を行った。これらのパラメーターをさらに変化させ、エネルギー変換の大小を調べることが次の課題として挙げられる。

List of symbols

A	Amplitude of oscillation of the cylinder
A^*	Non-dimensional amplitude of oscillation of the cylinder
C	Structural damping of the system
C_D	Drag coefficient
C_L	Lift coefficient
d	Diameter of tripping rods
D	Diameter of the cylinder
E	Generated voltage
f^*	Non-Dimensional frequency of oscillation of the system
fn	Natural frequency of oscillation of the system
$fosc$	Frequency of oscillation of the cylinder
fs	Vortex-shedding frequency
F	Total force acting on the cylinder
F_D	Drag force acting on the cylinder
F_L	Lift force acting on the cylinder
F_m	Electromagnetic reaction force
g	Gravity acceleration
I	Inertia of the system
K	System stiffness
ℓ	Coil length
L	Cylinder length
m	System oscillating mass
m^*	Reduced mass

m_b	Magnetic bar coefficient
M	Mass of the coil
N	Total number of turns of the coil
P	Generated power
r_1	Distance of application of restoring force
r_2	Distance of application of hydrodynamic force
r_3	Distance of application of electromagnetic reaction force
R	Resistor
Re	Reynolds Number
S_G	Mass-damping parameter
St	Strouhal number
t	Time
V	Current velocity
V_R	Reduced velocity
Z	Vertical position of the cylinder
α	Coefficient of proportionality between the coil speed and the generated voltage
β	Tripping rods angular position
δ	Gap between the cylinder and the tripping rods
η	System efficiency
φ_F	Difference of phase between lift force and cylinder vertical position
φ_L	Phase of lift force
φ_Z	Phase of cylinder vertical position
ν	Kinematic viscosity
θ	Angular position of the bar

$\dot{\theta}$ Angular velocity of the bar

$\ddot{\theta}$ Angular acceleration of the bar

ρ Water density

ξ Damping ratio

ω Angular frequency of oscillation of the cylinder

1 Introduction

The world's energy supply is hardly dependent of fossil fuels. The World Energy Outlook 2007 predicted that coal, oil and gas will be responsible to meet 84% of energy demand in 2030 and it is of common knowledge that these non-renewable sources will deplete in a near future, however it is not a consensus when it will happens because lots of efforts have been made to delay it. The search for new oil fields is constant, as well the development of new drilling and extraction techniques to increase the volume of recovered oil. In parallel, the energy conversion efficiency of existing systems is being improved and renewable energy sources are being developed. The latest World Energy Outlook, released in 2012, estimates that is necessary to invest 4.8 trillion US dollars on the development of renewable energy systems until 2035 to meet the demand increase.

A promising source of renewable energy is the ocean. There are two basic principles on producing energy from it that are usually broached. The first one is thermal and relies on the difference of temperature between the surface and deep water. The warm water on the surface is used to vaporize a fluid, which has a low boiling point, and the vapor expansion turns a turbine that is connected to a generator, producing electricity. Then the vapor is directed deep into the ocean where it condenses, re-starting the cycle. The second one consists on using the mechanical energy of tides and waves. It is based on the principle that a floating body moves up and down under effect of tides and waves. The body is connected to a linear type generator that converts its vertical motion in electricity, but this kind of generation can be intermittent as depends of weather conditions.

There is a third potential source of energy on the oceans that is not explored: the currents. The main reason is because ocean currents have low speeds, usually less than 1.0 m/s at water

surface, and it is not efficient to use turbine type generators at such low speed. Efforts have been made on the development of new systems capable of extracting energy from these low speed flows efficiently. To work with such low speed flows there is the option to apply a dispositive that uses vortex-induced vibrations (VIV) phenomenon to convert the energy of the flow in electricity.

Vortex-induced vibrations are the result of the vortex shedding that occurs on a bluff body under influence of a steady flow. The vortex shedding process induces periodic forces on the body which can result in motions. The motions are perpendicular to the flow direction and are self-excited when the vortex-shedding frequency and system natural frequency are approximately the same, fact that makes possible to develop systems to extract energy from low flow speeds by only setting up their natural frequency. These aspects will be better discussed on chapter 2 of this thesis.

This work has focus on studying a manner of improve the conversion efficiency of a system which uses the vortex-induced vibrations of a circular cylinder under influence of a steady flow to generate electricity. It will be made by attaching two appendages to the cylinder surface, called tripping rods, in order to change the flow pattern around the cylinder and increase the forces acting on it. The use of tripping rods to increase the forces were never been tried before and that is the novelty of this doctoral research.

1.1 Background

VIV is a problem for most of engineering areas that involves the interaction of fluid flow and structure. Most of the studies about VIV are concerning its reduction or suppression by the attachments of appendages to the body with the objective of breaking the vortex formation behind

the cylinder, as compiled by Zdravkovich[1]. During the researches for VIV suppression one of the types of appendages, called tripping wire or tripping rod, showed an increase of the forces acting on the body according to their positioning around the cylinder, as showed in Nebres & Batil[2] and Alam et al.[3] results, but this effect was ignored because larger forces there were not useful application.

Recently, a group of researches of Michigan University studied the opposite. They wanted to increase the forces and amplitude of motions of VIV to produce electricity from a fluid flow. They developed a system called VIVACE[4] (Vortex-Induced Vibration Aquatic Clean Energy) that consists of an elastically mounted cylinder that is submerged on water and connected to an electricity generator. The first model of VIVACE[4] was equipped with a smooth cylinder and in order to improve the efficiency of their system they started to study the attachment of roughness strips over the cylinder surface to try to increase the system efficiency. It was the first documented effort about the use of attachments to increase VIV.

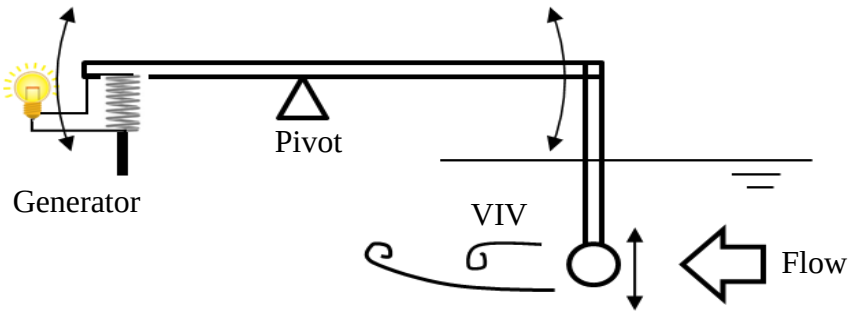

Figure 1.1: Schematic view of the energy generation system using VIV and principle of leverage.

Following VIVACE[4] steps, Nishi et al.[5.] developed a system that utilizes the vortex-induced vibrations of a cylinder and principle of leverage, which will be described along the next chapter. Their system transforms the translation motion of the VIV into a translation motion of the generator as shown in Figure 1.1. The aim of their work was to improve the system efficiency by tuning the distance between the pivot and the generator, changing the ratio between the cylinder motion and coil motion.

Nishi et al.[5.] experiments achieved a lower efficiency than expected and there was the necessity of increasing it. One of the ideas, which inspired this doctoral research, was the addition of attachments to the cylinder surface to change the flow characteristics around the cylinder in order to increase the fluid forces acting on it. The attachments chosen were tripping rods, which are cylinders with diameters much smaller than the main cylinder and are attached parallel to the main cylinder axis. The idea of using tripping rods is based on the results obtained by Alam et al.[3] in their experiments for reducing VIV. Although it was not their objective, when placing tripping rods at certain angular positions around the cylinder a large increase of lift and drag forces was detected.

Alam et al.[3] experiments were conducted only with non-oscillating cylinders and do not contained any information about the effects of the force increase in the amplitude of oscillation of a free-oscillating cylinder, condition necessary for energy generating purposes. It also did not covered the entire domain of angular positions To cover the lack of data about the response of a free-oscillating cylinder with tripping rods a series of tests with stationary and free oscillating cylinders were conducted and will be presented in this thesis.

1.2 Objectives

The objective of this doctoral research was to study experimentally the attachment of a pair of tripping rods to a circular cylinder under the influence of a constant flow in order to increase the energy conversion efficiency of a vortex-induced vibrations energy harvesting system. The objective was based on the idea that it is possible to find a region within the tripping rods can be positioned to increase the lift forces acting on the cylinder and, consequently, improves the system efficiency. It was the first time tripping rods are studied specifically with the purpose of increasing the lift forces and for that reason it was necessary to divide the study in smaller objectives.

The first objective was to study the most fundamental case of a non-oscillating cylinder under influence of a constant flow to obtain a curve that relates the position of tripping rods to their effects in the drag and lift forces and check if the tripping rods were capable of increasing the forces significantly.

After the curve is created, the next objective was to conduct free oscillation experiments with tripping rods attached at positions which presented large lift coefficients and check the influence it causes in the amplitude of oscillation of the cylinder and in the power conversion efficiency of the system.

1.3 Literature Review

Vortex-induced Vibrations (VIV) attracts much attention because it is a crucial factor on the design of structures that involve long slender bodies. The VIV exerts large steady and oscillatory forces that can lead to structural failure and fatigue. A lot of efforts have been made

thought understanding its fundamentals to find a way to reduce or, in an optimal circumstance, suppress it. On the other hand, some researchers started to develop a manner of enhancing VIV for energy harvesting purposes. Although these two branches of research have opposite objectives, both of them use the same principle of adding attachments or roughness over the body surface to change flow pattern around it. The flow changes depend of attachments size, form and position and can lead even to increase or decrease of VIV.

Zdravkovich[1] presented several means of VIV suppression, classifying tripping wires as attachments that disturb the spanwise correlation of vortex shedding. Igarashi[6] and Nebres & Batil[2] studied the effects of attaching a single tripping wire parallel to the main cylinder axis, at angular positions in relation to stagnation point, as will be discussed on chapter 2.

$$\mathrm{Re} = \frac{VD}{\nu} \qquad 1.1$$

Igarashi[6] tested several diameters of tripping wires positioned at 50^o and 60^o within Reynolds number (Equation 1.1) ranging from 1.3×10^3 to 9.6×10^4. He observed three different flow patterns that change in function of Reynolds number, tripping wire angular position and diameter ratio (defined as the ratio between the tripping wire and the cylinder diameters *d/D*). The first pattern, hereby referred to as pattern A, presents a separation over the tripping wire and an immediately reattachment behind it, followed by a posterior laminar re-separation. No significant changes on drag coefficients and strouhal number were observed in comparison to the smooth cylinder case, meaning that the tripping wire affects little the flow. This pattern is restricted to cases when tripping wires diameter is small or at low Reynolds numbers and was observed on both angular positions. With the increase of tripping wires diameter or Reynolds number the flow

exhibits pattern B, which is characterized by the separation over the tripping wire, a reattachment behind it and a turbulent re-separation that occurs further downstream than the smooth cylinder. Pattern B presents lower drag coefficients and higher strouhal number than the smooth cylinder. The third pattern, pattern C, presents a complete separation over the tripping wire and a wider wake than patterns A and B. In Igarashi's[6] experiments the pattern C appeared only when the angle was 60^o, being independent of Reynolds number when the diameter ratio was larger than 0.02. This pattern has lower strouhal number and larger drag coefficients than the smooth cylinder.

Nebres and Batil[2] experiments covered Reynolds numbers ranging from 1×10^4 to 4×10^4. They positioned a single tripping wire ($0.006 < d/D < 0.14$) at several angles within 0^o to 180^o and confirmed the three patterns observed by Igarashi[6]. In addition, they discussed how the effect of tripping wire depends on the angular position.

Hover et al.[7] and Alam et al.[3] studied the effects of positioning two tripping wires symmetrically in relation to the stagnation point. Hover et al.[7] conducted stationary and free oscillation tests with and without tripping wires. The tripping wires position and diameter ratio were fixed at 70^o and 0.003, respectively, and the Reynolds number was varied up to 4.6×10^4. Stationary cylinder tests showed that tripping wires with Reynolds number lower than 2×10^4 give almost the same lift and drag coefficients as those for the smooth cylinder. With Reynolds greater than 2×10^4 the drag and lift coefficients decrease and the strouhal number starts increases until Re $\approx 3.5\times10^4$,where they stabilize until the maximum *Re* tested. Despite there are no comments about the flow patterns on their work, it seems that there was a transition from pattern A to pattern B with the increase of Reynolds. In their free vibration tests, the attachment of tripping wires introduced changes on the amplitude of vibration response. The lock-in occurs within smaller

reduced velocities than the lock-in for smooth cylinder. The amplitude of oscillation and mean drag coefficients were lower than those for smooth cylinder, except for $4.5 < V_R < 5$, when it was slight higher. When the reduced velocity is greater than 6, the wires produce a sharp reduction of the amplitude, achieving nearly zero for $V_R > 7.5$. It suggests that tripping wires can be applied for reducing the amplitude of oscillation.

Alam et al.[3] conducted experiments of a stationary cylinder with tripping wires attached. Their experiments included a gap between the cylinder and tripping wires surfaces. The three diameter ratios tested, 0.08, 0.1 and 0.12, produced the smaller coefficients when tripping wires were positioned between 20^o and 40^o, reaching reductions up to 67% and 87% for mean drag and fluctuating lift coefficients, respectively, when compare to smooth cylinder. They reported also that the mean drag coefficients increases by 62% and the fluctuating lift coefficient increase by 63% then tripping wires were positioned between 50^o and 60^o. The analysis of the flow pattern using surface oil-film techniques confirmed the presence of flow patterns B and C on reduction and increase of coefficients, respectively.

Raghavan & Bernitsas[8] conducted experiments dedicated to VIV enhancement with Reynolds number ranging from 8×10^3 to 1.5×10^5. Based on Bernitsas et al.[9], instead of tripping wires, they attached roughness strips over the cylinder surface and found that the effect of roughness is dependent on grit size, angular position and Reynolds number. They determined that the best angular positions are between 57^o and 80^o and that there is a critical Reynolds number based on roughness grit size above which there is increase on the amplitude in comparison to smooth cylinder. Below this critical value, the amplitude is reduced inside the original lock-in region. In every case tested the lock-in range increases with the attachment of roughness. Their

system achieved a maximum amplitude ratio of 2.7 and the lock-in occurred for the reduced velocities ranging from 4 to 12.5.

On computational fluid mechanics field Nguyen & Nishi[10] (2012) applied the Lattice Boltzmann method to simulate the flow around a circular cylinder with tripping wires with Reynolds number ranging from 10^o to 50^o and diameter ratios of 0.08, 0.10 and 0.11. They found that when positioning the tripping wires between 50^o and 90^o lift and drag coefficients increase. Using the numerical results obtained, they interpreted the increase is a result of the forced separation induced at tripping wires position. The interaction of tipping wires with the surrounding fluid widens the wake region, producing larger pressure difference between the upper and lower sides of the cylinder and, consequently, larger coefficients. Their interpretation has the same characteristics of pattern C obtained experimentally.

As far as we know, only Nebres and Batil[2] investigated the entire range (0^o~180^o) of angular positions; however, their study was restricted to stationary cylinder experiments and measured only the drag force. The response of a free-oscillating cylinder with a pair of tripping wires attached at angular positions larger than 60^o remains to be examined experimentally. It means that we have no complete knowledge about which angular positions is most effective on enhancing or reducing VIV. Experimental results on this aspect can provide with an important suggestion for refining the design of the structures mentioned above.

2 Theoretical Aspects

This chapter of the thesis contains the theoretical aspects about the flow-induced vibrations (FIV) of a bluff body under influence of a constant flow and the basic principles of using these vibrations for generating electricity. Firstly, it will be presented the basic principles of the flow around circular cylinders. It will be followed by the presentation of the mechanisms involved in the appearance of hydrodynamic forces acting on the cylinder.

Section 2.3 will present the flow-induced vibrations phenomena and introduce the most common types of FIV, with special attention to the vortex-induced vibrations phenomenon, which is the actuating phenomenon in the energy harvesting system used in this work that will be presented in section 2.4. Finally, the last section of this chapter will show the known aspects of the effects of tripping rods in the flow around a circular cylinder.

2.1 Flow around circular cylinders

There are two main classifications of bodies under influence of a flow: slender body and bluff body. Circular cylinders are classified as a bluff body. An easy to understand definition of what a bluff body is has been made by Bearman[11]: "Bluff bodies are the ones that, when submitted to a constant flow, present a substantial proportion of its submerged surface exposed to the flow separation phenomena". It means that, in a slender body the streamlines are always attached to the body surface, without separation. In a different manner, the streamlines of the flow around a bluff body separates from the body's surface, creating a region of separated flow.

The separation phenomenon may occur because the body geometry and the conditions of the boundary layer. If the shape of the body is not smoothly tapered but terminates abruptly, the flow that follows a stream line close to the surface will suffer an interruption due to a suddenly change in the pressure field. This interruption occurs because of an adverse pressure gradient in the flow direction forcing the flow deceleration and subsequent separation. The effects of turbulence in the boundary layer also influence the phenomenon of separation. As the boundary layer becomes turbulent separation point moves to the rear (downstream) of the body. The streamlines of the flow around a slender and a bluff body are represented in Figure 2.1.

In these two cases presented, the body surface is continuous and do not have edges or irregularities. Some types of bodies, as a square cylinder, have non continuous surfaces. The discontinuity in the surface of the body disturbs the boundary layer radically and forces the separation, resulting in well-defined separation points, differently from what happens to continuous bodies, in which the separation point varies with the flow conditions.

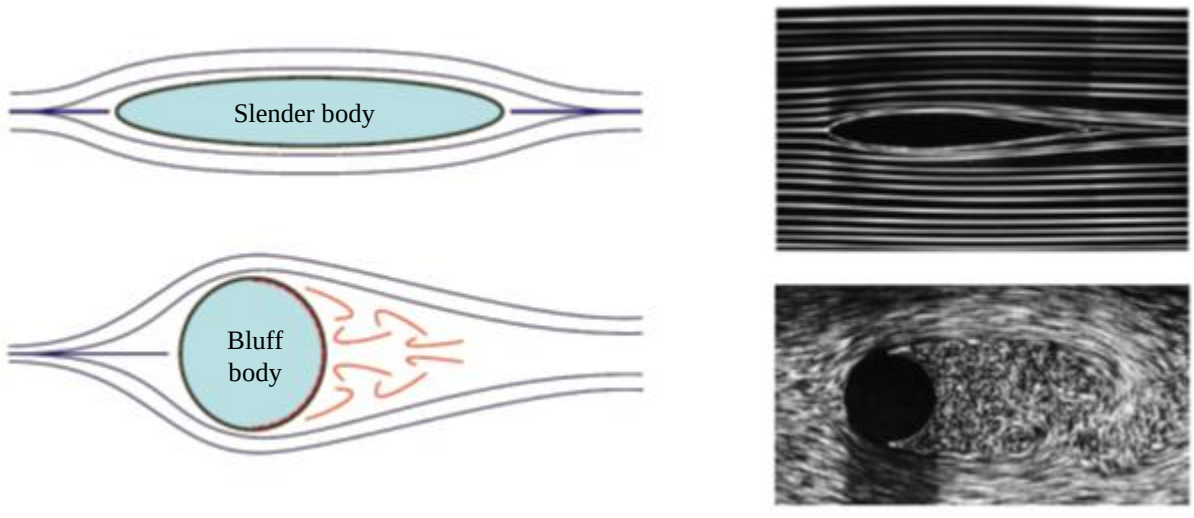

Figure 2.1: Streamlines around slender and bluff bodies. In red it is highlighted the bluff body region exposed to the separated flow. Reproduced from Van Dyke[12].

The phenomenon of separation is governed by the Reynolds number (*Re*). This dimensionless quantity presented in equation 1.1, relates the magnitude of inertial and viscous forces in the flow. As the Reynolds number increases, the flow undergoes successive transitions assuming different flows patterns around the body. These transitions are related to turbulence in the boundary layer and are sensitive to small perturbations.

When the Reynolds number is very small the flow is considered highly viscous, because the viscous forces are larger than the inertial forces and the flow do not separate from the body surface. This condition is commonly called "creeping flow" in the literature. However, as the Reynolds increases, there is growth of bubbles in the recirculation area near the wake. As long the flow maintains low speeds these bubbles remain stable, near the surface of the body in a symmetrical configuration. This sequence of growth of recirculation bubbles can be seen in Figure 2.2.

When the Reynolds number exceeds a certain critical value, the flow becomes unstable and the bubbles are draw inside wake region far from the body. Figure 2.3 shows the changes in the wake of a circular cylinder in six different ranges of Reynolds. When Re = 32, the bubbles remain near the body surface and do not affect the wake region downstream of the cylinder. Increasing for Re = 55, the wake starts to present signs of instability. From Re = 65, the unstable behavior of the wake is already clear. The oscillations in the wake begin even during the laminar regime and will continue until high values of Reynolds, when the flow presents turbulent regime.

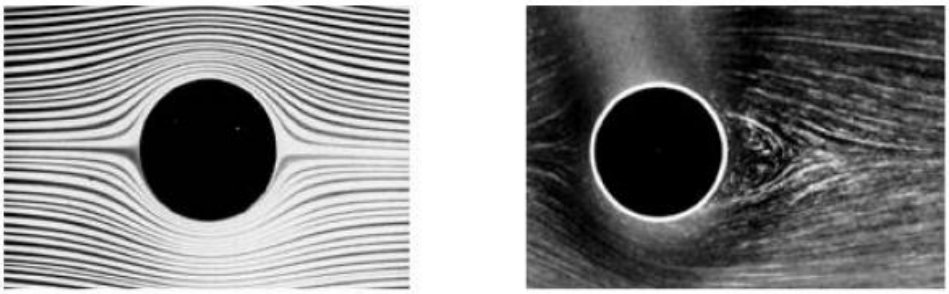

Without Separation Re = 13

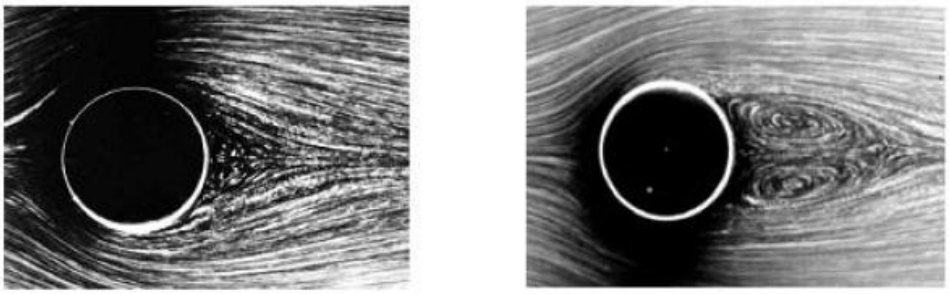

Re = 9.6 Re = 26

Figure 2.2: Steps of the flow separation and formation of recirculating bubbles at the near wake region. Reproduced from Van Dyke[12].

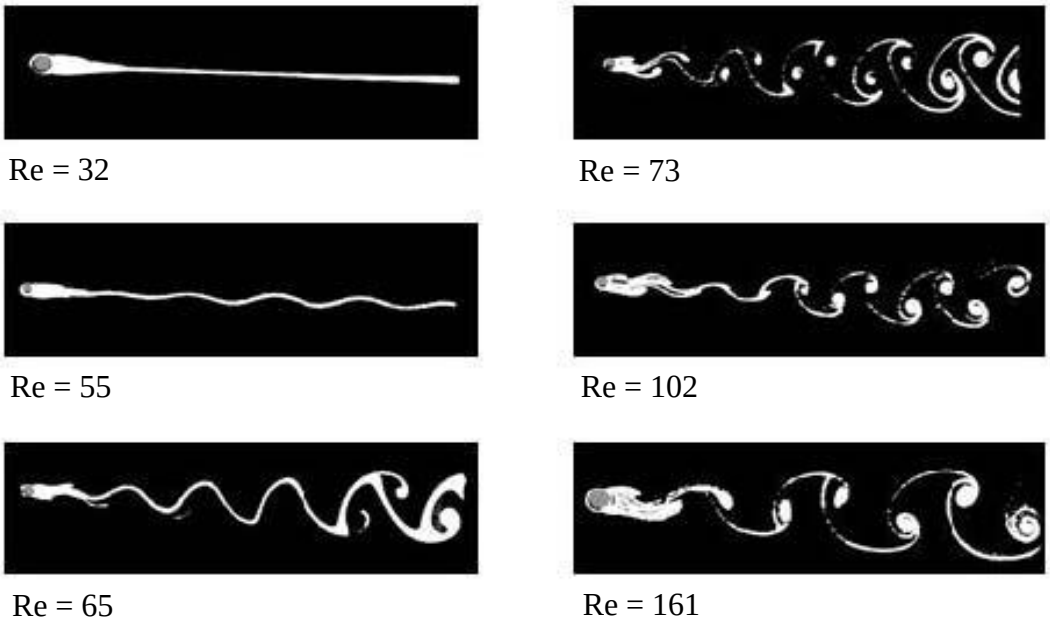

Re = 32 Re = 73

Re = 55 Re = 102

Re = 65 Re = 161

Figure 2.3: Beginning of the wake instability in the laminar flow condition. Reproduced from Batchelor[14].

This peculiar behavior assumed by wake attracted the attention of scientists since antiquity. Leonardo da Vinci outlined the wake downstream of flat plates and even some types of foils. However, only in the early 20th century, two researchers, Henri Bernard[14] and Theodor von Kármán[15] described the phenomenon by observing the alternating vortex formation behind cylinders. This phenomenon was called the von Kármán vortex street and has a key role in the instabilities that cause the flow-induced vibrations in cylinders.

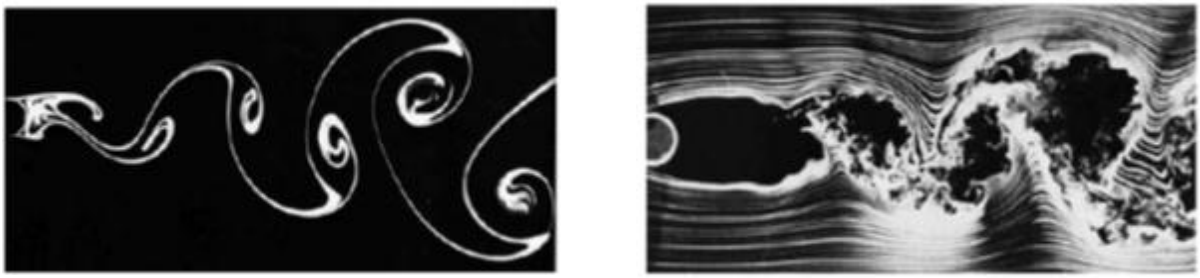

Figure 2.4: Von Kármán vortex street for two flow conditions: on the left side the flow is laminar (Re=140) and on the right side the flow is turbulent (Re = 10^4). Reproduced from van Dyke[12].

The alternate vortex shedding is present in the wake region of any bluff body, not just circular cylinders, whenever there are interactions between the shear layer downstream the body. The vortices generation is not symmetrical. When a vortex is separating from the body in the direction of the wake region a new one is starting to form in the opposite side of the body. This alternation gives the wake region the aspect observed in Figure 2.4. The vortex formation downstream of a circular cylinder, called vortex shedding frequency (f_s), has a characteristic frequency that is defined below:

$$f_s = \frac{VSt}{D} \qquad 2.1$$

Where V is the flow speed, *D* is the cylinder external diameter and *St* is the Strouhal number. The Strouhal number is obtained experimentally and is well known for circular cylinders. Figure 2.5 shows the Strouhal number variation in function of Reynolds number.

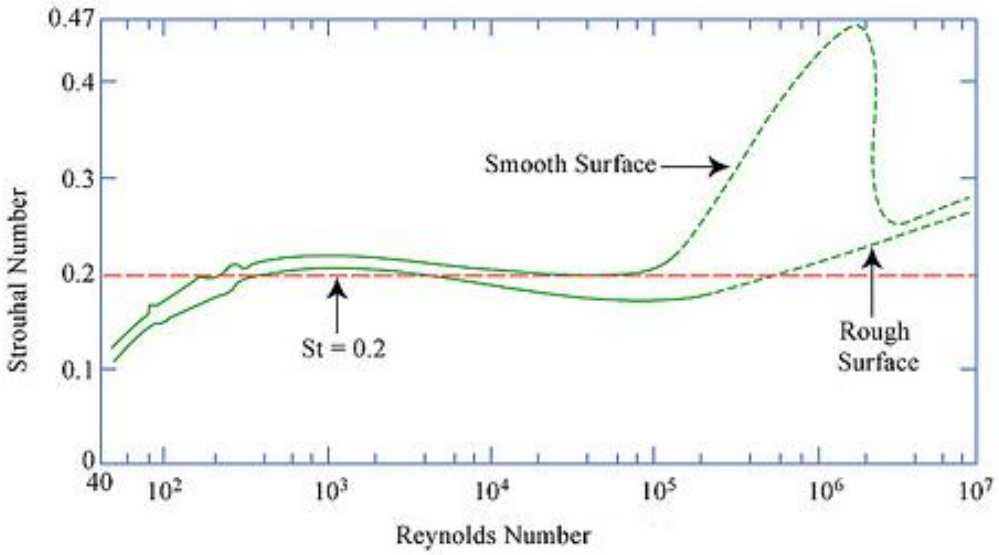

Figure 2.5: Srouhal number variation in function of the Reynolds number. Reproduced from Roshko[16].

2.2 Hydrodynamic Forces

The velocity field of the flow around a cylinder generates a pressure distribution around the wall, which when integrated results in the forces acting on the body. Two forces are usually considered: drag force (F_D) and lift force (F_L). The drag force acts on the body at the same direction of the fluid flow; meanwhile, the lift force acts transversally to the flow direction. The pressure distribution in the ideal case, without vortexes formation, is symmetric in relation to the stagnation point, as shown in Figure 2.6. In this case, only the drag force will appear.

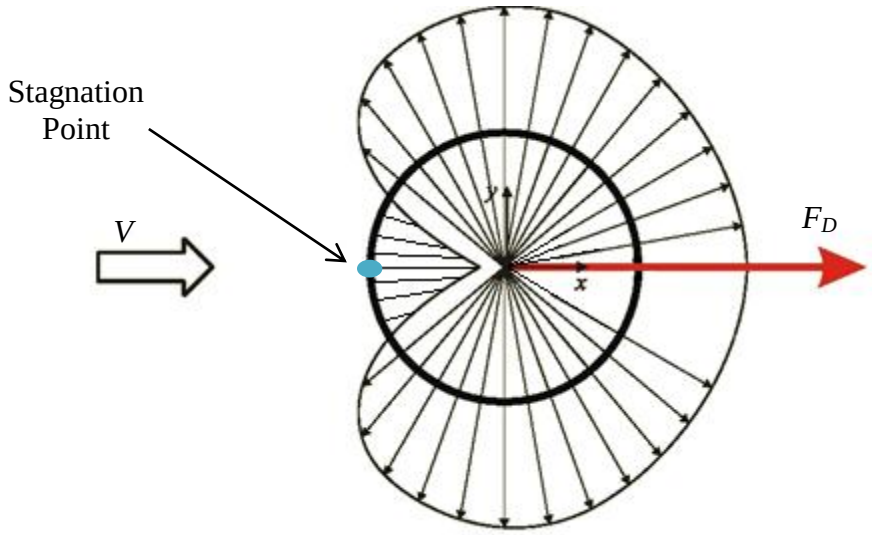

Figure 2.6: Symmetrical pressure distribution and the resultant drag force F_D.

Because of the vortex formation process, the pressure distribution around the cylinder is not symmetric along the time, as shown in Figure 2.7 and results in lift forces acting on the body.

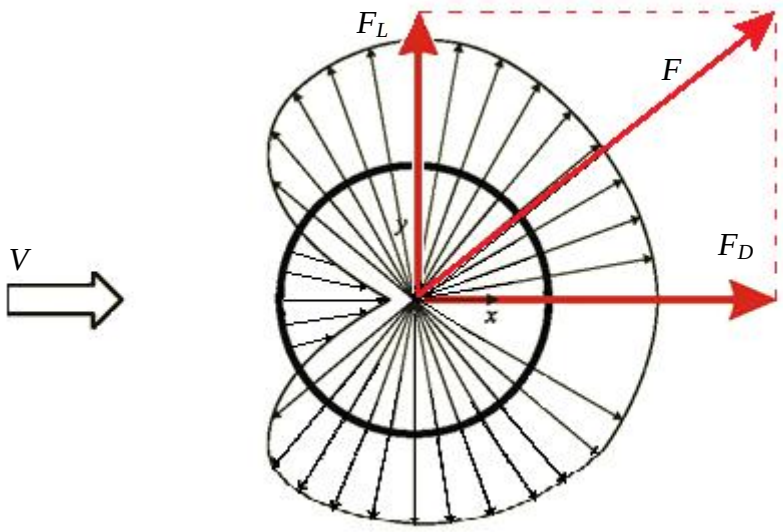

Figure 2.7: Asymmetrical pressure distribution and the resultant force decompose in the Lift (F_L) and drag (F_D) forces.

The drag and lift forces are usually represented, respectively, as the non-dimensional coefficients C_D and C_L. They can be calculated from the force as:

$$C_D = \frac{2F_D}{\rho DLV^2} \qquad 2.2$$

$$C_L = \frac{2F_L}{\rho DLV^2}, \qquad 2.3$$

The drag and lift coefficients of a circular cylinder changes in function of the Reynolds number. Figure 2.8 shows the behavior of the coefficients and the behavior of the regime of the wake region for a wide range of Reynolds. From Re ≈ 5 to 40 the flow is laminar and the bubbles are restricted to the wake region near the cylinder. In the range 40 < Re < 180 the alternating vortex shedding starts and the separation became permanent. With alternating vortex detachments behind the cylinder, the pressure field begins to oscillate and loses the symmetry, resulting in lift forces. In Re ≈ 350 vortexes far from the body surface in the wake region present transition to turbulent flow, but the shear layers will still laminar until Re ≈ 10^4.

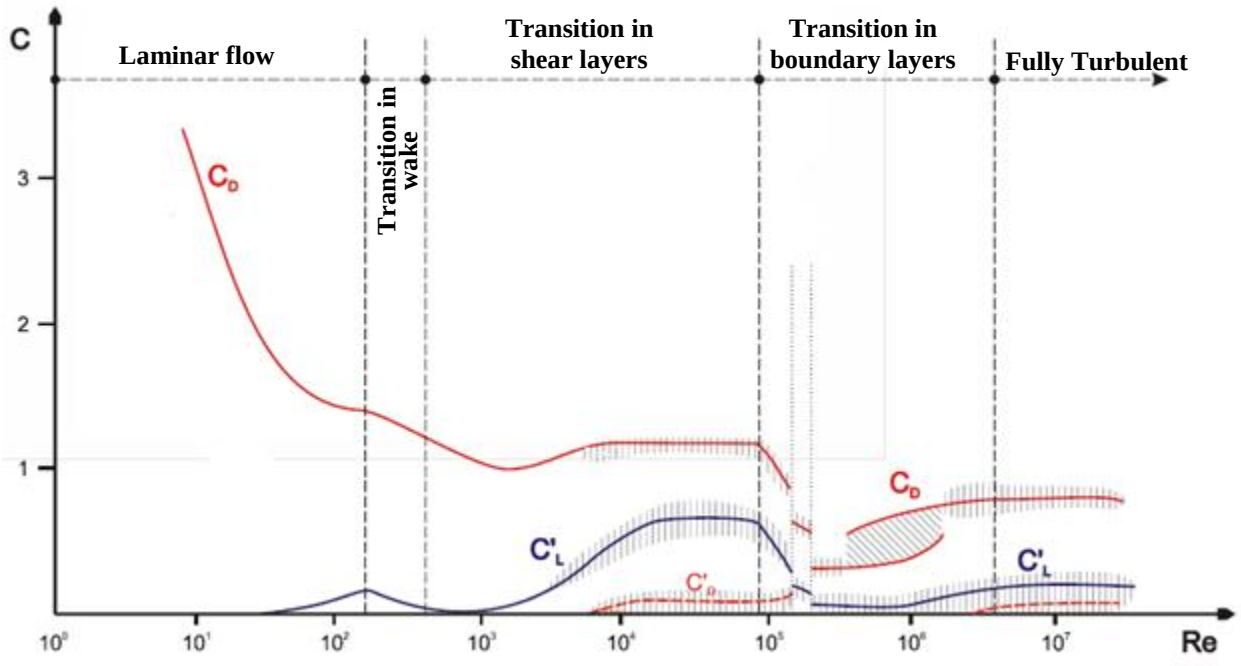

Figure 2.8: Lift and drag coefficients variation in function of the Reynolds number. Adapted from Zdravkovich[17].

The fluctuation of drag coefficient starts when there is formation of vortexes in the wake region. Around $Re \approx 10^4$, the fluctuation in drag coefficient C_D is obtained experimentally, as reported by Zdravkovich[17] However, when the boundary layer changes to turbulent, around the critical number $Re \approx 3 \times 10^5$, there is a sharp drop in the drag coefficient. The regime remains critical until $Re \approx 3.5 \times 10^6$, when the fully turbulent regime starts. For $Re > 3.5 \times 10^6$, there is the formation of fully turbulent wake that will continue for the rest of the range of Reynolds.

2.2.1 Wake of a non-oscillating circular cylinder

For many decades, many researchers presented works mapping the behavior of vortexes wake region. Perry et al.[18] showed in great detail the points of vortex formation with instantaneous streamlines. More recently, Williamson[19] compiled a work detailing the dynamic behavior of the wake downstream of a circular cylinder. Figure 2.9 shows stable wakes for a wide range of Reynolds (laminar and turbulent regimes). Every time the wake region of a non-oscillating cylinder is stable, only one vortex shedding pattern can be observed occurring on both sides of the cylinder. This shedding pattern, as reported by Bernard[14] and Kármán[15,] is now known as 2S mode. This nomenclature means that two isolated vortices are detached from the body to the wake region in one cycle of oscillation.

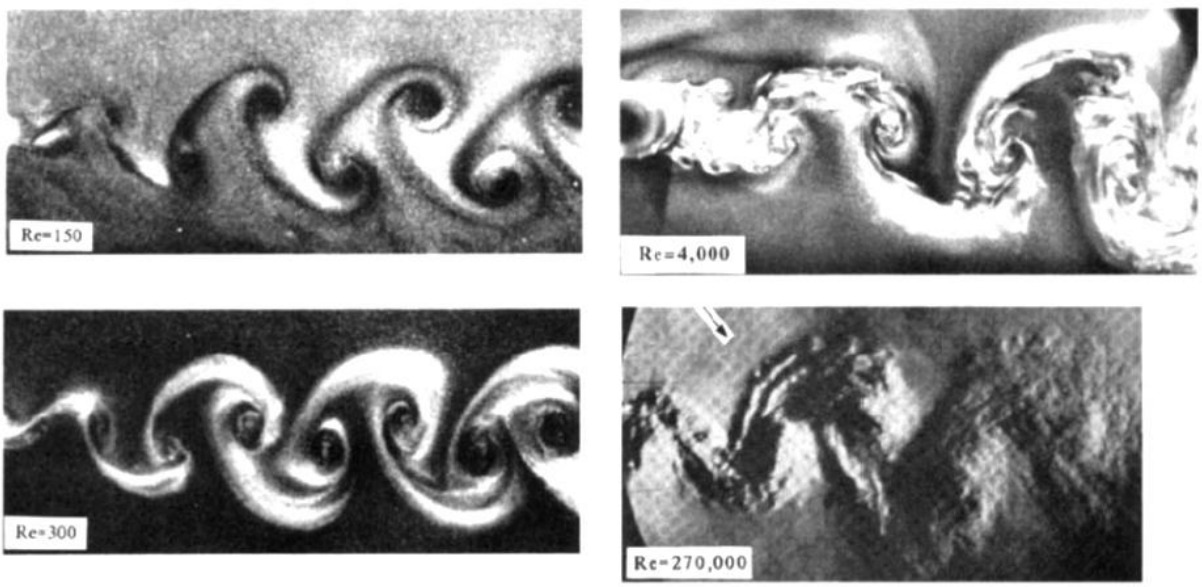

Figure 2.9: Stable wakes for a wide range of Reynolds number. Adapted from Willianson[19].

The dynamics of the 2S wake of a single cylinder is well described in the literature. In the wake region far away from the cylinder a lengthy region can be observed in which the stable 2S pattern. When the distance from the cylinder is large enough, an instable pattern take places. Within the stable region, some interesting relations were established. One example is that the longitudinal spacing between the centers of the vortexes is 0.28D for a wide range of Reynolds number.

2.2.2 Wake of an oscillating circular cylinder

The wake region of a cylinder changes when the body passes from the static configuration to a transverse oscillation condition. Basically, the vortex shedding modes are related to the amplitude and frequency of the oscillations. In a detailed study, Williamson & Roshko20 mapped the shedding patterns in function of these two parameters. They carried out forced oscillation

experiments with a rigid cylinder and observed several patterns substantially different from the 2S regime observed for a non-oscillating cylinder.

Figure 2.10 summarizes their work and presents the emission modes found for a cylinder with forced oscillation. From several distinct patterns observed, three deservers more attention because occurs more frequently: the familiar 2S ("two single"); 2P mode ("two pairs"), and the P + S mode ("single+pair"). As seen earlier, in 2S mode two isolated vortices are detached in each emission cycle, one from the each side of the cylinder. In the 2P mode, two pairs of vortices are detached in direction to the wake in each cycle. Finally, in P + S mode, a composition of a single vortex and a pair of vortices are detached from the cylinder in each cycle emission.

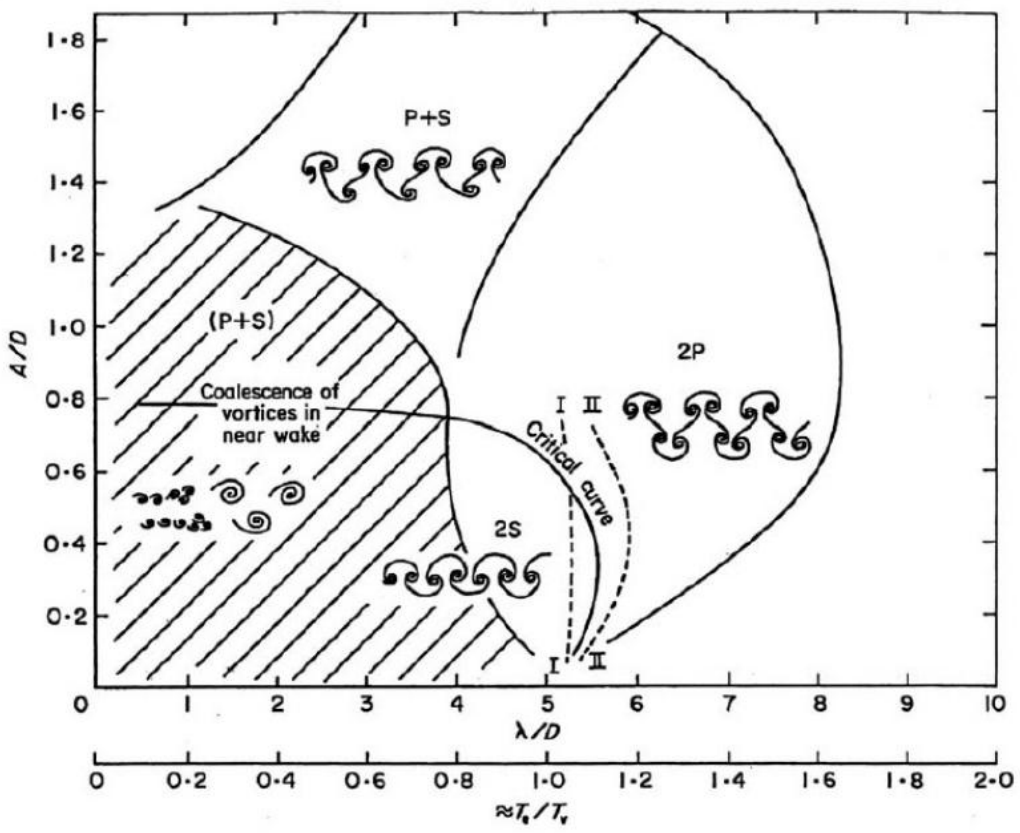

Figure 2.10: Vortex-shedding modes of a circular cylinder in forced oscillation experiments. Reproduced from Williamson & Roshko[20].

The experimental techniques of flow visualization and numerical simulations perfectly illustrate these modes. Figure 2.11 shows the 2P mode, where it is possible to observe two pairs of vortexes at each side of the wake. In the left image they used a visualization technique with aluminum particles in suspension, while the image on the right is a numerical simulation. In the 2P mode, the pair of vortexes generated at one side of the cylinder has opposite rotation directions.

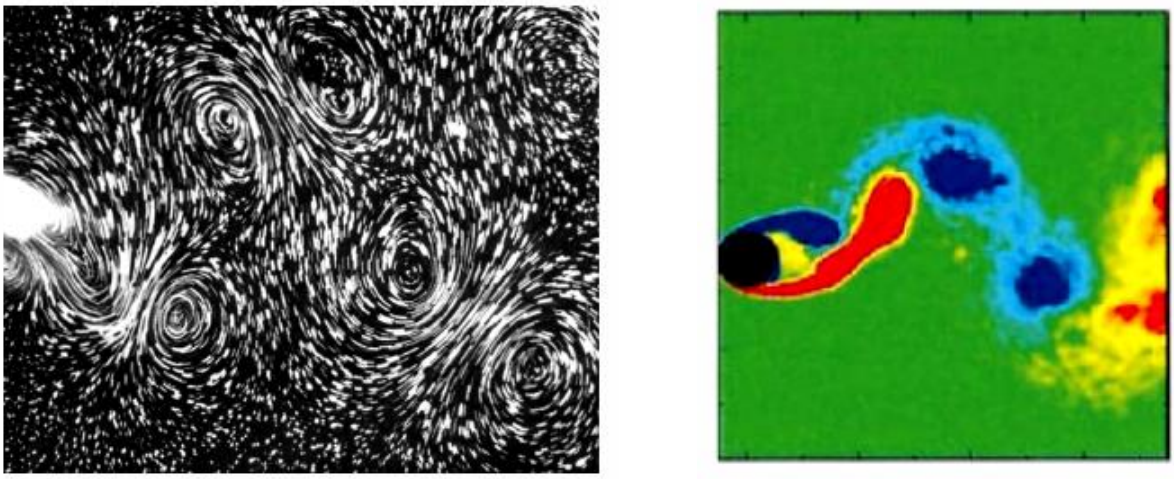

Figure 2.11: Vortex-shedding mode 2P: (left) experimental visualization from Willianson & Roshko[20]; (right) numerical simulation by Blackburn et al[21].

Besides all of these vortex emission patterns have been observed for a cylinder under forced oscillations, not all of them were verified when an isolated cylinder is free to oscillate transversely to the flow. As will be discussed in the following sections, when we will address the phenomenon of Vortex Induced Vibrations, a cylinder oscillating freely presents only the 2S and 2P modes for the speed range of interest in this work.

An additional phenomenon occurs when a cylinder is freely oscillating: the vortex shedding frequency no more varies according the equation in the entire range of flow velocities. When oscillating, the vortex shedding frequency will assume the same frequency as the system natural

frequency within a certain range of flow speeds. This phenomenon is called lock-in and will be described in detail along this thesis.

2.3 Flow induced Vibrations

In engineering, the flow-induced vibrations (FIV) are present in most systems which have structures with a bluff profile which are under influence of a fluid flow. The effect of the force fluctuations inherent to FIV can cause destructive vibrations and, for that reason, numerous efforts have been made to study how to reduce or suppress the FIV. Recently, some researchers found a useful application of FIV for energy extraction purposes and opened a new field of study about how to control and enhance FIV to achieve a better efficiency on energy conversion.

There are several types of FIV, each one associated with a specific flow phenomenon or the compositions of these phenomena. They can be classified according to their nature. Table 2.1 summarizes two types of FIV and their associated fluid phenomena.

Table 2.1: Two examples of flow induced vibrations phenomena and their causes.

VIV – Vortex Induced Vibrations	The vibration of the structure is caused by the interaction between the dynamics of the body and the periodic fluid forces generated by the changes in the pressure field caused the vortex-shedding process at the near wake region.
Galloping	Caused by the oscillation of lift force resulted from the variation of the angle of attack of the body in relation to the flow.

The excitation force has their origin from the fluid flow around the body. The body and the fluid are coupled by the surface of the body. The fluid forces exerted on the surface deforms or displaces the body, which takes a new orientation in relation to the flow and then the fluid forces may switch to the new configuration. The fluid exerts force on the structure and it responds to exerting opposing force on the fluid, establishing the mechanism of interaction between the fluid and the structure. The fluid forces applied to the structure is originated from the pressure field around the bluff body. If the fluid phenomenon has a cyclic behavior, the pressure field oscillates cyclically on the body surface and the resultant force will be periodic.

As discussed before, the pressure field can generate a resultant force on the body that has a lift component not null, inducing an excitation in the transverse direction of the flow. As in all dynamic systems it is common to describe the system in function of the excitation force, frequency of excitation, structural mass, restoring force, damping, etc. All the terms pertinent to describe the dynamic of a system under influence of flow induced vibrations will be described in this section.

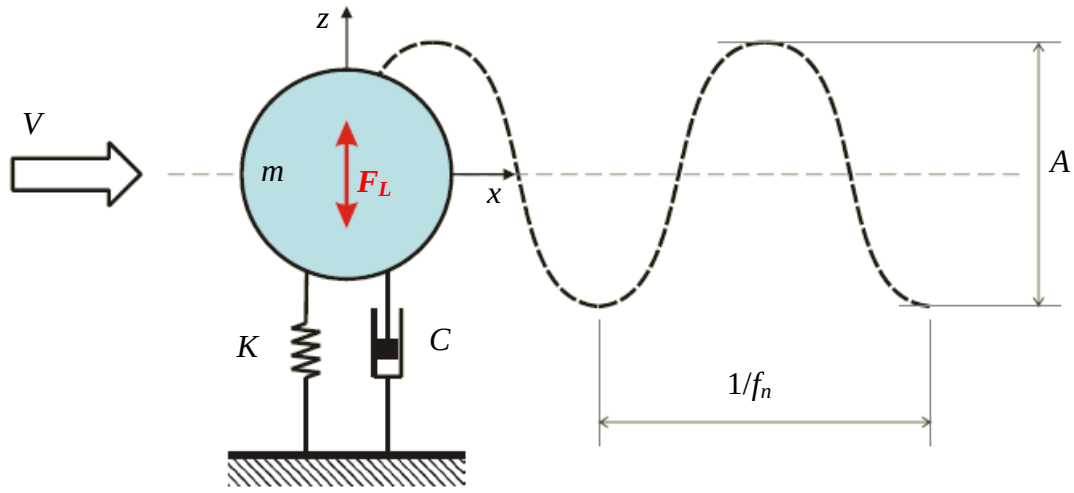

Figure 2.12: Dynamic system of an oscillating cylinder with one degree of freedom.

$$m\ddot{z} + C\dot{z} + Kz = F_L(t) \qquad 2.4$$

$$F_L(t) = \overline{F_L}\sin(\omega t + \varphi_L) \qquad 2.5$$

$$z(t) = A\sin(\omega t + \varphi_Z) \qquad 2.6$$

The dynamic system considered in this section has only one degree of freedom, only moving transversely to the flow direction. The rigid cylindrical body is considered as the entire structure of the dynamic system, meaning that it will concentrate the structural mass, the restoring force and the damping of the system, as shown in Figure 2.12. Thus, the transverse motion $z(t)$ of the cylinder can be expressed by Eq. 2.4: m is the mass of the whole oscillating system, C is the structural damping, K *is* the constant of proportionality of the restoring force and $F_L(t)$ is the fluid excitation force in the transverse direction.

When the frequency of oscillation of the cylinder is synchronized with the excitation of the fluid force, a good approximation for the force F_L(t) and the response z(t) of the cylinder are shown in Eqs. 2.5 and 2.6, where: $\overline{F_L}$ is the magnitude of the lift force, φ_L is the phase of the lift force; A is the amplitude of oscillation of the body, φ_Z is the phase of the cylinder position and $\omega = 2\pi f_n$ is the angular frequency of oscillation of the body. Blevins[21] states that the phenomena of FIV, especially the VIV, have harmonic characteristics thus can be modeled in this way. Like any dynamic system, the natural frequency of oscillation depends on the ratio between the restoration and the inertia of the oscillator, as defined in Eq. 2.7.

$$\omega_n = 2\pi f_n = \sqrt{\frac{K}{m}} \qquad 2.7$$

To study FIV several dimensionless parameters are defined. The use of these parameters is useful to the comparison between different experiments because the system response is ruled by them. It means that the response of two different systems is expected to be almost the same if the dimensionless parameters are equal. Table 2.2 presents a summary of the most important dimensionless parameters.

Table 2.2: Non-dimensional parameters

$A^* = \frac{A}{D}$	Non-dimensional amplitude: ratio between the oscillation amplitude and the cylinder diameter.
$V_R = \frac{V}{f_n D}$	Reduced Velocity: non-dimensional velocity obtained by dividing the flow speed by the natural frequency of the system and the cylinder diameter.
$m^* = \frac{m}{m_\nabla} = \frac{m}{\frac{\pi D^2}{4} L\rho}$	Mass ratio: ratio between the oscillating mass (m) and the mass of the fluid displaced by the cylinder.
$f^* = \frac{f}{f_n}$	Non-dimensional frequency: ratio between the oscillation frequency (f) and the system natural frequency.
$\zeta = \frac{C}{2\sqrt{Km}}$	Damping ratio: ratio between the structural damping (C) and the critical damping.

2.3.1 Vortex Induced Vibrations

The vortex induced vibrations (VIV) are one of the types of flow-induced vibrations which occur in bluff bodies. As discussed in previous sections, the generation and release of alternating vortices generates a pressure field that varies cyclically in time. Consequently, there is a periodic fluctuation in the transverse force in the same the frequency of the emission of these vortexes.

Thus, the excitation force in VIV phenomenon is generated by the alternating vortex generation which causes periodic changes in the pressure acting to the cylinder surface.

Figure 2.13 illustrates the variation of force in approximately one third of the vortex emission cycle in a cylinder. It is possible to observe that the pressure field in the cylinder surface is synchronized with the formation of vortices in the wake. When a vortex is formed in one side of the cylinder it causes a drop in pressure, generating a lift force in this direction. In a complete cycle of vortex shedding, the lift goes form its maximum positive value, reaches its maximum negative value (when the opposite vortex is being formed) and returns to the initial positive value. Thus, the fluctuation of the lift force has the same frequency of issuance of the vortices to the wake.

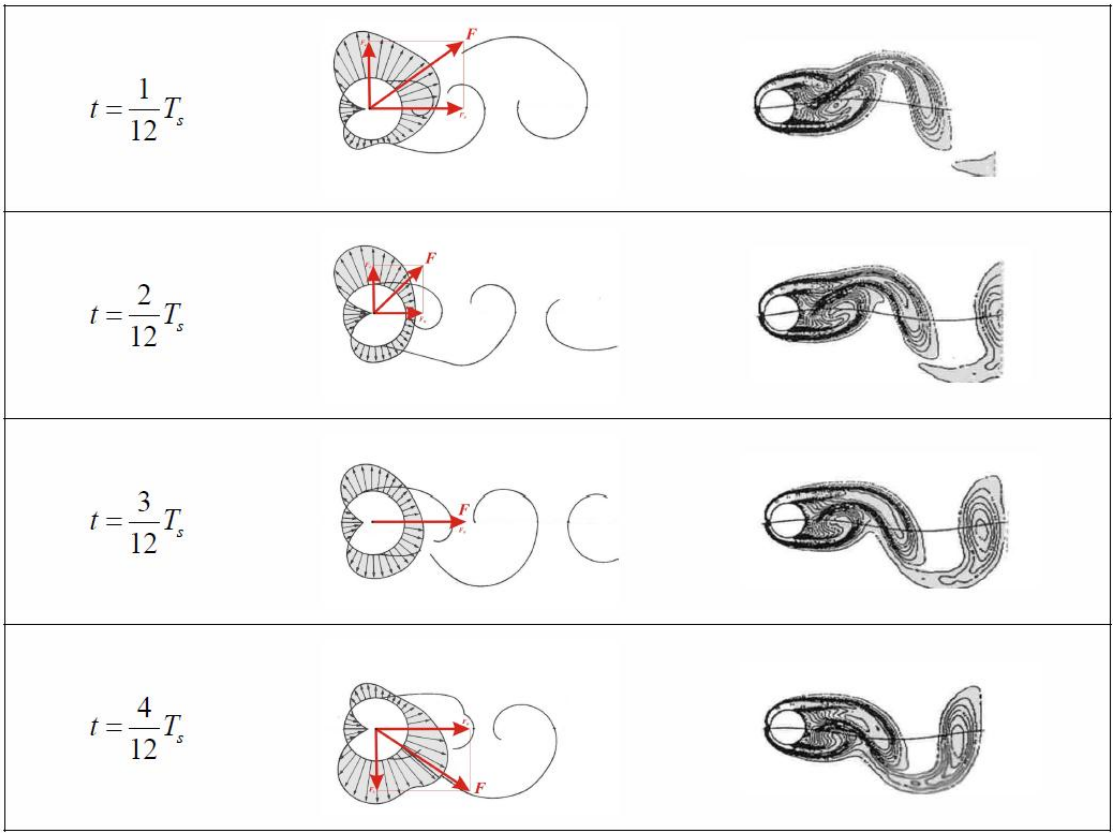

Figure 2.13: Pressure field variations for one third of the vortex shedding cycle. Adapted from Blevins[21].

Following the same principle, the drag force will also change over emission cycle. However, unlike the lift, the drag force does not change direction, but suffers only a fluctuation in its magnitude always pointing in the flow direction. However, over a cycle a vortex is detached from each side of the cylinder, making the pressure field changes twice in one cycle. Consequently, the frequency of fluctuation of drag force is twice the of vortex shedding.

Therefore, the phenomenon of VIV excites the vibration of the cylinder in both directions: longitudinal and transverse to the flow. However, the fluctuation of the forces in the transverse direction is greater than in the longitudinal direction resulting in a large oscillation in the first direction. Thus, the oscillation amplitude in the direction of drag is smaller and has double the frequency. Briefly, the source of the effects of VIV is the interaction between the cylinder and the pressure fields modified by the emission of vortices in the wake. According to Williamson & Govardhan[22] "VIV is a phenomenon of feedback between the dynamics of the body and the wake."

Following the description of this text, it is easy to see that there are two characteristic frequencies involved in the phenomenon of VIV. The frequency of vortex shedding f_s governs the fluid excitation force, and the natural frequency of the system f_n governs the dynamic response of the cylinder oscillation. Thus, as any dynamic system, an oscillating cylinder is subject to the resonance phenomenon, which is the amplification of the vibrations which occur when the excitation frequency approaches the system natural frequency.

From this point, an analysis of the behavior of an elastically mounted cylinder with one degree of freedom will be made, using the oscillator presented on last section. The natural frequency of vibration depends on the weight and rigidity of the system, as shown in Eq. 2.7. In general, all linear oscillators oscillate at the same frequency of the excitation. When the external

excitation frequency coincides with the natural frequency of the system the resonance phenomenon takes place and a large amplification of the oscillation is observed. However, a system under influence of VIV response has a different and very interesting response that will be described below.

As discussed before, the external excitation frequency is equal to the vortex shedding frequency. With the increase of the flow speed, the vortex shedding frequency also increases. The cylinder frequency of vibration is equal to the vortex shedding frequency until it approaches the system natural frequency. As the excitation in VIV is a phenomenon that suffers a feedback generated by the cylinder wake, the oscillations interfere on the vortex shedding process and the system natural frequency takes control of the vortex shedding process and its frequency, making them synchronized with a value near the system natural frequency even with increase of the flow speed. At the end of the band of synchronization, the vortex shedding frequency is no longer controlled by the system natural frequency and the system starts to oscillate with the vortex shedding frequency again. Typically, the lock-in phenomenon is classified as the regime in which the emission frequency of vortices f_s is controlled by the frequency f_n. Thus, synchronization occurs when $f_s/f_n \approx 1$.

Several experimental investigations have shown the variation in Strouhal number as a function of Reynolds Number remains close to the value St ≈ 0, 2 for a wide range of Reynolds number ($10^2 < Re < 10^6$). Therefore, it is possible to estimate the flow speed in which the resonance $f_s = f_n$ occurs. The synchronization range can be observed in Figure 2.14, from reduced velocities 6 to 13.

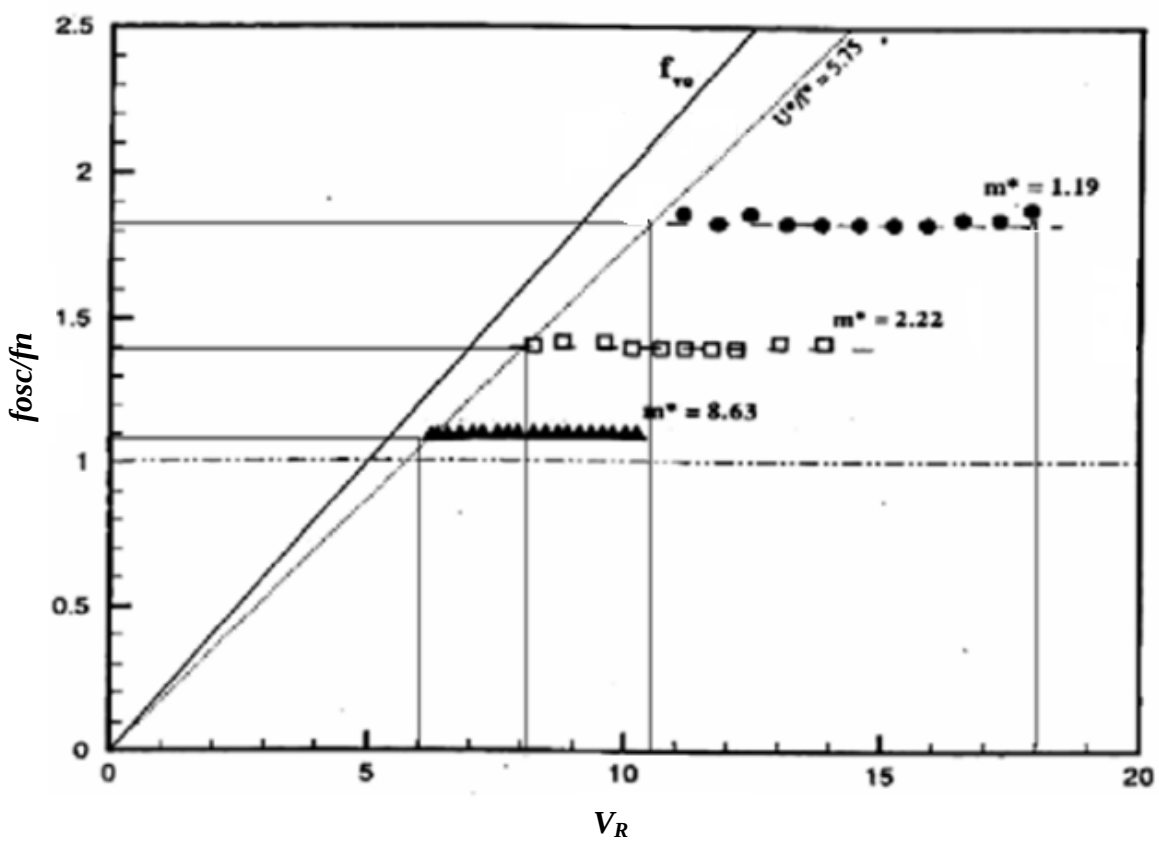

Figure 2.14: Frequency responses of experiments with different mass ratios. Reproduced from Bernitsas et al.[9]

The amplitude of oscillation of an elastically rigid cylinder undergoing VIV are directly associated with the mass and damping parameters of the system. As a first example, Figure 2.15 presents results for two cases of rigid cylinders mounted elastically. Feng[23] achieved peak amplitude at resonance around 0.6 diameters, while the experiment Khalak & Williamson[24] reached peak amplitude around 0.9. It is necessary to notice that the mass ratio m* of the systems are very different, with Feng[23] experiments presenting a mass ratio more than 20 times larger than the one conducted by Khalak & Williamson[24].

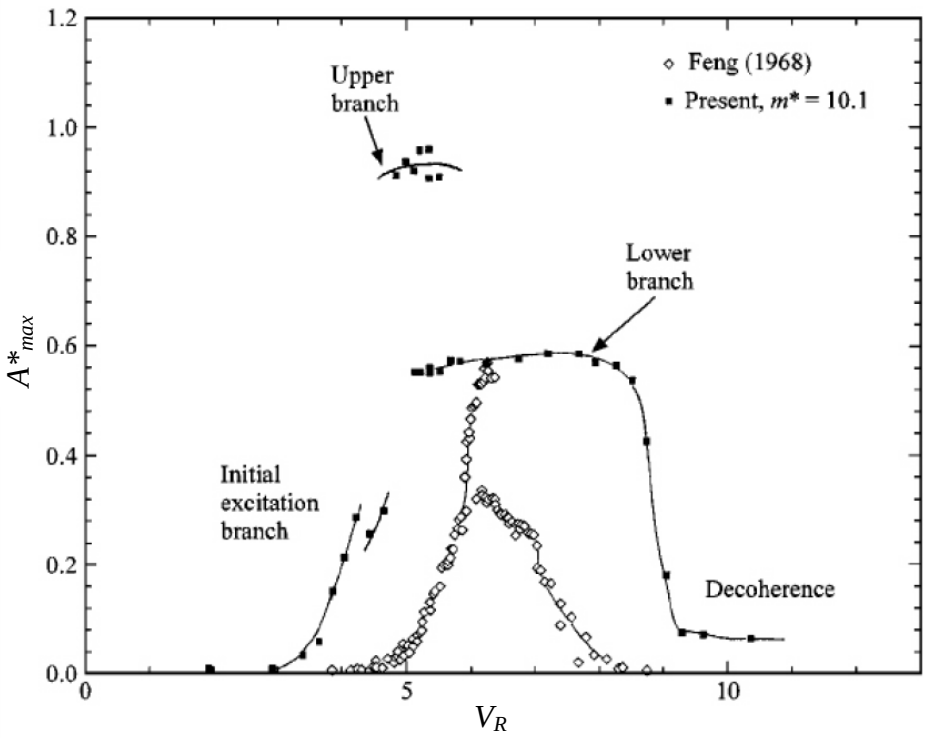

Figure 2.15: Response amplitude for two cases of elastically mounted cylinders with different characteristics oscillating transversally. Feng[ref]: m^*=248 and $m^*\zeta \cong 3.28$; Khalak & Williamson[24]: m^*=10.1 and $m^*\zeta$=0.13. Adapted from Khalak & Williamson[24].

Khalak & Williamson[24] explain the difference of the answer of the two cases: "The maximum amplitude depends on the mass-damping parameter (m*ζ); the higher this parameter is smaller will be the amplitude of the resonance peak". Feng[23] has the combined parameter $m^*\zeta \cong 3.28$, while the experiment of Khalak & Williamson[24] presents $m^*\zeta = 0.13$, about 4% of the value of Feng's experiment, justifying the difference between peaks.

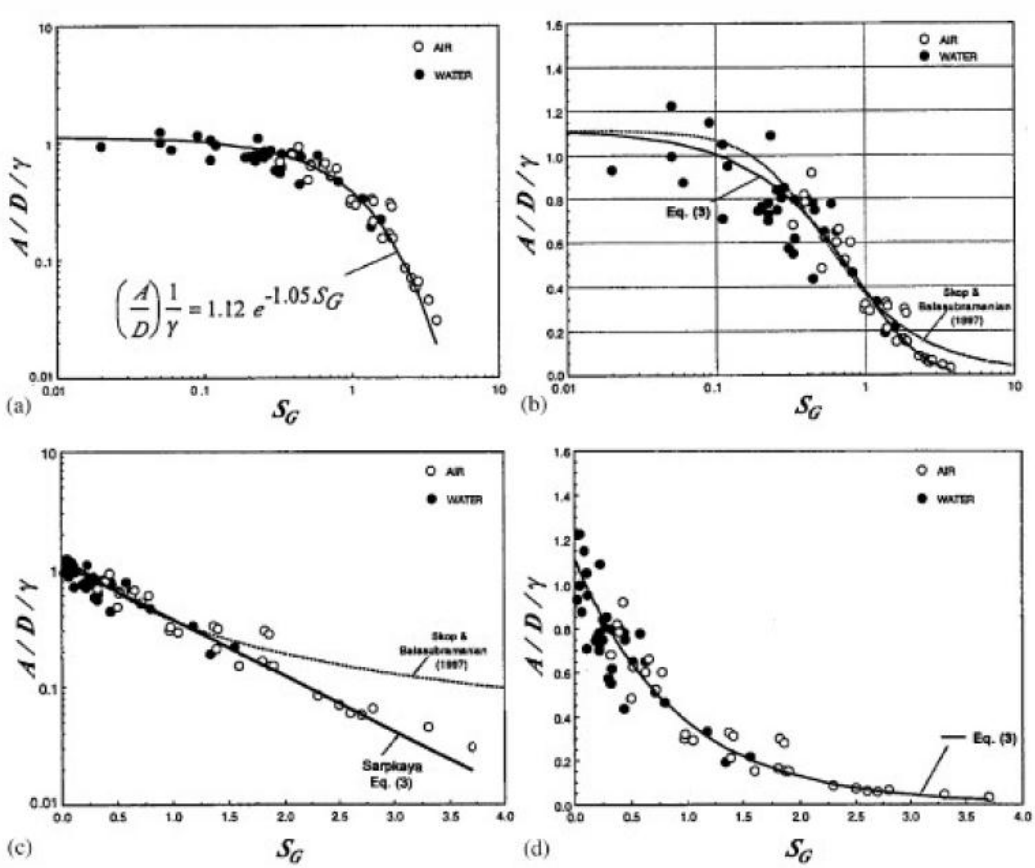

Figure 2.16: Griffin plot showing the behavior of VIV amplitudes in function of the mass-damping parameter S_G=m*ζ. Reproduced from Sarpkaya[25].

Several authors have collected the maximum amplitudes of different works and tried to propose analytical models to find and approximation that represents the amplitude of VIV in function of the mass-damping parameter. The most accepted model was presented by Griffin et al.[26] and is known as the Griffin plot. In this curve, shown in Figure 2.16, it is possible to analyze the behavior of the maximum amplitude of VIV of lots of experiment as a function of the mass-damping parameter. It is clear that the maximum amplitude always decreases with the increasing of the mass-damping parameter.

Another peculiar behavior can be seen in Figure 2.15. The case with lower m*ζ has not only the highest peak, as well as an almost constant amplitude of oscillation around 0.6 that present from reduced velocity 5 to 9. In contrast, the high m*ζ suffer a sharp decrease on the amplitude just after the peak. From this comparison, Khalak & Williamson[24] concluded that the mass and damping parameters also influence the range of reduced velocities in which the lock-in occurs. Thus, the phenomenon of lock-in is not only characterized by a peak centered in the neighborhood of reduced velocity 5, but by a range within the amplitude of oscillations are amplified. The dynamic behavior of the cylinder is then analyzed under the assumption of three branches of response: initial branch, upper branch and lower branch.

The initial branch is where the excitation and the lock-in begin. When the frequencies are very close to the resonance the amplitude increases sharply to the upper branch. Increasing the reduced velocity, the response falls to a lower level, called lower branch. However, only systems with low mass-damping present these three branches. When the mass-damping parameter increases the response presents only the initial and the lower branches. Khalak & Williamson[24] state that "the maximum amplitude achieved in the upper branch has a strong dependence of the mass-damping parameter, but the widening of the high and lower branches is only dependent of the mass ratio parameter." Figure 2.17 illustrates exactly what was discussed now. It is necessary to pay attention to the dependence of the mass and damping parameters and transition effects between modes.

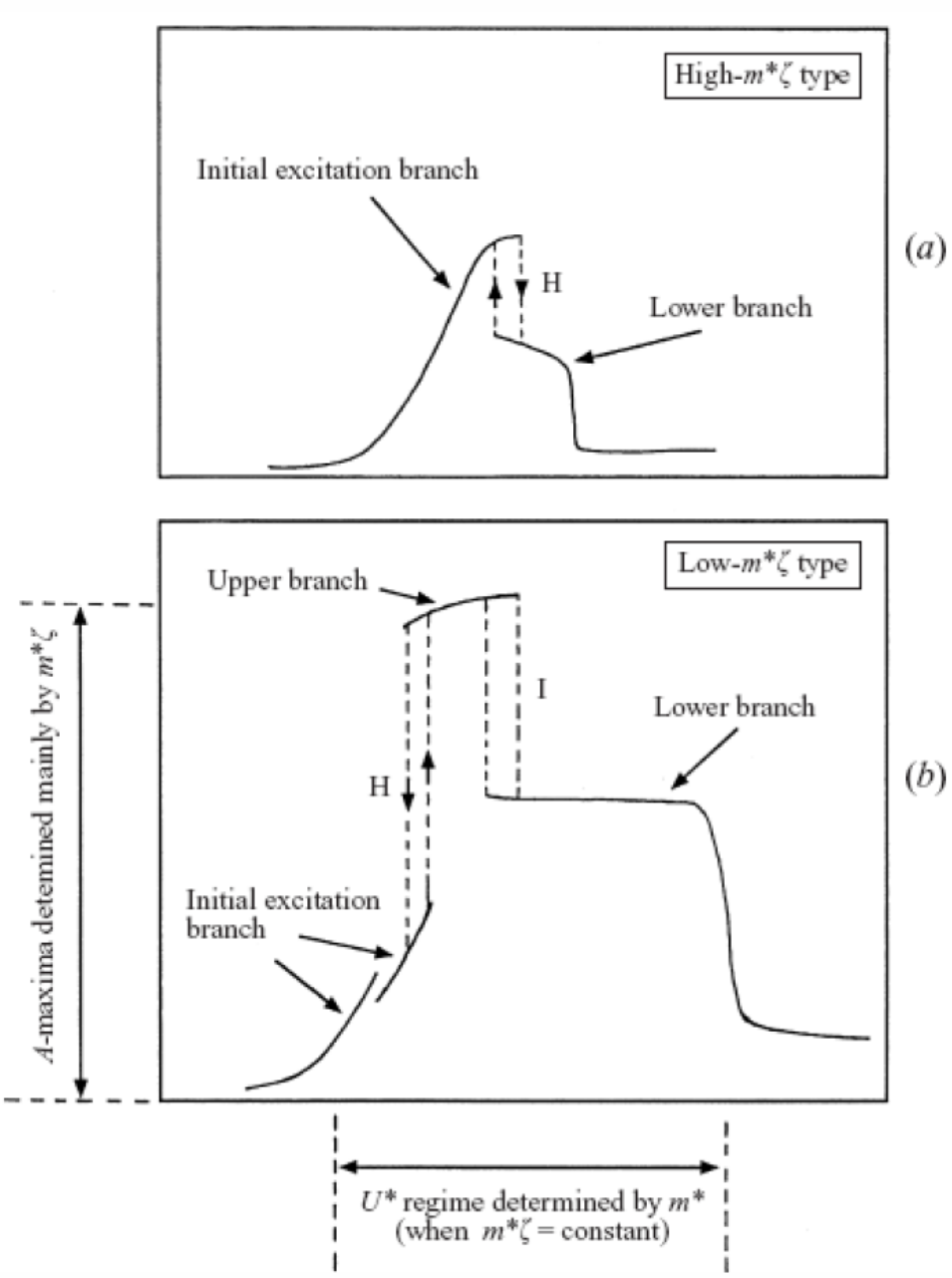

Figure 2.17: Response modes of an elastically mounted rigid circular cylinder. It is necessary to pay attention to the dependency of the mass-damping parameter and the transition effects between modes. Adapted from Khalak & Williamson[24].

Another phenomenon observed for a system which has a low mass ratio parameter is observed at the behavior of the non-dimensional frequency $f^*=f_s/f_n$ usually used to illustrate the VIV response. The phenomenon of synchronization, as defined at the beginning of this section,

occurs at values different from $f^*=1$. Experiments showed that f^* assumes levels within two branches of response. The greater m* is, the nearest f^* is to the unit. This fact led to a review of the lock-in phenomenon. Sarpkaya[25] defined it as "the band of lock-in occurs when the frequency of the lift force synchronizes with the oscillation frequency." Later, Khalak & Williamson[24] considered the synchronization when "the frequency of the vortex-shedding mode in the wake synchronizes with the cylinder oscillation frequency", remembering that the vortex-shedding modes in an oscillating cylinder may involve more than one pair of vortices per cycle.

Also in Figure 2.17 it is necessary to highlight another two important points of VIV phenomenon that is associated with the vortex-shedding modes: the hysteresis (identified by the letter H) and the phenomenon of intermittency (identified by the letter I). Feng[23] had already noticed during his experiments that the transition between the branches of response showed hysteresis, fact identified in the case with high $m^*\zeta$ parameter of Figure 2.17. Khalak & Williamson[24] found that when the system has a low $m^*\zeta$ parameter and shows three branches of response, the first transition between the initial branch and upper branch also had characteristics of hysteresis. Moreover, the second transition between the upper branch and the lower branch presented an alternation between the branches (Figure 2.17). These hysteresis phenomena have been attributed to the jumps in the phase angles between the lift force and the oscillation of the body caused by the change in the vortex-shedding modes.

Williamson & Roshko[20] mapped the vortex-shedding modes in the wake region for a wide range of speeds within there was oscillation of the cylinder. As the result of their work, they created a map showing the modes of vortex-shedding, as presented in Figure 2.18. Later, Willianson & Govardhan showed a clear correlation of the mode 2S with the initial branch and of

the mod 2P with the lower branch, as shown in Figure 2.17. Only these two modes, 2S and 2P, are obtained when a cylinder is free to oscillate transversely. The other modes in the map of Figure 2.19 were observed in experiments with forced oscillations.

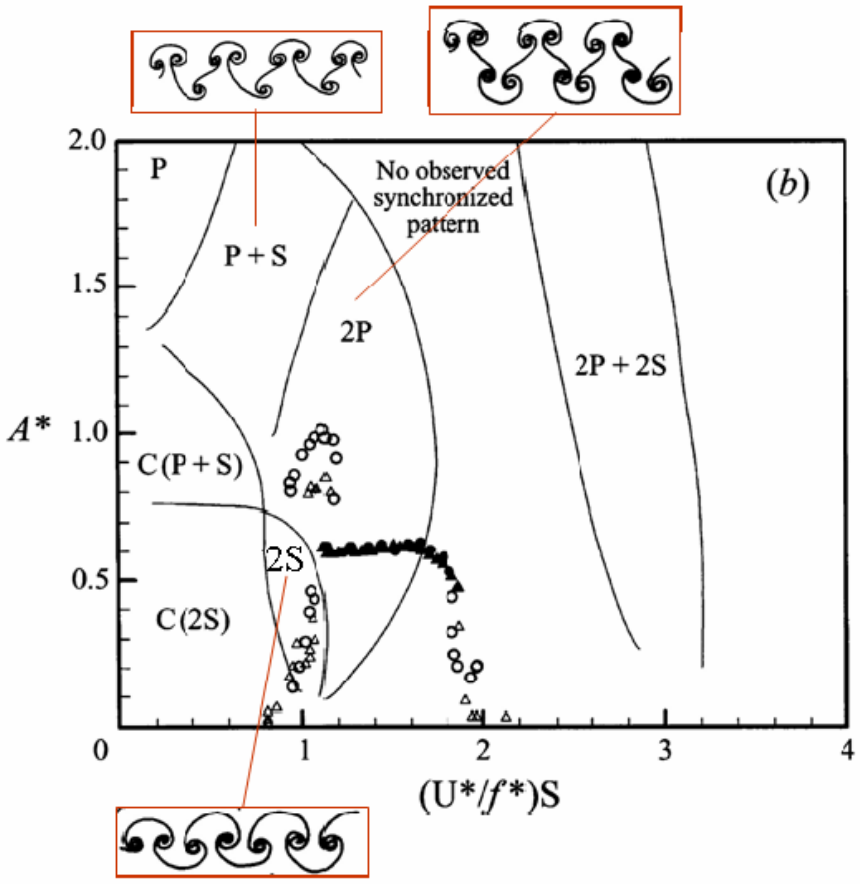

Figure 2.18: Map of the vortex-shedding modes in function of the non-dimensional amplitude of oscillation and reduced velocity. Adapted from Willianson & Govardhan[22].

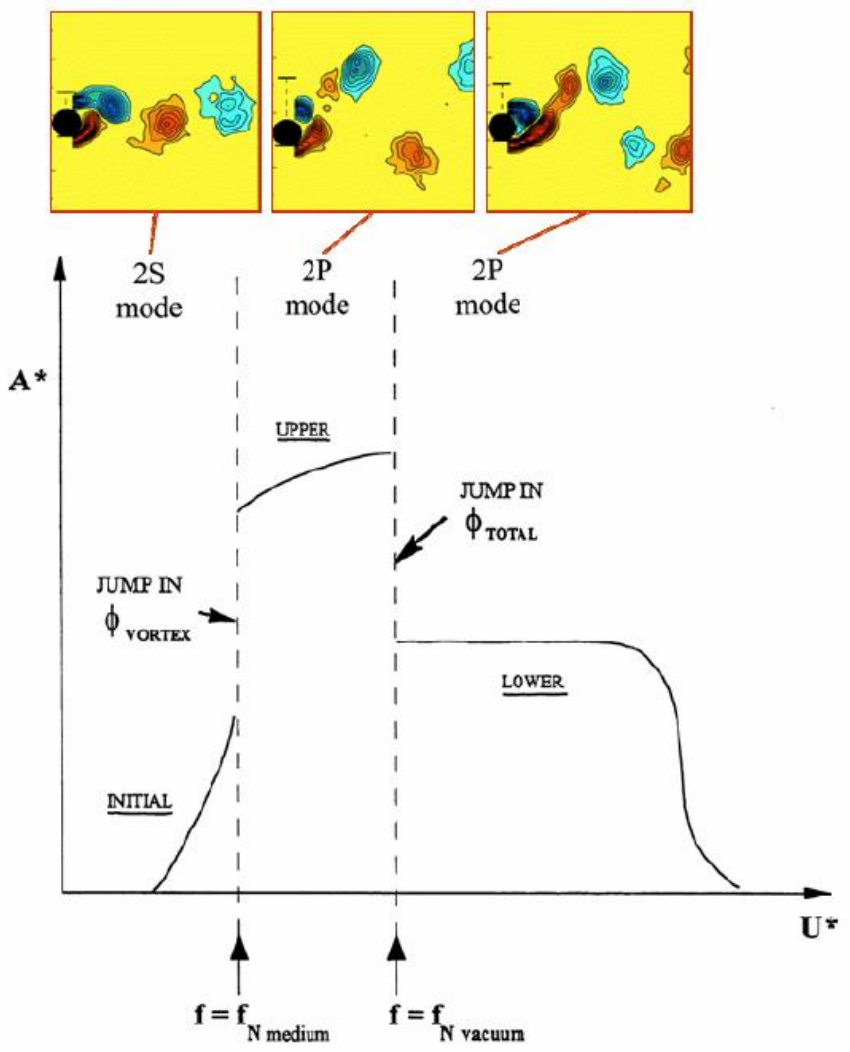

Figure 2.19: Vortex-shedding modes and the transition between the response branches. Adapted from Williamson & Govardhan[22].

2.4 Energy harvesting systems using VIV

The first well succeeded system that used the vortex-induced vibrations phenomena to convert energy from a fluid flow into electricity was the VIVACE[4], developed by a group of researchers from University of Michigan. The self-excited motion characteristic of vortex-induced vibrations aroused their interest in the development of an energy harvesting system which uses the motions of a circular cylinder to move an electricity generator.

The motions of the cylinder are the result of the alternating vortex shedding which creates asymmetry in the pressure distribution around the cylinder, resulting in a oscillatory lift force. The cylinder in VIV oscillates perpendicularly to its axis and transversely to the flow velocity. Thus, the cylinder in VIV absorbs energy from the fluid and converts it into motion.

There are several options to convert this motion of the cylinder in electricity and two of them are presented in Figure 2.20. The simplest option is to use a linear generator, which can be used without the necessity of a mechanical dispositive to convert the translational motion of the cylinder into rotational motion to use a rotatory type generator. Because of the simplicity, the linear generator was chosen to be used in the energy harvesting system used in the experiments for this thesis.

The second option is more complex because needs a rack & pinion system to convert the translational motion of the cylinder in rotational motion. The advantage of this system is that the rotatory type generators are more efficient than the linear type, but a careful analysis must be made to balance if the better efficiency of the generator compensates the extra damping resulted from the inclusion of the rack & pinion system.

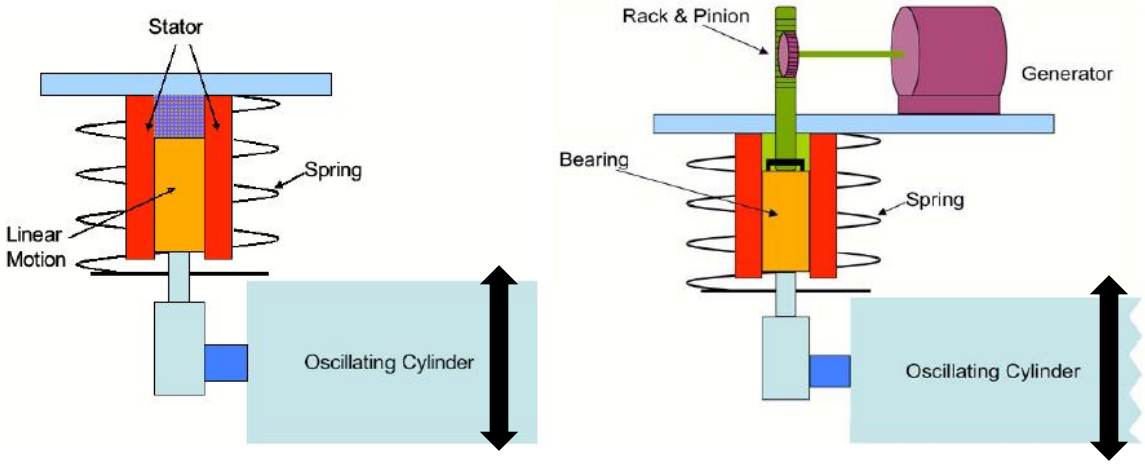

Figure 2.20: Conversion of cylinder motion into electricity. On left a linear generator and on right a rack & pinion system converts the translational motion in rotatory motion to activate the generator.

The common part for all the generating systems is that to achieve large amount of energy generation is necessary to lead with large damping factors. As VIV amplitudes are greatly dependent of the resonance phenomena it suffers large influence of variations in the damping factor. To balance the extra damping from the generator larger lift forces are required in order to achieve a better conversion efficiency and most of the recent efforts are being made in that direction. The research of this doctor course also follows this direction as the use of tripping rods has the objective to increase the lift forces acting on the cylinder and, consequently, the system efficiency.

2.4.1 VIV and leverage system for efficiency enhancement

With the objective of increasing the efficiency of the energy conversion using VIV Nishi et al.[5] developed a system that utilizes the vortex-induced vibrations of a cylinder and principle of leverage. Their system transforms the translation motion of the VIV into a translation motion of the generator as shown in Figure 2.21. The aim of their work was to improve the system efficiency by tuning the distance between the pivot and the generator, changing the relation between the cylinder motion and coil motion.

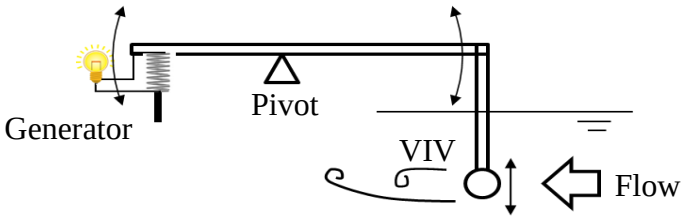

Figure 2.21: Schematic view of the leverage system used to improve the conversion efficiency.

To analyze the idea behind the use of the leverage system to increase the conversion efficiency it is necessary to show the system mathematical model. The leverage can be represented as a single rigid bar that rotates around a pivot, as shown in Figure 2.22. Fluid force from VIV and electromagnetic reaction forces are applied at distances r_2 and r_3, respectively, from the pivot, while spring restoring force is applied at distance r_1. The dynamic equation of the system is written as:

$$I\ddot{\theta} + C\dot{\theta} + k\theta + kr_1^2 \sin\theta\cos\theta = F_L r_2 \cos\theta + Mgr_3 \cos\theta - F_m r_3 \cos\theta \qquad 2.8$$

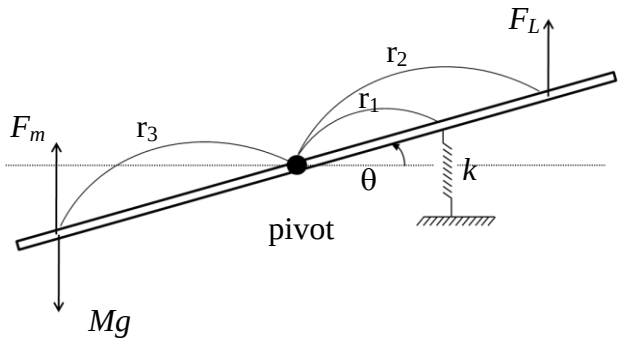

Figure 2.22: Representation of the leverage system as a single rigid bar with the forces and their points of application.

The voltage generated on the generator is proportional to the velocity of the coil's translation motion and can be written as:

$$E = \alpha r_3 \dot{\theta} \cos\theta \qquad 2.9$$

Where α is the constant of proportionality obtained experimentally. The electromagnetic reaction force is:

$$F_m = \frac{\alpha m_b r_3 N}{\ell R}\dot{\theta}\cos\theta \qquad 2.10$$

By solving the equation of motion and considering the frequency of lift force equal to the system's natural frequency it is possible to obtain the equation of maximum generated voltage:

$$E_{\max} = \frac{\alpha F_L}{\frac{C}{r_2 r_3} + \frac{\alpha m_b N}{\ell R}\frac{r_3}{r_2}} \qquad 2.11$$

Using the parameters presented in Table 2.3 into equation 2.9 it is possible to obtain the curve that shows the maximum generated voltage in function of the r_3/r_2 relation, as presented in Figure 2.23. The position of the maximum in this curve changes with the variation of the system parameters.

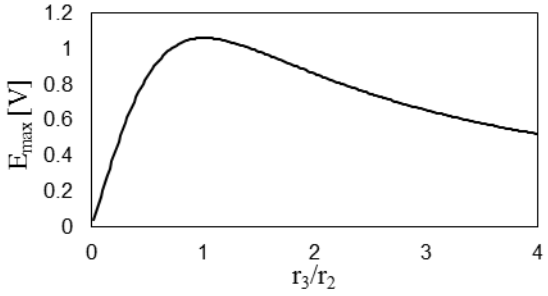

Figure 2.23: Theoretical maximum voltage response in function of r_3/r_2.

Table 2.3: Parameters of the system to calculate the maximum voltage generated curve.

Symbol	Definition	Value
C	Damping coefficient	$2\zeta\sqrt{Ik}$ [kg m s^{-1}]
F_L	Amplitude of lift force	- [N]
F_m	Electromagnet reaction force	- [N]

g	Gravity acceleration	9.81 [kg m s^{-2}]
I	Moment of Inertia of the bar and coil	$0.48 + Mr_3^2$ [kg m^2]
k	Spring stiffness	540 [N m^{-1}]
ℓ	Coil length	0.043 [m]
m_b	Magnet bar coefficient	0.637×10^{-3} [Wb]
M	Coil mass	0.548 [kg]
N	Total number of turns of the coil	2000
R	Resistor connected to the generator	100 [Ω]
r_1	Distance between pivot and spring	0.5 [m]
r_2	Distance between pivot and cylinder	0.5 [m]
r_3	Distance between pivot and generator	variable [m]
α	Empirical coefficient	29.76 [V s m^{-1}]
ζ	Damping ratio	0.079 [-]
θ	Angular position of the bar	- [rad]

2.5 Tripping rods

In this chapter the tripping rods and their known effects in the flow around a circular cylinder will be presented. Tripping rod is the name giver to small diameter cylinders that are attached to a main cylinder with the objective of changing the flow patterns around the cylinder. The flow modifications caused by the tripping rods are different in function of four parameters of the system:

- Angular position
- Diameter ratio
- Gap ratio
- Reynolds Number

As result of the flow modifications caused by the presence of tripping rods the hydrodynamic effects of the flow on the cylinder will also suffer modifications. The most important modification can be observed in the fluid forces acting on the cylinder, which can increase or decrease in comparison to the smooth cylinder, according to the combination of the three system properties cited before.

The possibility of using tripping rods for reducing the fluid forces acting on the cylinder motivated researchers[2,3,6] to study and obtain the flow patterns present in a cylinder with tripping rods attached. As shortly presented in the literature review of this thesis, there are three flow patterns that take place in a cylinder with tripping rods. These three patterns are presented in Figure 2.24. Each pattern is associated with one of the three possibilities that can occur with the hydrodynamic forces acting on the cylinder, which can increase, decrease or suffer no alterations.

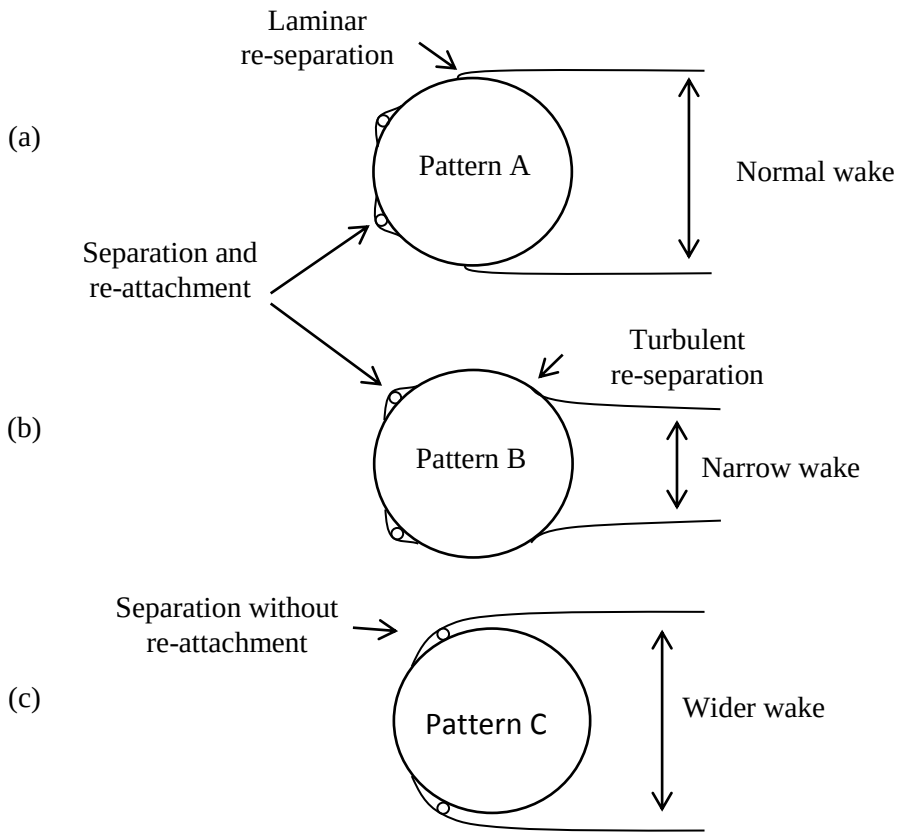

Figure 2.24: Flow patterns around a cylinder with tripping rods.

The first pattern, called pattern A in this thesis, is associated to the no alterations in the forces acting on the cylinder. The reason for it occurs is that the tripping rods do not cause significant changes in the flow to alter the wake region behind the cylinder. This pattern is usually present when the diameter of the tripping rods or the Reynolds number is too small. This pattern is characterized by a separation of the flow just before the tripping rod and a re-attachment just behind it, followed by a laminar re-separation which occurs at the same place as the observed in the smooth cylinder. This pattern is shown in Figure 2.24a.

The second pattern, called pattern B, is the most studied because is associated to the reduction of fluid forces acting on the cylinder. In this case, presented in Figure 2.24b, there is a separation before the tripping rod and an immediately reattachment behind it, as occurs in pattern A. The difference appears in the re-separation of the flow, which will occur more downstream than the observed in the smooth cylinder and will be turbulent. As a result of the alter re-separation, the wake region will be narrow than the observed for the smooth cylinder and the energy in the wake will be lower, fact that results in the smaller forces acting on the cylinder.

The third and last pattern, called pattern C, is the most important for the present work because the increase of forces acting on the cylinder are associated with it. In this case, the separation occurs just before the tripping rods and there is no re-attachment behind it. As a consequence of the earlier separation the wake region becomes wider than the observed for the smooth cylinder. As a consequence, the energy present in the vortexes in wider wake region will be larger, resulting in the larger forces observed. This flow pattern can be observed in Figure 2.24c.

Explained the flow patterns that appear in a cylinder with of tripping rods, it is necessary to remember the definitions of the tripping rods angular position and the diameter ratio already made in chapter 1. Figure 2.25 presents a schematic view of the cylinder with a pair of tripping rods symmetrically attached in relation of the stagnation point, at angular positions β. The tripping rods diameter is represented by d and the diameter ratio is defined as the ratio between the tripping rods diameter and the cylinder diameter D. Another important factor that influences the forces is the gap ratio, which is the ratio between the gap (δ) from the cylinder to the tripping rod surface and the cylinder diameter.

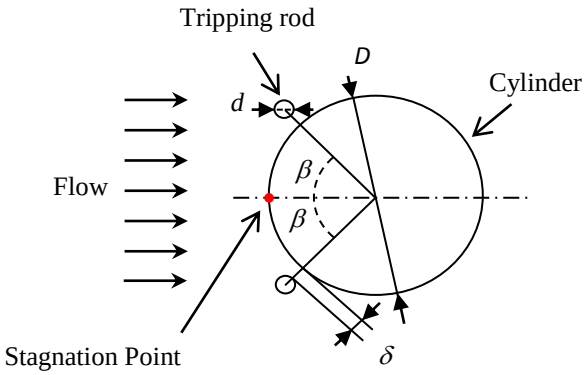

Figure 2.25: Tripping rods positioning around the cylinder.

The following sections will show the effects of the variation of each one of the four parameters of the system in the forces acting on the cylinder.

2.5.1 Effects of angular position

The angular position of the tripping rods is the parameter that most affects the force acting on the cylinder. It is possible to change between the three flow patterns only by variation of the angular position. Figure 2.26 shows an example of lift coefficient variation obtained by Alam et al in function of tripping rods position. When tripping rods are positioned from 20 to 40 degrees the lift coefficients are smaller than those for the smooth cylinder and the flow pattern B can be observed. Above 40 degrees there is a sharp variation and the lift coefficient response and it present values larger than those for the smooth cylinder. It happens because when positioning the tripping rods more near to the angular position where the separation naturally occurs for the smooth cylinder, easier is to the tripping rods to induce the separation.

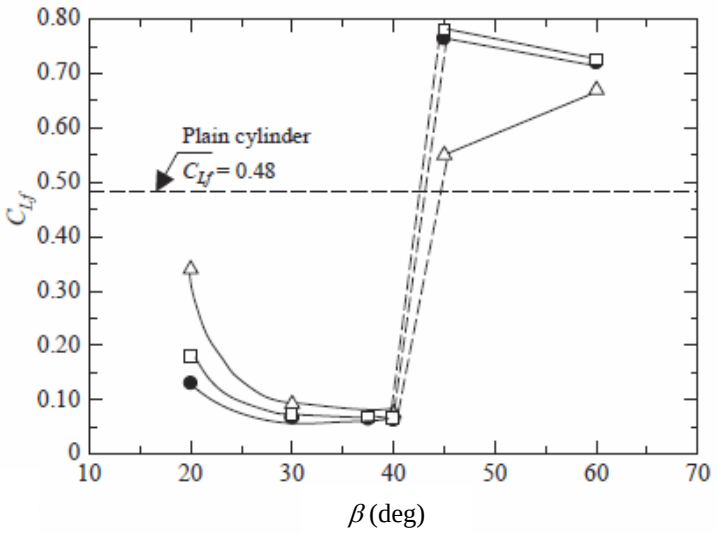

Figure 2.26: Variation of the fluctuating lift coefficient in function of tripping rods angular position. reproduced from Alam et al.[3]

This is the variation that will be studied in this work to improve the generating system efficiency.

2.5.2 Effects of the diameter ratio

The variation of the diameter ratio also cause alterations in the flow properties and, consequently, in the forces acting on the cylinder. The relation between the diameter of the tripping wire and the thickness of the boundary layer is an important factor in the transition between the flow patterns. As the tripping rod diameter starts to overcome the thickness of the boundary layer the tripping rod induces the transition of the boundary layer from laminar to turbulent and even can induce an earlier separation of the flow. Figure 2.27 shows an example of three different diameters of tripping rods.

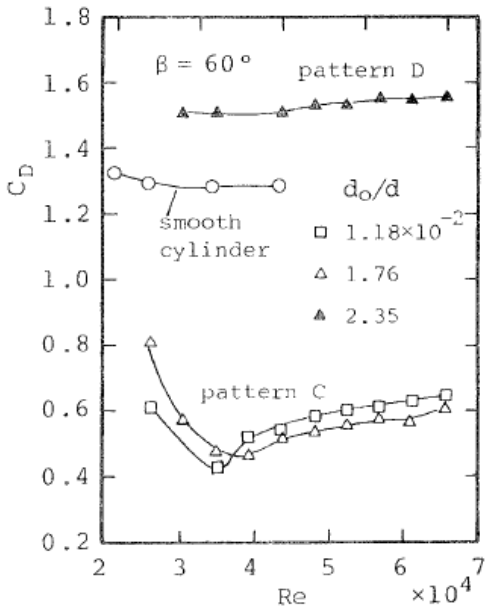

Figure 2.27: Drag coefficient variation in function of the diameter ratio. Nomenclature: □: (d/D = 0.0118); △: (d/D = 0.0176); ▲: (d/D = 0.0235). Reproduced from Igarashi[6].

It is possible to notice in this figure that the two smaller tripping rods caused a significant reduction of the drag coefficient, characteristic of pattern B. As the tripping rod diameter ratio increased, the drag coefficients also increased in comparison of the smooth cylinder. It was caused because the larger tripping wires induced a separation of the flow at tripping rod position, causing the transition from pattern B to pattern C.

In the experiments that will be presented in this thesis, the diameter ratio was maintained constant during all the experiment.

2.5.3 Effects of gap ratio

There is not much information about the gap ratio influence in the hydrodynamic coefficients of the cylinder. Alam et al. is the only known work that shows its effects, as presented in Figure 2.28.

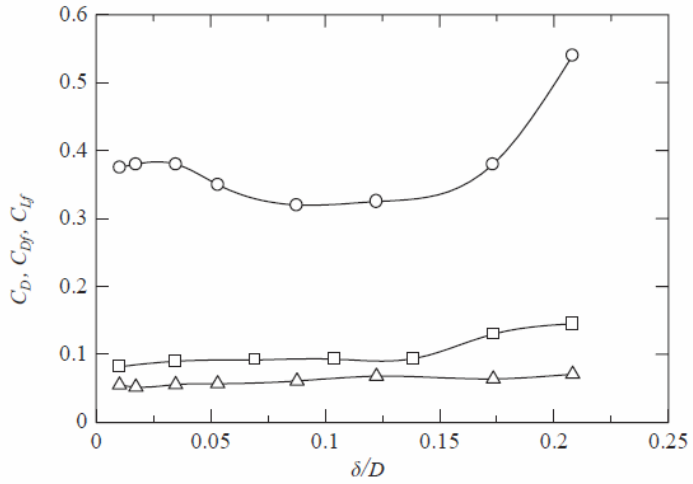

Figure 2.28: Force coefficient variations in function of the gap ratio. Reproduced from Alam[3].

In this thesis the only parameter of the tripping rods that will be varied is the angular positioning but it is necessary to know the effects of the gap ratio because small variations on the gap ratio are expected once the tripping rods used during the experiments are very long and have only to fixing points at their ends. By observing in Figure 2.28, it is possible to see that all the coefficients present an almost constant value when the gap ratio is around 0.1. To avoid that the small gap variation along the cylinder spanwise affects the measured data it is necessary to set the gap ratio as near as possible to 0.1.

2.5.4 Effects of Reynolds number

The Reynolds number is a non-dimensional value that relates the dynamic forces and the viscous forces. As discussed in sections 2.1 to 2.3, the flow characteristics around a bluff body suffer lots of modification in function of the Reynolds number. The same occurs in the case of the flow around a cylinder with tripping rods attached. The dependency of the Reynolds number can be verified in Figure 2.29, where the drag and lift coefficients and the Strouhal number are presented in function of the Reynolds number for a cylinder with and without tripping rods. The diameter ratio and the angular position of the tripping wires were fixed and only the Reynolds number was varied.

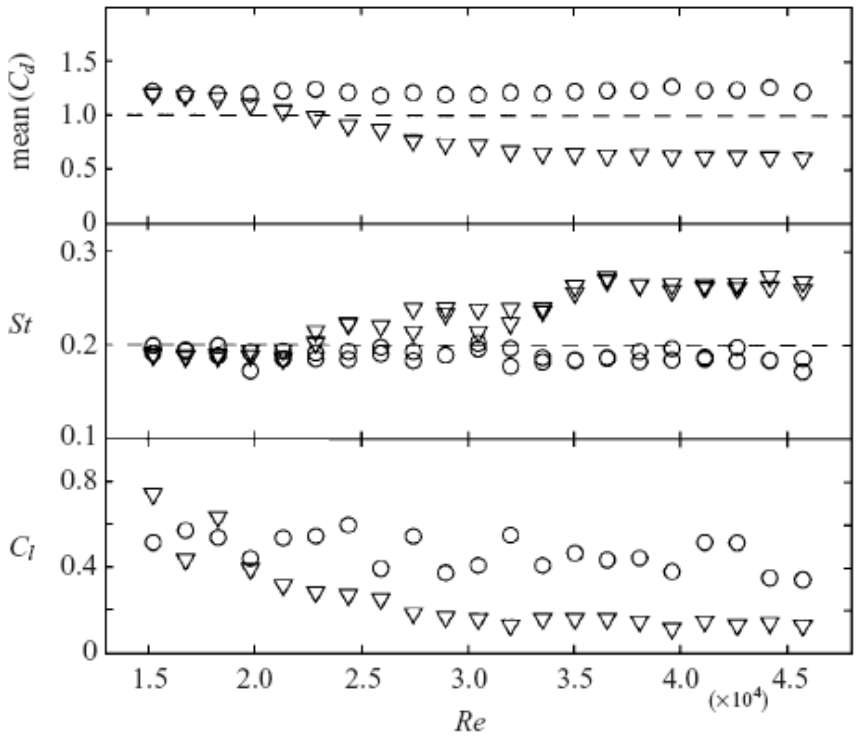

Figure 2.29: Force coefficients and strouhal number variation in function of the Reynolds number.

From this figure it is possible to notice that the presence of tripping wires reduced the lift and drag coefficients for Reynolds numbers higher than 2.0×10^4 in comparison to the smooth cylinder. The reduction is associated with the transition of the flow from pattern A to pattern B, which is also associated to the transition in the boundary layer from laminar to turbulent.

At Reynolds numbers lower than 2.0×10^4 the presence of the tripping rods is not able to induce the transition of the boundary layer because the size of the tripping rod is smaller than the boundary layer thickness. The thickness of the boundary layer decreases gradually with the increase of the Reynolds number. At Reynolds 2.0×10^4 the thickness of the boundary layer and the size of the tripping rod are getting closer. Above this value, the tripping rods size starts to overcome the thickness of the boundary layer causing the transition of the flow.

3 Experimental Setup

This chapter contains detailed information about the experiments conducted. Section 3.1 presents the experimental approach that was chosen to understand the changes that the attachment of tripping rods causes on fluid forces and VIV response amplitude in function of the angular positioning. Then, in section 3.2, a schematic view of the system configuration is presented with a discussion about the advantages and disadvantages of the current configuration. It will be followed by a description of all measurement equipment used, in section 3.3, and an explanation about the process to obtain the load cells calibration factor, in section 3.4. Finally, section 3.5 contains information about the adjustment of the system natural frequency and the process to measure the damping coefficient of the system.

3.1 Experimental approach

As mentioned in chapter one of this thesis, the objective of this study is to improve the efficiency of an energy harvesting system that uses VIV to convert the energy of the fluid flow into electricity. It will be made by attaching tripping rods to the cylinder of the harvesting system. There are no previous records on the literature about other works using tripping rods to increase VIV forces and amplitudes of oscillation because all previous works with tripping rods were conducted with the objective of reducing/suppressing VIV. Besides there was no interest on VIV amplification, the works of Nebres & Batil[2] and Alam et al.[3] showed evidences of an increase in lift and drag forces acting on the cylinder when placing tripping rods at angular positions between 50^o and 90^o.

The lack of information about the effects of tripping rods on the increase of VIV amplitudes led to a careful approach in the experiments, starting from the simplest case and then adding complexity to the system step by step. At the first moment, it was necessary to understand the phenomena and obtain a curve that describes the lift and drag coefficients in function of tripping rods angular positioning. The best method to obtain such data is with the most basic test: a stationary cylinder under influence of a constant flow. It was decided to investigate the entire range of angular positions, including regions behind the cylinder in which it was expected that the tripping rods had no influence on the flow. To cover the entire range, the tripping rods were positioned from 15^o to 165^o, with a 7.5^o interval.

The data provided from the non-oscillation experiments was necessary to define the tripping rods positions to run the second set of experiments, now with the cylinder in free-oscillation condition. Differently from the non-oscillation tests, where only one current speed was necessary, the free-oscillation tests requires running several different current speeds to cover the entire range of reduced velocities from 2 to 12 within VIV is expected to occur. To restrict the number of experiments only the two positions that presented high lift coefficients in non-oscillation experiments were chosen to conduct free-oscillation tests.

The free-oscillation tests were divided in two: with and without energy generation module attached. Following the principle of adding complexity step by step, the second set of experiments experiments were conducted without the generation system. In this configuration, the system presents low mass ratio and low mass-damping parameter. Systems with these characteristics are common in the literature, as presented in chapter 2, and were the best choice to start the free-oscillation experiments due to the large amount of data for comparisons. In this part, the objectives

were to compare the system response of the smooth cylinder case with other literature results to check anything out of normal and also to obtain the effects of the attachment of tripping rods in the amplitude of VIV response.

The third and last set of experiments is the most complex case. The attachment of the energy generation module to the system increased the mass ratio and the mass-damping parameter. To maintain the consistence of the work the same configurations of the case without generator were repeated. It is expected that the damping and extra mass resulted of the addition of the generator would change significantly the system behavior, thus this tests are the most important in order to obtain information about the changes in energy conversion efficiency that tripping rods could cause. In the next section, the system configuration will be described in details.

3.2 System configuration

The system for harvesting energy used in the experiments of this thesis had already been used before by Nishi et al.[5] The previous results and experience with the system is an important advantage and led to the decision of using the same system in the current work. Besides the advantage using the same system there is a disadvantage regarding the operational range. The diameter of the cylinder of the system is fixed, d = 25mm, and the operational speed range of the towing carriage is from 0.01 to 0.8 m/s. As presented in chapter two of this thesis, the VIV phenomenon is expected to occur between reduced velocities 2 and 12. Therefore, the system stiffness was adjusted to cover this entire range of reduced velocities and respect the towing carriage maximum speed, as will be presented in section 3.5. The restrictions of the system and the

towing carriage resulted in Reynolds number ranging from 3.45×10^3 to 2.04×10^4, which do not corresponds region of maximum lift coefficients, as presented in Figure 3.1.

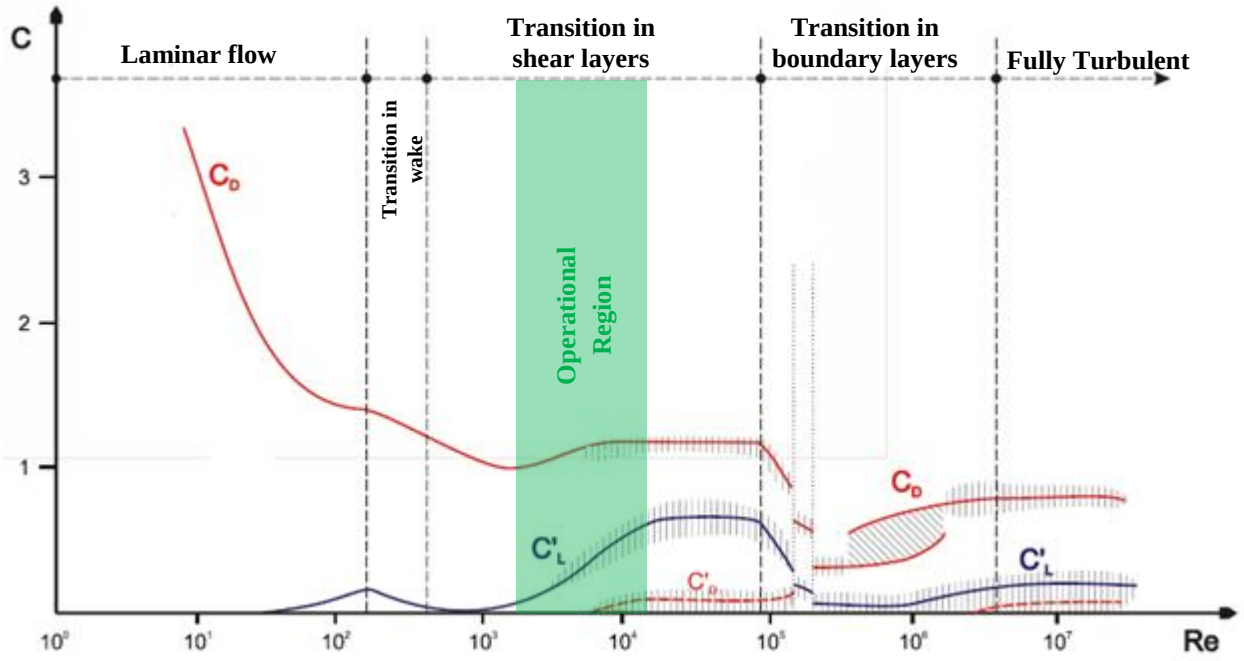

Figure 3.1: Operational region of the experiments. Adapted from Zdravkovich[17].

The system arrangement is presented in Figure 3.2. The system was built of aluminum bars connected by bearings. Two towing directions are shown and are related to the angle of tripping rods tested. In a towing tank it is usually necessary to go in one direction and return to the start position before doing the next test run. As the system tested was symmetric, except by tripping rods positioning, it was possible to make measurements when running in both directions, saving a lot of time during the experiments. When going forward, the tripping rods were positioned from 15^o to 90^o and, complementary, when going backwards, from 90^o to 165^o.

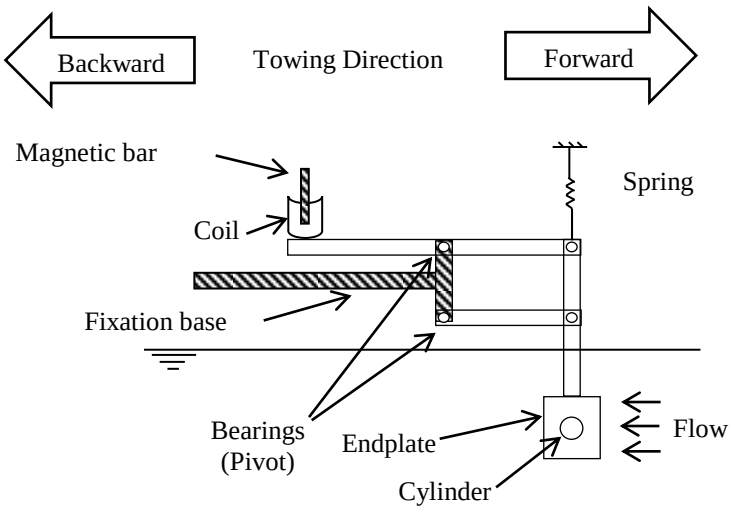

Figure 3.2: Schematic view of system configuration. Dashed shapes represent non-moving parts of the system.

Figure 3.3 contains a simplification of the system as a rigid bar. The positions if the pivot point, the cylinder and the coil position are shown. The distance of the cylinder to the pivot point is r_2=0.5 and the distance from the coil to the pivot point r_3 can be varied. A rapid observation of Figure 3.2 indicates that because of the system geometry the movement of the cylinder is not perfectly translational in the vertical direction. In fact, the geometry results in a small horizontal movement. As the maximum expected amplitude of the oscillation is 0.025m and the distance between the cylinder and the pivot is r_2 = 0.5m, the maximum displacement of the cylinder in the horizontal direction will be 6.25×10^{-4} m, much smaller than the vertical. Due this large difference, the cylinder motion will be approximated as a pure translational motion in the vertical direction.

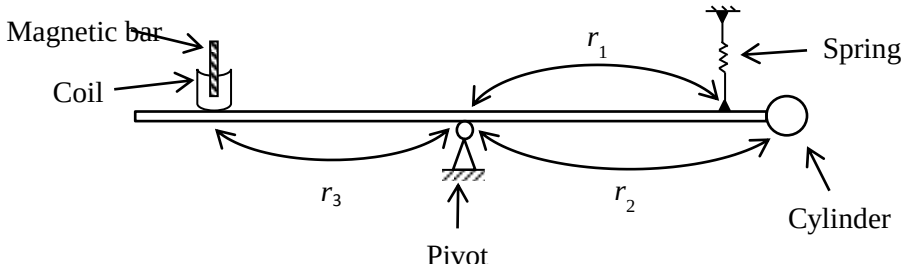

Figure 3.3: Simplified system representation as a rigid bar.

As presented in chapter 2, the translational displacement of the cylinder is transmitted by the leverage system to a translational displacement of the magnet bar, which moves inside the coil to generate electricity. The distance r_3 is adjustable and defines the ratio between the cylinder and magnet bar displacements. The adjustment of this distance is used to set up the system to generate the maximum voltage, as presented in Eq. 2.11.

The cylinder is supported on both ends by two bi-axial load cells which are responsible for measuring the drag and lift forces acting on it. The load cells will be described with more detail in the next section when the measurement equipment is presented. The load cells are connected to endplates, shown in Figure 3.4, which guarantees the bi-dimensionality of the flow around the cylinder, avoiding end effects.

Another role of the endplate is to support the tripping rods at pre-determined angular positions around the cylinder and make sure that they do not touch the cylinder surface and do not cause interferences on the forces measured. Endplates are shown in Figure 3.4. Tripping rods positioning holes are restricted to angles lower than 90^o and two pairs of endplates were necessary to obtain the desired 7.5^o interval because it was impossible to arrange all holes in only one. Each

endplate had holes with 15^o interval. One of the pairs covered the angles from 15^o to 90^o and the other pair covered angles from 22.5^o to 82.5^o.

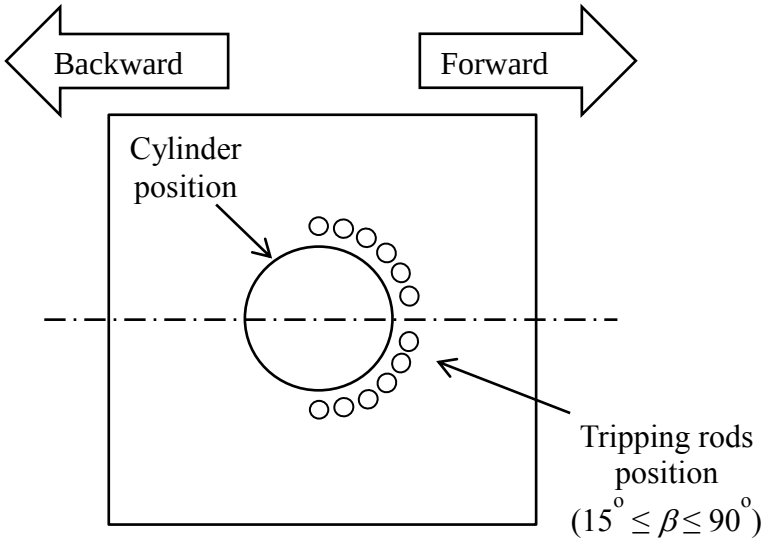

Figure 3.4: Endplate with holes for tripping rods positioning.

A photo of the cylinder and tripping wires connected to the endplates is presented in Figure 3.5.

Figure 3.5: Cylinder and tripping wires connected to the endplate.

System stiffness was given by springs attached at a distance r_1 from the pivot. The adjustment of the stiffness is important to setup the system natural frequency approximately the same as the vortex shedding frequency, main requirement to obtain VIV response. More details about the adjustment of system natural frequency are provided in section 3.4 of this thesis.

The energy generator is composed by a magnetic bar that moves inside a coil. The magnet, shown on Figure 3.6, is cylindrical and is 100mm long with a 25mm diameter. The magnetic bar charge is 6.38×10^{-4} Wb. The coil is shown in Figure 3.7. It was built using magnetic wire and a reel. The magnet wire was wrapped around the reel until reach 2000 turns, resulting in a 42Ω resistance.

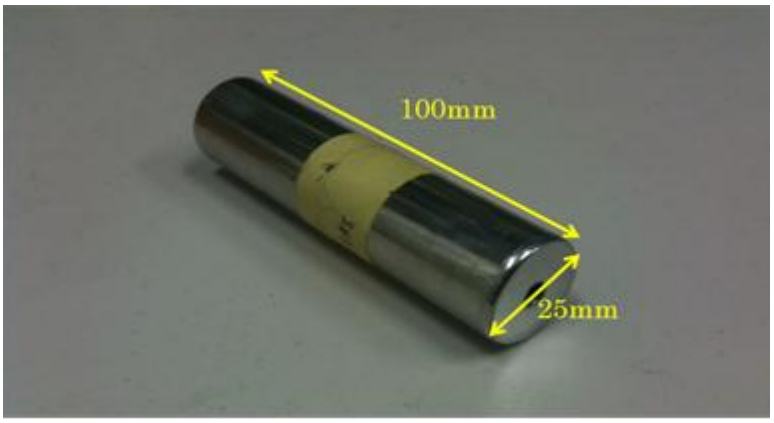

Figure 3.6: Magnet bar

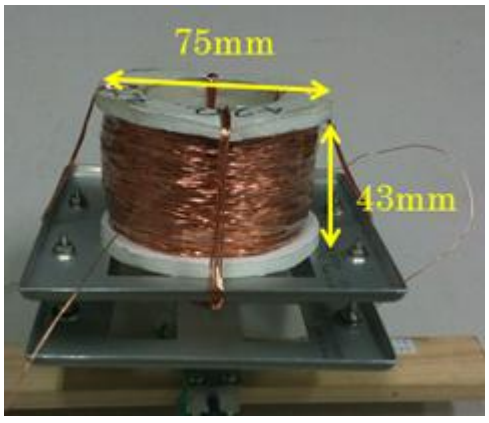

Figure 3.7: Coil construction.

The system damping changes according to the load attached to the generator because the reaction forces increase with the increase of the output current required by the load. To represent the load of the system a 100Ω resistor was attached to the coil. The power generated will be calculated as the power dissipated by the resistor.

3.3 Measurement Equipment

Four different measurements were made during the experiments: cylinder vertical displacement, drag and lift forces, flow speed (which is equal to carriage speed) and generated voltage. All the measurements were recorded by a digital data logger connected to a personnel computer.

The vertical displacement of the cylinder was measured with a laser displacement measurement positioned over the cylinder, as shown in Figure 3.8. This system is manufactured by Keyence and is has a maximum amplitude range of 0.1m. Its output is given in volts and the calibration factor is 0.01 m/volt.

The vertical displacement was measured to calculate the non-dimensional amplitude of oscillation of the cylinder presented in Table 2.2. The displacement of the cylinder is also necessary to calculate the cylinder vertical velocity and acceleration. The acceleration is important to calculate the inertial force of the cylinder to subtract it from the force measured by the load cells and obtain the lift force acting on the cylinder in the free oscillation tests.

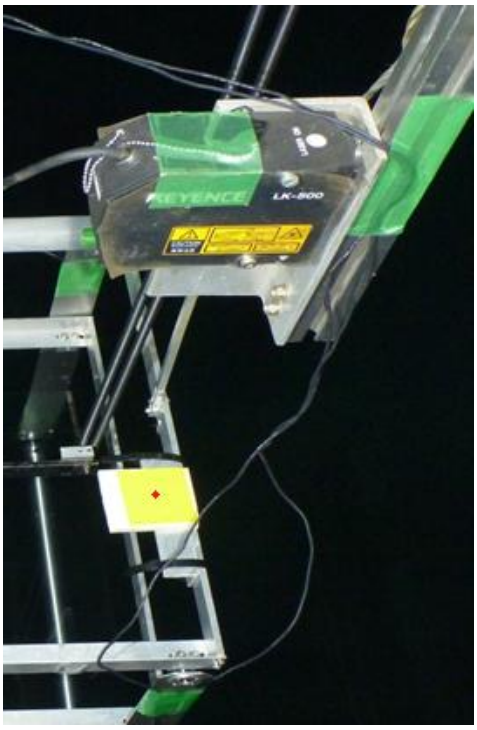

Figure 3.8: Laser displacement measurement device positioned over the cylinder.

To measure the forces acting on the cylinder a pair of load cells was attached to both ends of it, as presented in Figure 3.9: Cylinder assembled with the two load cells attached on both ends.. The load cells used are capable of measuring the forces in two directions and their measuring axes were positioned to measure the lift and drag forces. A schematic view of the load cell configuration and its positioning inside the cylinder is presented in Figure 3.10. The load cells are composed by two sets of strain gages, each one responsible to the measurement in one of the directions. The force is applied on the free end of the load cell by the cylinder and the moment caused by the force causes small deformations which cause a variation on the resistance of the strain gauges and, consequently, a voltage variation which is used to measure the force. The voltage variation is directly proportional to the force applied and the proportionality factor is obtained through a calibration process, which is presented in the next section of this work.

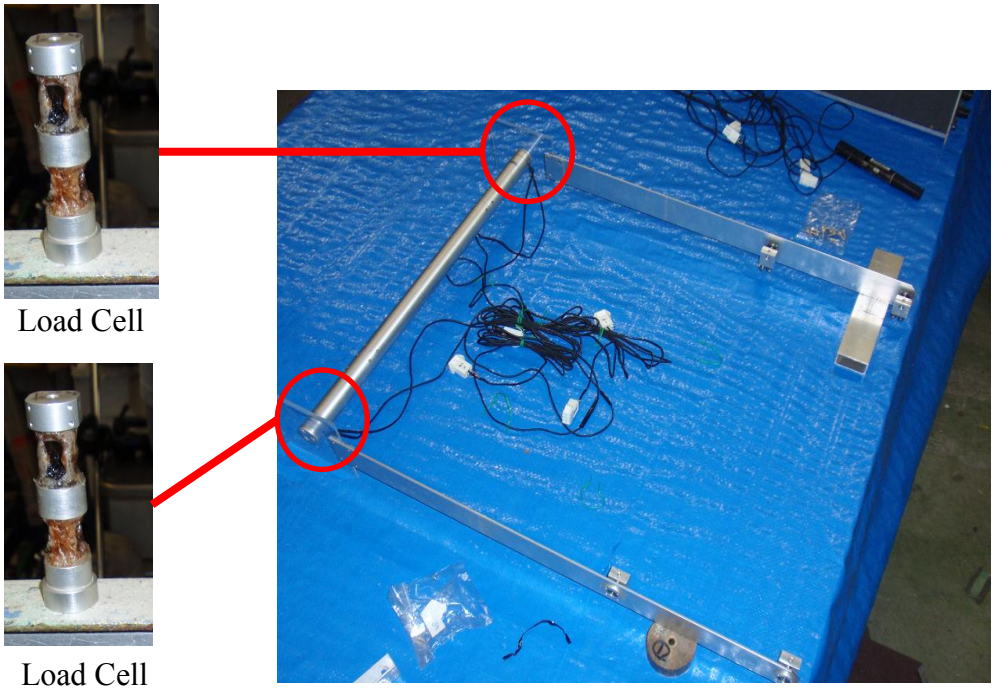

Figure 3.9: Cylinder assembled with the two load cells attached on both ends.

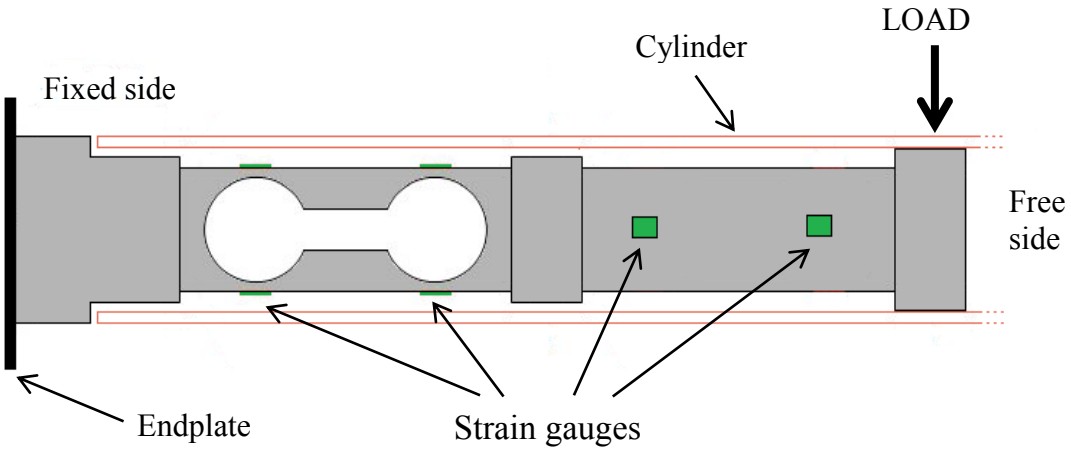

Figure 3.10: Load cell schematic view.

The flow speed is obtained through the measurement of the towing carriage speed. This measurement is made with the use of a rotatory encoder placed on the rail and a frequency to voltage converter, which converts the frequency of rotation from the encoder to an output voltage.

The equipment is shown in Figure 3.11. The calibration factor that relates the carriage speed to the output voltage is $0.1488\frac{m/s}{Volt}$.

Figure 3.11: Rotatory encoder and frequency/voltage converter used to measure the towing carriage speed.

The voltage generated was measured by connecting the data logger to the 100Ω resistor, as shown in

Figure 3.12.

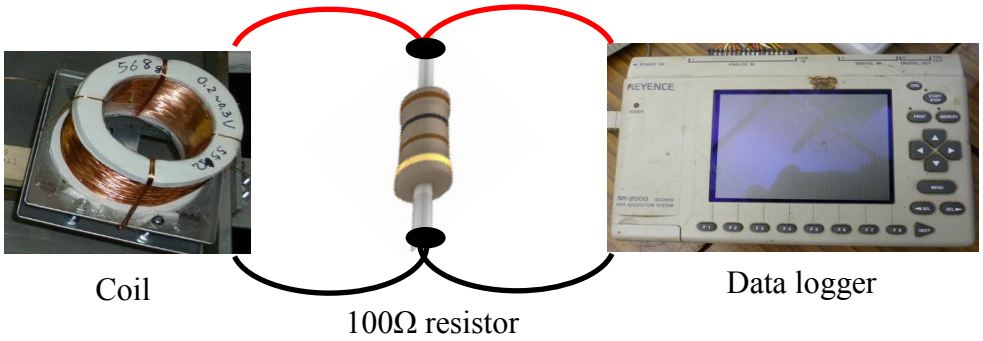

Figure 3.12: Measurement of generated voltage.

A summary of the measurement equipment and how they are connected is shown in Figure 3.13.

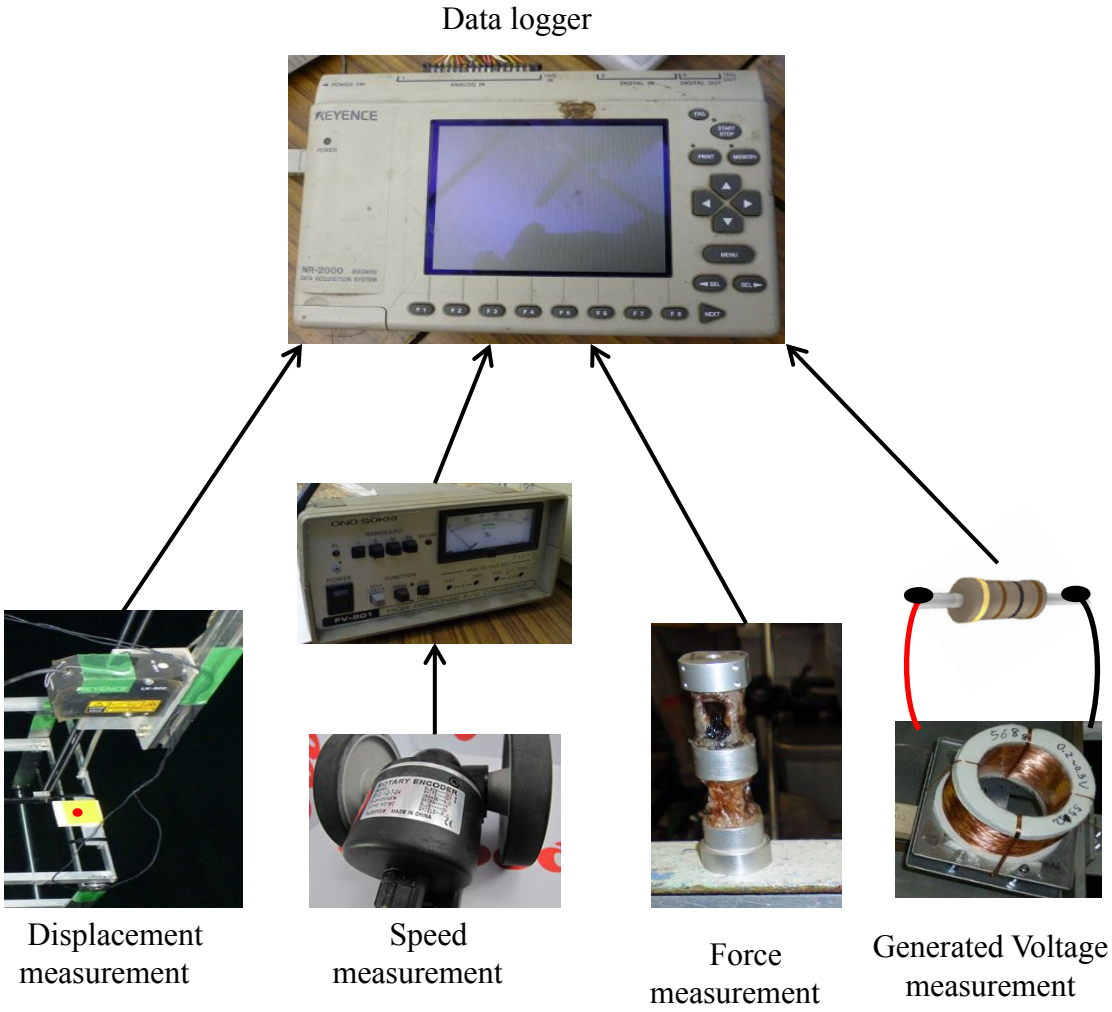

Figure 3.13: Summary of data measurement process.

3.4 Load cell calibration

The objective of load cell calibration is to find the calibration factor that relates the forces applied on the free side of the load cell and the resulting voltage measured. It is necessary to carry the calibration during the preparation of experiments, even if a calibration already was made on a previous experiment because the calibration factor can have small changes due external conditions, like ambient temperature, humidity or even small differences between the amplifiers that are attached to the load cells.

The process of calibration is simple, but needs to be carried accurately. It consists of the addition of known weights, as shown in Figure 3.14, to the free side of the load cell and then measure the voltage output to create a curve of weight versus voltage. The first step of the calibration is to fix the load cell and make sure that the axis that is going to be calibrated is positioned at the vertical direction. Figure 3.15 shows an example of the fixation of a load cell with two axes in order to calibrate the negative direction of the X axis. It must be repeated for all directions.

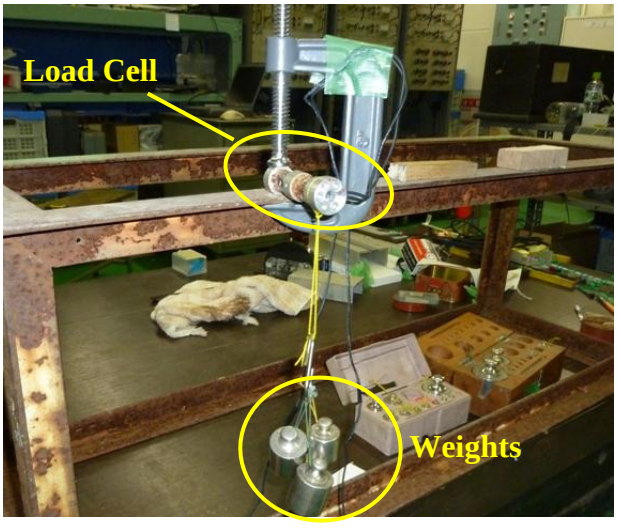

Figure 3.14: Load cell calibration by the addition of known weights.

As mentioned before, the calibrations must be done before start each set of experiments. This work was divided in three sets of experiments as described in section 3.1, but only two calibrations were necessary because the first two experiments, stationary and free oscillating without generator, were carried out consecutively, without disassembling the experimental setup. The calibration was carried out with weights ranging from 0 to 1000g, with a 100g increment. The results of both calibrations are shown. The calibration factors are highlighted in red on the figures and its unit is grams/Volt.

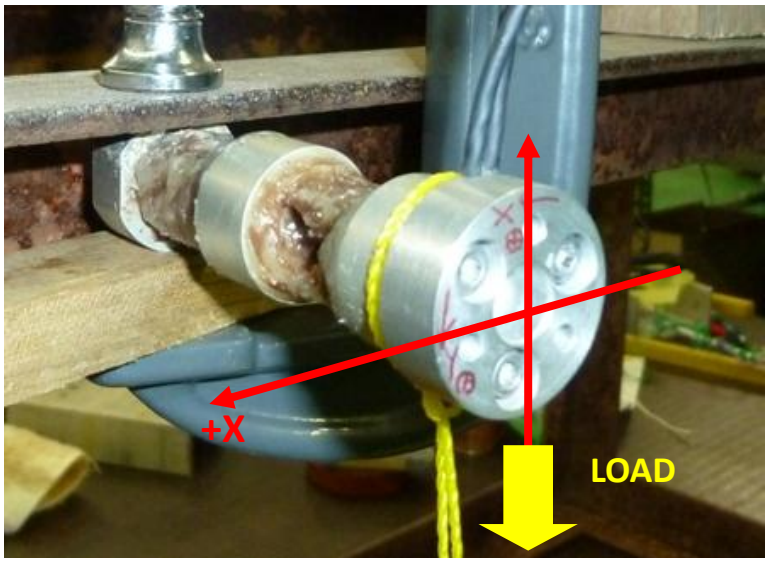

Figure 3.15: Fixation of load cell to calibrate the negative direction of X axis.

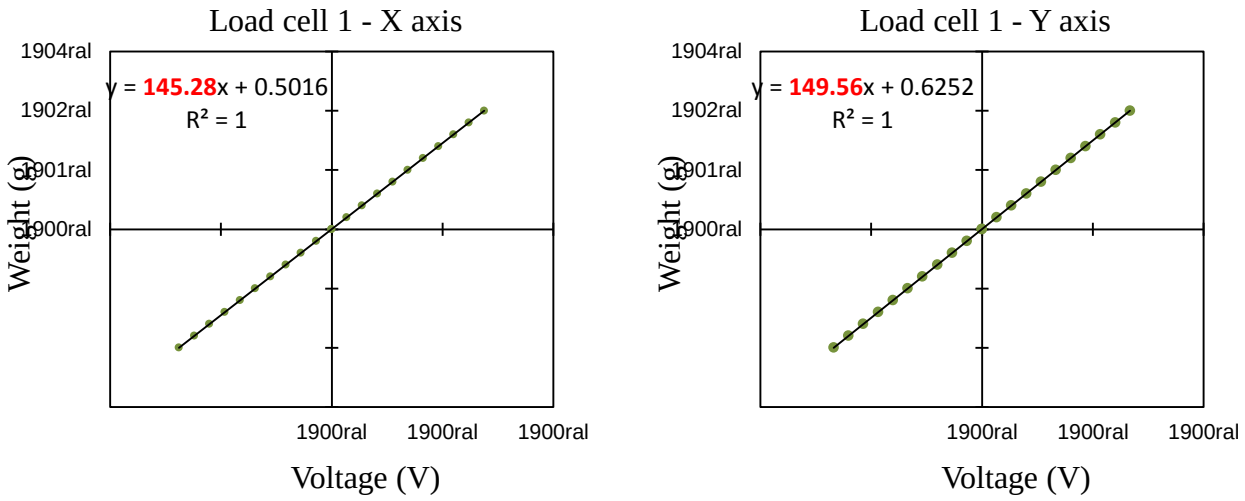

Figure 3.16: Calibration of load cell number 1 for stationary and free oscillating cylinder without generator experiments.

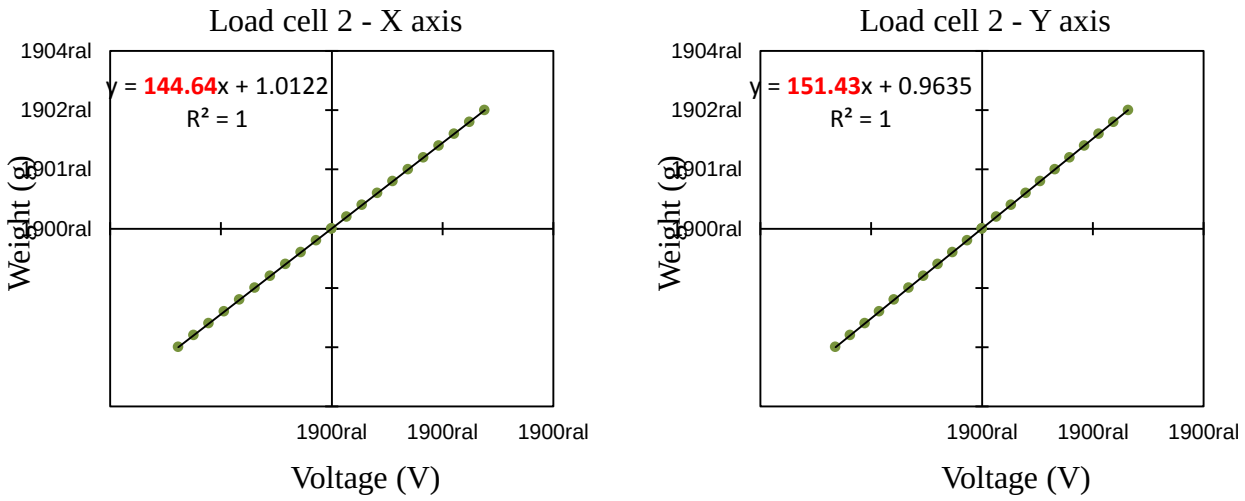

Figure 3.17: Calibration of load cell number 2 for stationary and free oscillating cylinder without generator experiments.

A summary of the calibration factors for the stationary and free oscillating cylinder without generator experiments is shown in Table 3.1.

Table 3.1: Summary of load cell calibration factors for stationary and free oscillating cylinder without generator experiments

Calibration factors for stationary and free oscillating cylinder without generator experiments		
Load cell number	Direction	Calibration Factor (gf/V)
1	X	145.28
	Y	149.56
2	X	144.64
	Y	151.43

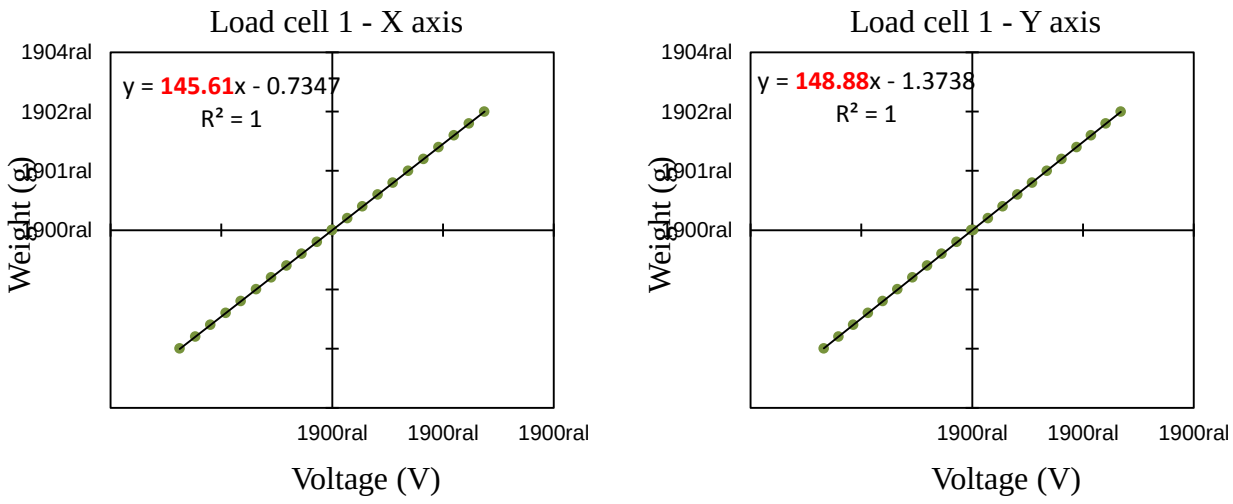

Figure 3.18: Calibration of load cell number 1 for free oscillating cylinder with generator experiments.

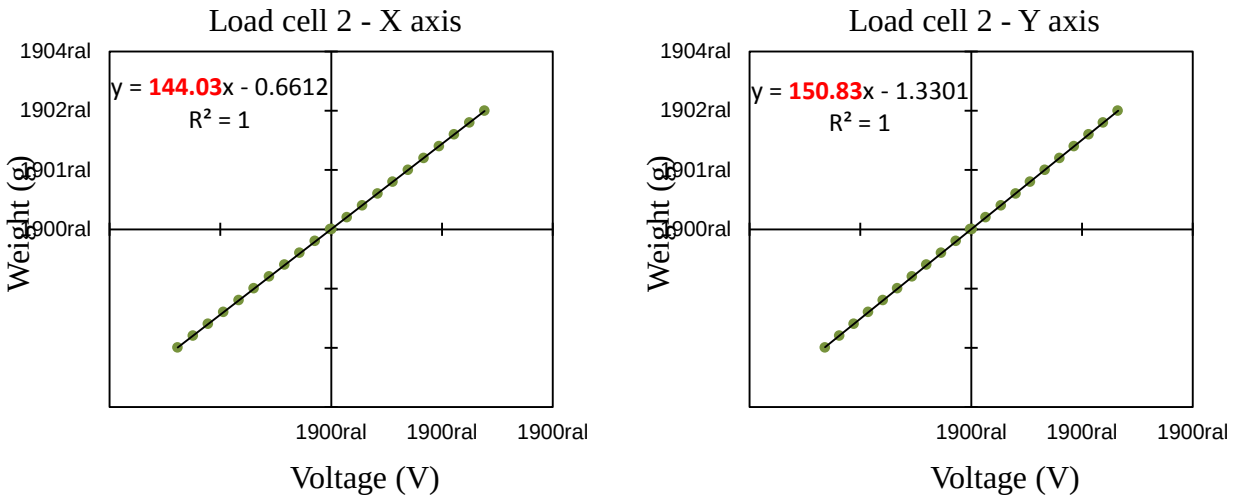

Figure 3.19: Calibration of load cell number 2 for free oscillating cylinder with generator experiments.

A summary of the calibration factors for the stationary and free oscillating cylinder without generator experiments is shown in Table 3.2.

Table 3.2: Summary of load cell calibration factors for free oscillating cylinder with generator experiments

Calibration factors for stationary and free oscillating cylinder without generator experiments		
Load cell number	Direction	Calibration Factor (gf/V)
1	X	145.61
	Y	148.88
2	X	144.03
	Y	150.83

3.5 Adjustment of system natural frequency and damping ratio measurement

VIV occurs when the natural frequency of the system and the vortex shedding frequency are approximately the same. The vortex shedding frequency is a function of the cylinder diameter, flow speed and strouhal number, as shown in equation 2.1. As the strouhal number is well known for circular cylinder the shedding frequency is easily calculated.

Once known the shedding frequency inside the desire Reynolds number range it is necessary to adjust the system natural frequency as near as possible to it. The experimental apparatus used has a very complex geometry, with several types of materials mixed, making very difficult to determine the system inertia theoretically. The best way to determine it is to execute a free decay experiment with springs of known stiffness.

The free decay experiment consists of moving the cylinder away from its equilibrium position and then releasing it to measure its motion. An example of the measured data in one free decay experiment is shown in Figure 3.20. From this data is possible to obtain information about oscillating frequency, which is the natural frequency of the system, and also the damping ratio.

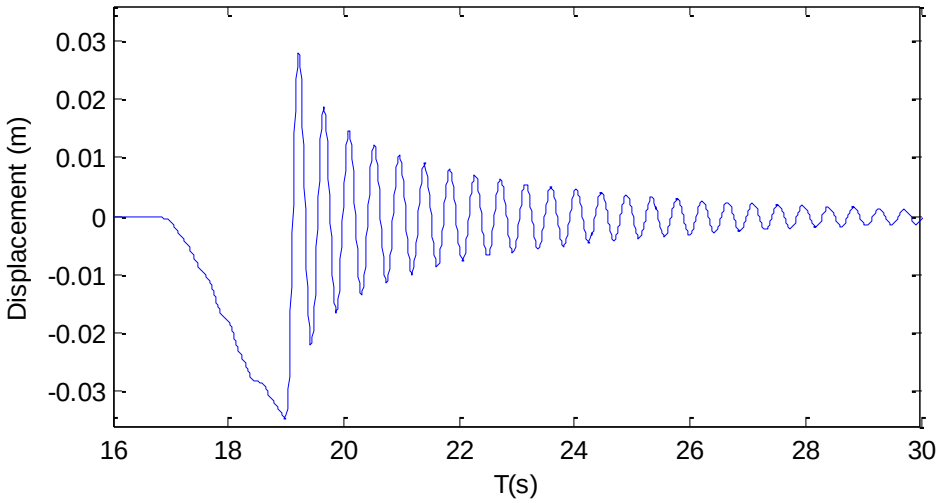

Figure 3.20: Example of free decay test.

The frequency of oscillation (f_{osc}) is calculated from the periods between peaks. A peak detection function is used to find the peaks of a selected part of the signal, as shown in Figure 3.21 and then it is only necessary to calculate the average difference of time between consecutive peaks.

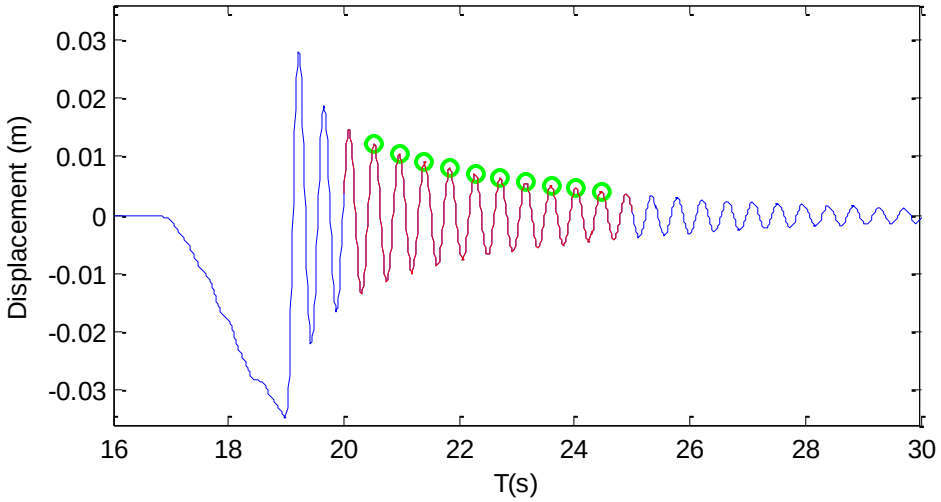

Figure 3.21: Peak detection on the free decay test.

The system inertia can be calculated as:

$$I = \frac{kr_1^2}{4\pi^2 {f_{osc}}^2} \qquad 3.1$$

Once known the Inertia, it is possible to calculate the spring stiffness necessary to achieve a natural frequency equal to the vortex shedding frequency.

$$k = \frac{4\pi^2 I {f_n}^2}{r_1^2} \qquad 3.2$$

where $f_s = f_n$.

Other important information that can be obtained from the free decay test is the system damping ratio. On the current study it was possible to consider a linear damping ratio because it had a good agreement at the amplitude range which is expected. The damping ratio can be obtained by adjusting an exponential function to the peaks, as shown in Figure 3.22. The exponential function is written as:

$$Z(t) = Z_o e^{-\zeta 2\pi f_n t} \qquad 3.3$$

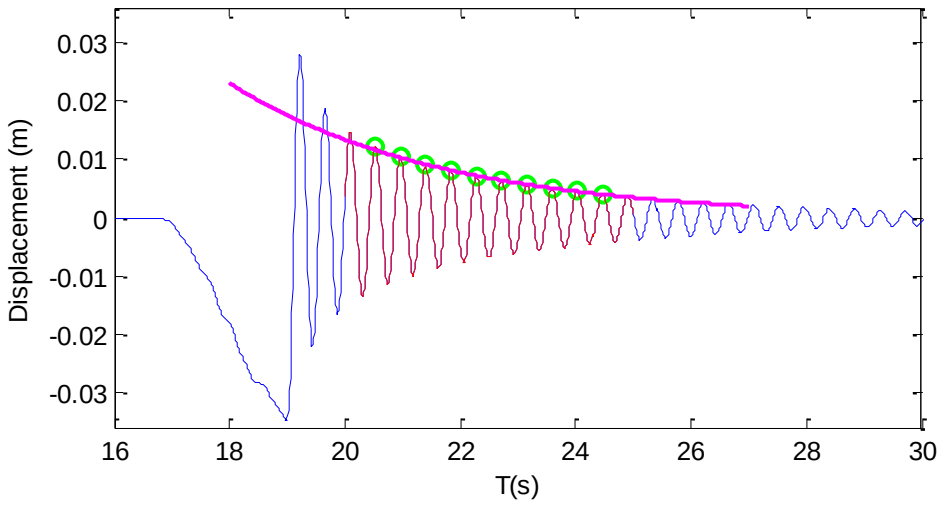

Figure 3.22: Adjustment of exponential curve to obtain the damping ratio.

The damping ratio was calculated using this method for each system configuration tested and its value is shown in the results section.

4 Data processing

This section of the thesis will describe how the measured data was processed. The measured data was:

- Drag and lift forces acting on each end of the cylinder.
- Towing carriage speed, considered equal to the flow speed.
- Cylinder vertical displacement.
- Voltage on the resistor.

Each type of data requires a specific analysis to extract the useful information from them and will be described in this section. However, there are some steps that are common to all the measurements, as zero adjustment, signal filtering and selection of region of analysis. These common steps will be presented now.

The first step of data analysis is the adjustment of the zero of the signal. This step is important because during the experiments it is common that the signals suffer a gradual shift because of small changes in the experiment conditions, like temperature, humidity and even alterations inherent to the signal amplifiers components condition. Despite the shift in the signal, usually the calibration factors do not change, the only change is in the initial value of the voltage.

To adjust the zero it is necessary to measure the initial conditions before each test run. The initial conditions are measured with all the system stopped. It is also necessary to assure that nobody is moving in the towing carriage and there are no waves in the water. After the conditions for measuring the zero is verified, the data starts to be acquired. At the current experiment it was assumed that a minimum of 5 seconds should be necessary for each run to measure the initial conditions. Ended the acquisition time, the carriage is started and the test run is conducted. Figure 4.1 shows the selected regions of the signal within the initial conditions are obtained.

Once selected the signal region the mean value of the selection is calculated and then subtracted from all the signal, as represented by the green line in Figure 4.1.

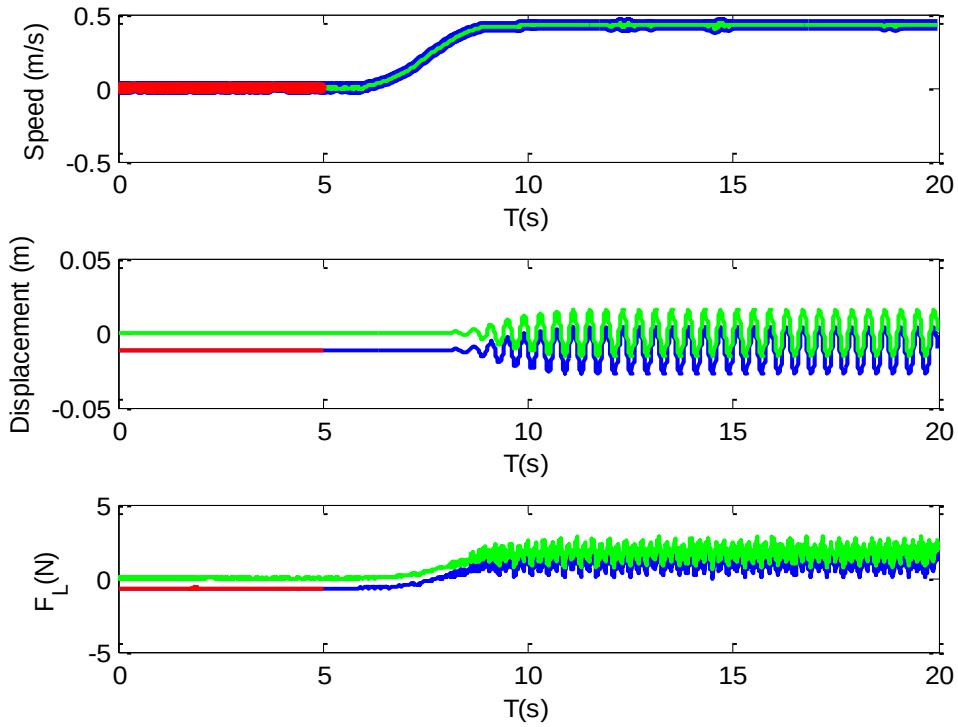

Figure 4.1: Zero region selection and signal adjustment. Blue: original signal; Red: Zero region; Green: Adjusted signal.

The second step of the data analysis is the signal filtering to clean the signal from undesired noise. The signal filtering was made using a low-pass digital filter created in Matlab. The low-pass filter was set-up to cut frequencies greater than 10Hz, about 4 times the system natural frequency. Figure 4.2 shows the signal before and after filtering and Figure 4.3 show the zoom of the drag force for a better observation.

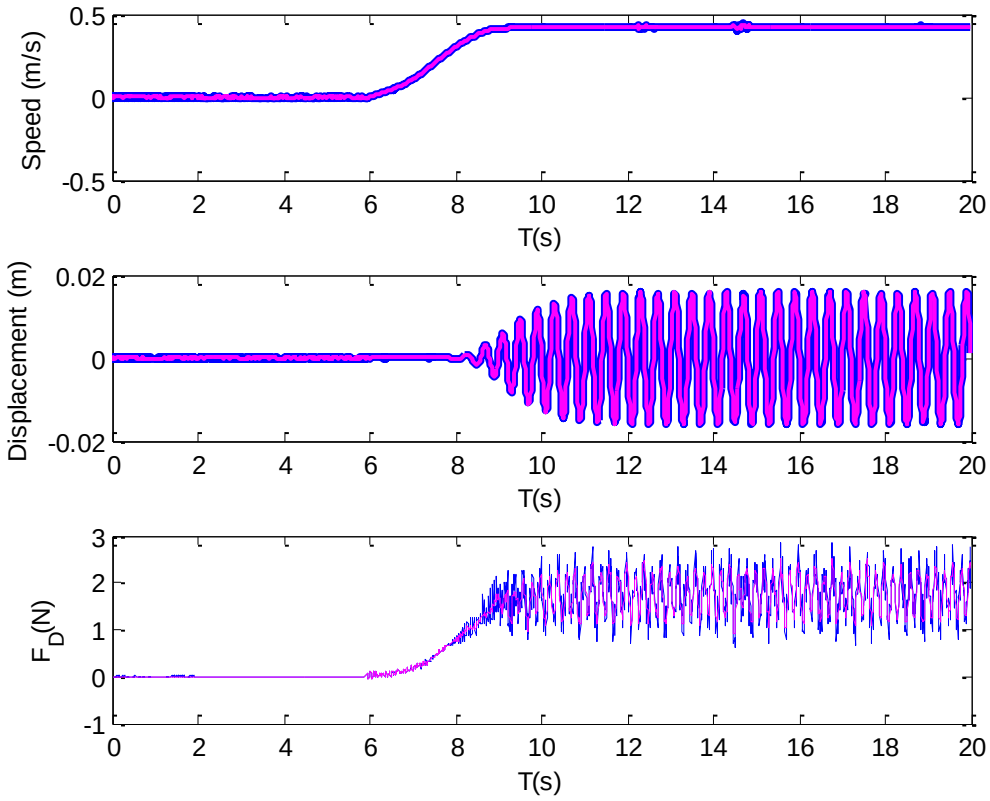

Figure 4.2: Signal filtering. Blue: Zero adjusted signal; magenta: Filtered signal.

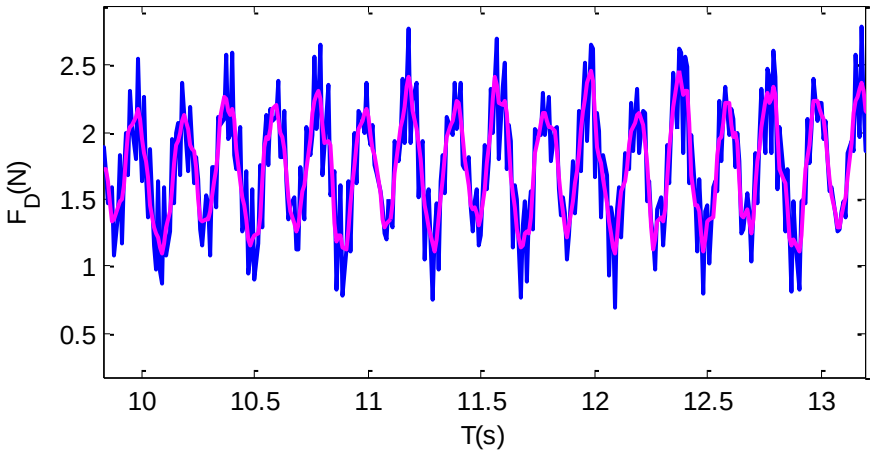

Figure 4.3: Zoom view of the Drag force signal to see the signal filtering result. Blue: Zero adjusted signal; magenta: Filtered signal.

The noise present in the signal may be result of harmonics of the frequency of the signal or from another external source, like the electric power frequency that is used to turn on the measurement equipment. To try to verify the origin of the noise the Fast Fourier Transform (FFT) of the unfiltered signal was calculated. Figure 4.4 shows the FFT of the drag force that was is calculated to check the frequencies present in the signal. The maximum amplitude is obtained when the frequency is 5.0Hz. This main frequency present in the drag force signal is the double of the cylinder oscillation frequency, which also is present in the signal as a harmonic of the response. As discussed in chapter 2 of this thesis, the frequency of oscillation of the drag force is the double of the oscillating frequency because in one period of cylinder oscillation there are two vortexes are formed in each side of the cylinder.

There are other two large peaks present in the example FFT, at 33.4 and 35.9 Hz. It was possible to identify the source of this noise by analyzing the vortex shedding frequency that is expected to occur in the tripping rods. The tripping rods diameter is 3 mm, the flow speed is 0.48 m/s and the strouhal number can be approximated as 0.21. By substituting these values in equation X.X, we obtain an expected vortex shedding frequency equal to 33.6 Hz, a value very near to the frequency of the noises.

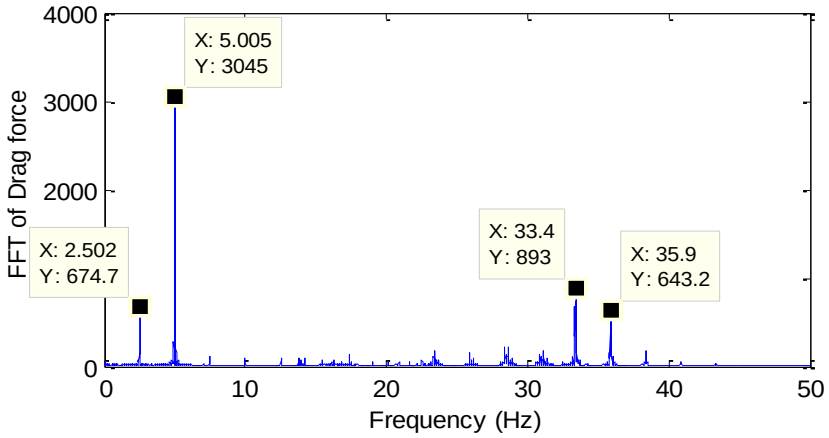

Figure 4.4: Fast Fourier Transform of the drag force signal.

The third and final step common to all the signals is the selection of the region of interest for analysis. This selection is made manually from the observation of the signal behavior. It is necessary to cut off the transient response caused by the acceleration and deceleration of the towing carriage and select only the region where the system achieves a regime in the response. Figure 4.5 and Figure 4.6 shows two examples of signal selection region. In Figure 4.5 the transition region is very short and the response achieves a regime soon after the speed stabilizes. Differently, in Figure 4.6, it is possible to notice a longer transient region from around 10 to 19 seconds of acquisition.

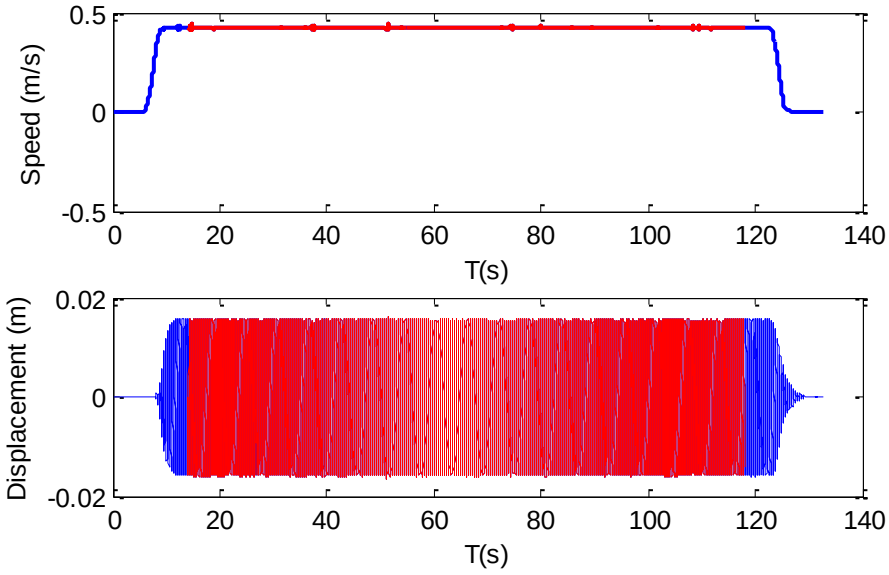

Figure 4.5: Example of the selection of region for analysis of a signal with short transient. Blue: filtered signal; Red: selected region for analysis.

All the signals are cut with the same starting and ending times. After the selection of the region of analysis each signal is submitted to a specific treatment according to the data it is necessary to extract from it. This treatment can be conducted in the time domain or in the frequency domain through the FFT of the signal. In the next section all the data extracted from the signals will be described.

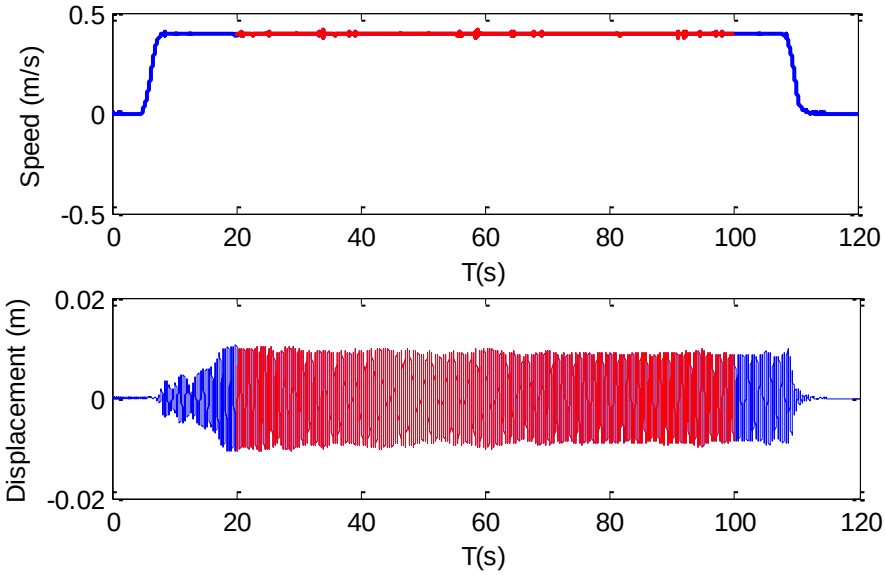

Figure 4.6: Example of the selection of region for analysis of a signal with a long initial transient. Blue: filtered signal; Red: selected region for analysis.

4.1 Time domain Analysis

4.1.1 Flow speed

The flow speed is measured through the measurement of the towing carriage speed. The behavior of the carriage speed can be observed in the top graph of Figure 4.6. The carriage speed is calculated as the mean value of the region of analysis.

4.1.2 Drag force

The drag force can be divided in two: a steady force and an oscillatory force. When the carriage starts to move, the drag force increases gradually until reach a mean value, called mean drag force. After the carriage speed stabilizes, the drag force starts do fluctuate around the mean value as a result of the vortex shedding, as shown in Figure 4.7. This parcel is called fluctuating

drag force. The frequency of the fluctuations of the drag force is the double of the frequency of oscillation of the cylinder.

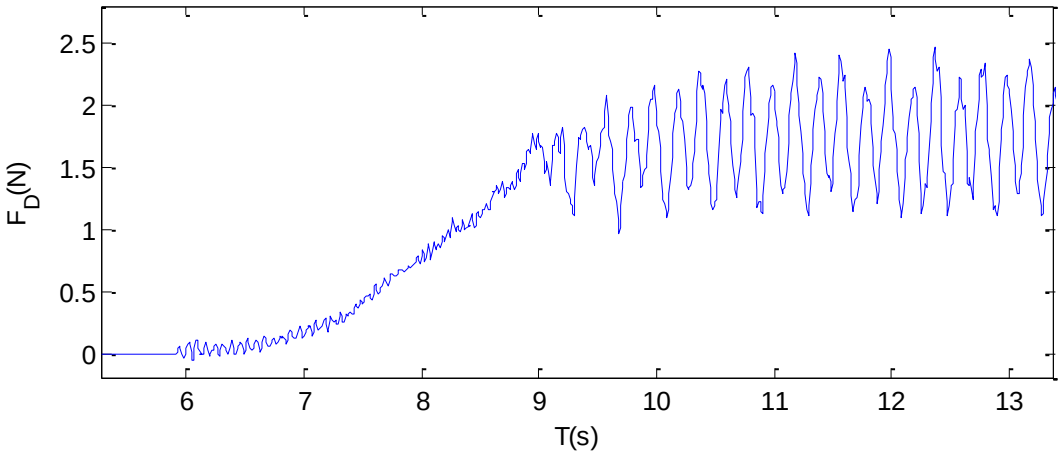

Figure 4.7: Drag force signal showing the fluctuations around a mean value.

In this thesis it will be considered only the mean drag force, which is calculated as the mean value of the selected region of the signal for analysis. To make comparison between different experiments it is common on VIV analysis to consider a non-dimensional coefficient, which is called drag coefficient (C_D). The drag coefficient is calculated as:

$$C_D = \frac{2F_{D\,mean}}{\rho D L v^2} \qquad 4.1$$

4.1.3 Lift Force

The lift force is an oscillatory force which is originated from the vortex shedding process. This force oscillates around zero, as shown in Figure X.X, and the most common approach to analyze the lift force is to calculate its root mean square (RMS) value. The root mean square of the

signal is calculated as:

$$F_{L\,rms} = \sqrt{\frac{1}{n}\sum_{i=1}^{n} F_{Li}} \qquad 4.2$$

The same way as presented for on last section, it is common to calculate the non-dimensional coefficient, called lift coefficient to make possible the comparison between experiments. The lift coefficient is calculated as:

$$C_L = \frac{2F_{L\,rms}}{\rho D L v^2} \qquad 4.3$$

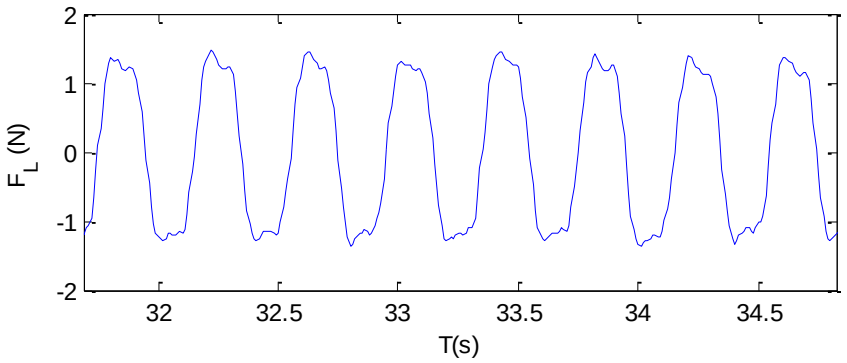

Figure 4.8: Example of lift force signal.

4.1.4 Amplitude of oscillation of the cylinder

There are two possibilities to present the amplitude of oscillation of the cylinder. It is possible to calculate the root mean square value of the signal or to calculate the average of the maximum amplitudes. Both ways are commonly used in the presentation of VIV results and the choice is made by the researcher. In this work the amplitude that will be presented uses the calculation of the average of the maximum amplitudes because most of the references presented

during this thesis presented their results in that way.

Then, a peak detection routine was written in Matlab® to calculate the average of the maximum amplitudes. Figure 4.9 shows an example of the amplitude of the oscillation of the cylinder with the peaks detected by the routine. Once the peaks are all found, the amplitude of oscillation is calculated as:

$$A_{\max} = \frac{1}{n}\sum_{i=1}^{n}\left|A_{peaks_n}\right| \qquad 4.4$$

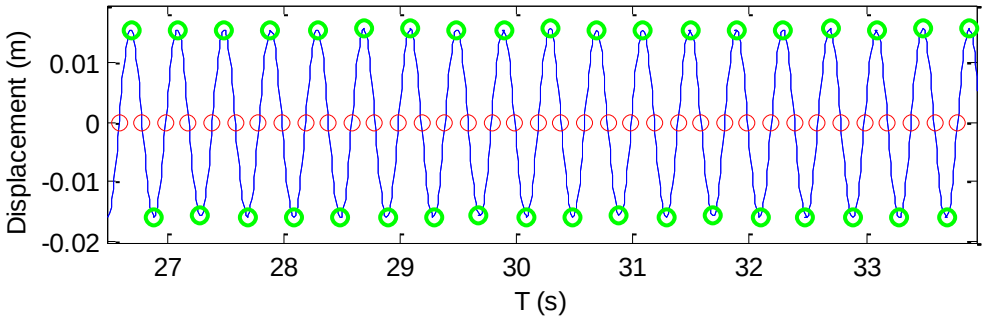

Figure 4.9: Signal showing the amplitude of oscillation of the cylinder and the peaks selected for analysis.

One more time, it is usual to calculate use a non-dimensional value to present the results. The non-dimensional value is calculated by dividing the amplitude by the diameter of the cylinder, as:

$$A = \frac{A_{\max}}{D} \qquad 4.5$$

4.1.5 Conversion Efficiency

The energy conversion efficiency is calculated as the ratio of the power dissipated on the resistor and the power of the fluid flow acting on the cylinder. The electric power in the resistor can be calculated as:

$$P = \frac{1}{T_E - T_S}\int_{T_E}^{T_S} \frac{E^2}{R} dt \qquad 4.6$$

And the power of the fluid flow can be calculated as:

$$W_{water} = 0.5\rho V^3 DL \qquad 4.7$$

Thus, the conversion efficiency is:

$$\eta = \frac{P}{W_{water}} = \frac{\frac{1}{T_E - T_S}\int_{T_E}^{T_S} \frac{E^2}{R} dt}{0.5\rho V^3 DL} \qquad 4.8$$

4.2 Frequency domain Analysis

The frequency domain analysis is useful to obtain certain properties of the signals, as the frequencies and phases of oscillation. In this thesis, the time domain analysis will be applied to obtain the frequency of the cylinder oscillation and the frequencies of the drag and lift forces. Special attention must be paid to the frequency of lift force, which is the same frequency of vortex shedding. The value of the vortex shedding frequency is important to calculate the strouhal number, which can suffer variations caused by the presence of tripping rods.

The phase of oscillation is another important data that is necessary to obtain, specially the phase of the lift force and the cylinder vertical position. The relative phase between the lift force and the cylinder vertical position can give a lot of information about the system behavior. In this thesis, the relative phase (φ_F) between these two signals will be calculated as:

$$\varphi_F = \varphi_L - \varphi_Z \qquad 4.9$$

Where φ_Z and φ_L denote the vertical posision and lift force phases, respectively. This definition of φ_F means that the lift force excites the vibration when φ_F ranges from 0 to 180^o, while the lift force decays the vibration when φ_F ranges from -180^o to 0^o. It is important to notice that if the phase difference is 90^o, the force is working in a pure excitation mode, what mean that as near the difference of phase is to 90^o, larger will be the amplitude of the vertical oscillation of the cylinder. The understanding of this definition will be useful during the data analysis section, that will be presented next in this thesis.

5 Results and Discussion

The results and the discussion of the results presented in this chapter of the thesis will be divided in three sections, according to the experiment characteristics. In section 5.1 will be presented the hydrodynamic coefficients and strouhal number obtained during the non-oscillating cylinder experiments, which is the most simple case studied. In section 5.2 will be presented the results obtained from the free-oscillating cylinder without the electricity generator connected and, finally, this chapter will be closed with the results of the free-oscillating cylinder with the electricity generator connected.

5.1 Non-oscilalting Cylinder

The effects of tripping wires on the hydrodynamic coefficients were greatly dependent of their angular positioning around the cylinder, as shown on figure 5.1. Analyzing the lift and drag coefficients (figures 5.1a and 5.1b, respectively) it is possible to notice three distinct regions in function of tripping wires positioning.

The first region, regarding angles between 30^o and 52.5^o, presents a reduction on the coefficients in comparison to the smooth cylinder results, represented by the dotted line, and a small increase of strouhal number (figure 5.1c). The reduction of coefficients present on this region was also reported by Alam et al.[3], Hover et al.[7] and Nguyen and Nishi[10]. The mechanism responsible for these reductions are already well known and are attributed to a flow separation over the tripping wires and a reattachment behind them, followed by a turbulent re-separation (pattern B), which results in the narrowing of the wake region and a relaxation of the backpressure on the

cylinder. On the current experiments, the maximum reduction of lift and drag coefficients inside this region were 26% and 18%, respectively, and occurred for $\beta = 45^o$. The variations in Strouhal number were discussed by Alam et. al.[3] and they have direct relation to the variation on the coefficients. The increase in Strouhal number is associated with an energy decrease in the flow, which results in lower forces and consequently, in lower hydrodynamic coefficients. That explains also the higher hydrodynamic coefficients present in the second region because which will be discussed below.

The second region, covering the range between 60^o and 90^o, is characterized by the increase of the coefficients in relation to smooth cylinder and the reduction of strouhal number, which indicates the formation of larger and stronger vortexes. The increase of the coefficients achieved up to 68% on lift and 42% on drag during the experiments conducted. Besides there is no information about the lift coefficient on their works, Igarashi[6] and Nebres & Batil[2] reported an increase of drag coefficients during their experiments inside this same region, but it occurred only if the tripping wires diameter were large enough to induce a complete separation of the flow (Pattern C). Alam et al.[3] is the only work of our knowledge that contains information about both lift and drag coefficients increase, which occurred when tripping wires were positioned between 50^o and 60^o, but there are no comments about the increase of coefficients on their work because they were focusing only the study of the mechanism for reduction of coefficients.

The third and last region, concerning the angles larger than 97.5^o, presents a larger reduction of coefficients than the observed at the first region. The reduction in the third region was never reported before in other works. At this region, the strouhal number presented an irregular behavior and oscillated near the smooth cylinder values.

(5.1a)

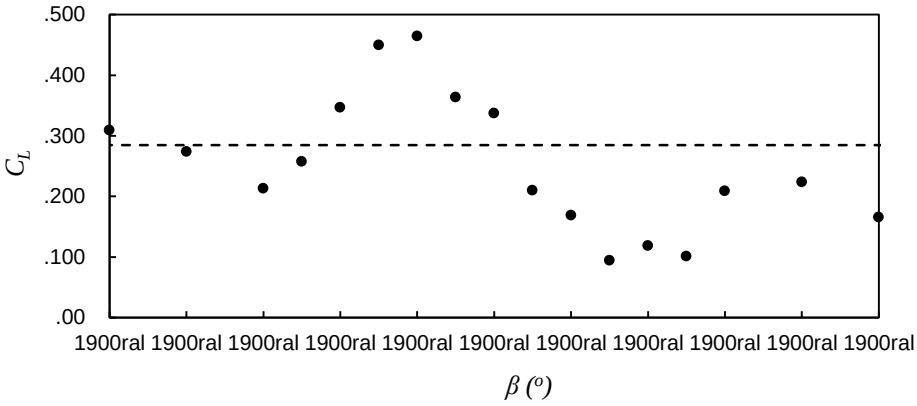

(5.1b)

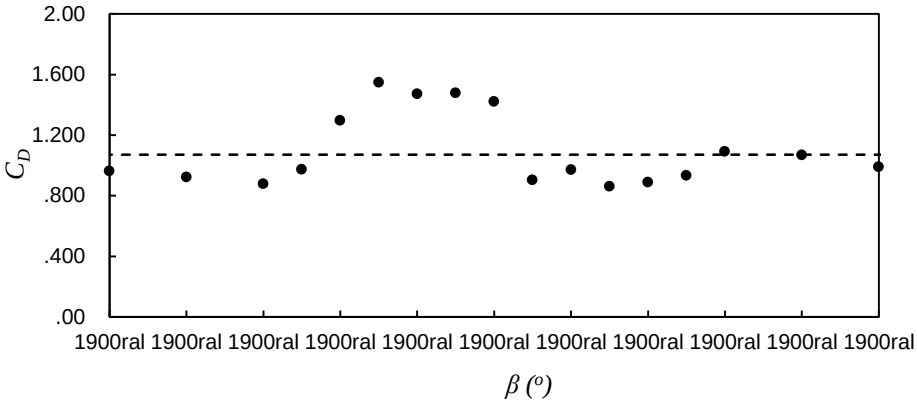

(5.1c)

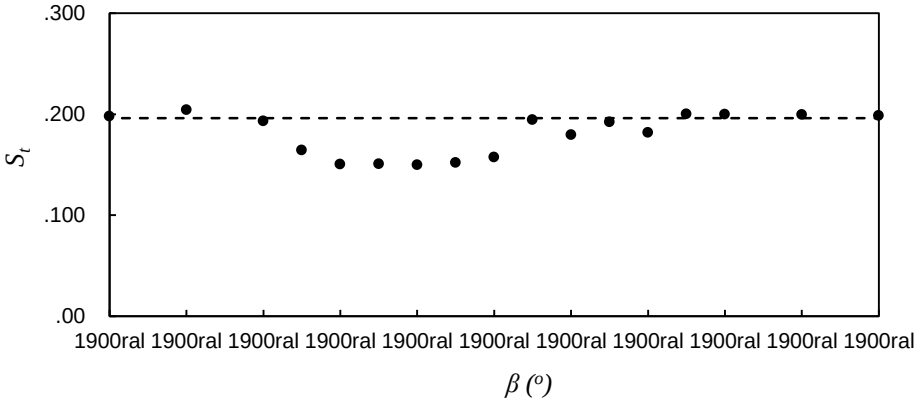

Figure 5.1: (a) Lift coefficient, (b) drag coefficient and (c) strouhal number in function of angular position β. The dashed lines represent the values measures for the smooth cylinder case.

Inside the third region were found the maximum lift and drag reductions on our experiments (respectively, 67% and 20%, at β = 112.5^o). This finding was never been reported before by other researchers because mostly researchers restrict the positioning of tripping wires to angles lower than 60^o based on previous works, as Pearcey et al.[27] and Nebres and Batil[2], which inferred that placing tripping wires above 60^o would have little effects on the flow and, consequently, on the hydrodynamic coefficients. The most plausible explanation of our results contrast with theirs is because we are working with larger diameter ratios and included a gap between the cylinder and tripping wires, what led to flow alterations never faced before at other experiments. These alterations still not clear because our experiments did not included flow pattern detection techniques.

The reduction of coefficients occurred together with a decrease on strouhal number, which means that the known relations between strouhal number and hydrodynamic coefficients is not valid in this case, which means that the flow around the cylinder with tripping wires positioned is substantially changed and further research is necessary understand the influence of the tripping wires on the flow patter for this case.

5.2 Free Oscillating Cylinder without generator

5.2.1 Smooth Cylinder experiments

Free oscillating tests were carried out firstly with a smooth cylinder to make comparisons with other researcher's experiments and to be used as a base case to quantify the changes causes by the tripping wires on VIV response. Figure 5.2 shows the amplitudes of vibration of smooth

cylinders obtained on this study and the results presented by Khalak & Williamson[24]. The response curves are similar: both of which have distinct initial, upper and lower branches. In contrast, our experiment exhibits smaller amplitudes, which can be attributed to our larger mass ratio (6.13 against 2.4) and damping ratio (0.016 against 0.011), as discussed by Govardhan & Williamson[22].

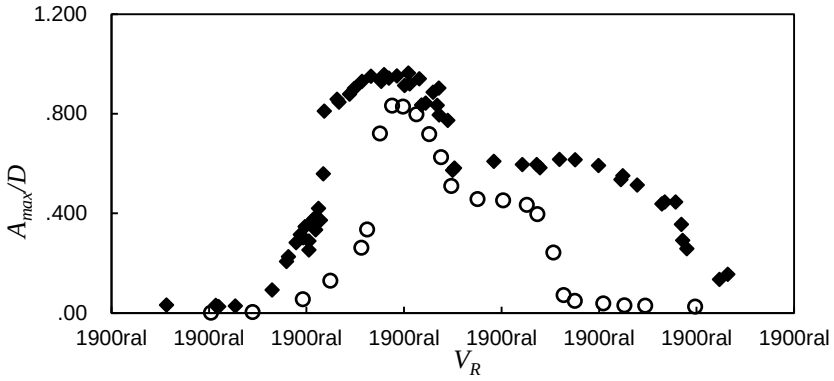

Figure 5.2: Dimensionless amplitude response of a smooth cylinder. Current experiment (○) and Khalak and Williamson (•) results plotted together.

5.2.2 VIV enhancement: Tripping wires at 60^o and 75^o

In this section the increase on the amplitude of oscillation of the cylinder caused by the presence of tripping wires will presented. The dimensionless amplitude and response frequency for smooth cylinder and cylinder with tripping wires at β = 60^o and β = 75^o are shown in figure 5.3. Considerable effects caused by tripping wires can be noticed when V_R is greater than 7: the amplitudes with tripping wires are larger than those for the smooth cylinder and there is a monotonically increase of the amplitude with the increase of V_R, reaching a maximum A/D = 1.27, for β = 75^o case, whereas the smooth cylinder shows small amplitude response when V_R is over 9. When β = 75^o, another fact that attracts attention is that the amplitudes are larger than the other two cases at lower reduced velocities ($3 \leq V_R \leq 5$).

Other important alteration caused by the presence of tripping wires occurs on the lock-in range. While smooth cylinder lock-in range is $5.5 \leq V_R \leq 8.75$, tripping wires cases increased the lock-in range to $5.5 \leq V_R \leq 12$ and $4 \leq V_R \leq 12$, for $\beta = 60^o$ and $\beta = 75^o$, respectively. The monotonically increase in amplitude and the widening of lock-in region were also reported by Raghavan and Bernistsas who placed roughness strips over the cylinder surface.

(5.3a)

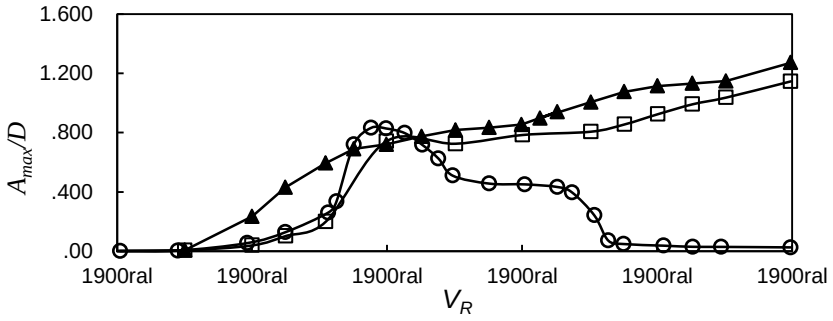

(5.3b)

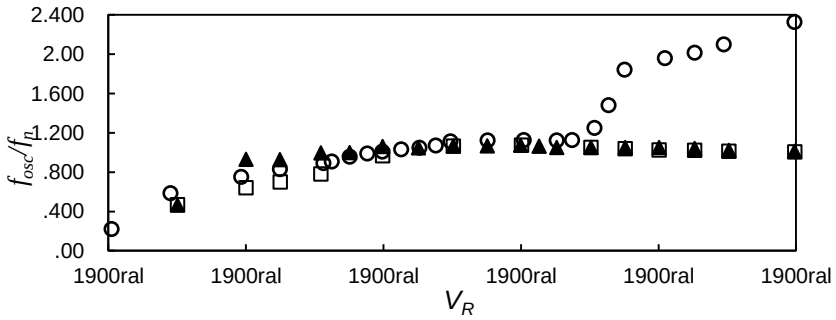

Figure 5.3: (a) Amplitude and (b) frequency responses. ○: smooth cylinder, □: tripping wires at $\beta = 60^o$, ▲: tripping wires at $\beta = 75^o$.

The lift and drag coefficients and the phase difference φ_F are shown in figures 5.4 and 5.5. Their analysis is important to uncover what drives the very large amplitudes when tripping wires are attached to the cylinder. There is no significant difference in the maximum coefficients and phase differences among the three cases at reduced velocities lower than 7. Besides the maximum amplitudes are similar, we can see a leftward shift on the lift coefficient for the case with $\beta = 75^o$ which is closely related to the earlier increase on the response amplitude observed on figure 6.

When V_R is larger than 7 the lift coefficient is mostly constant around 0.4 for the two cases with tripping wires. This stabilized lift coefficient do not justifies by itself the large amplitude of response obtained at this region, but if we check the phases we can notice that the smooth cylinder case presents a phase shift from 0^o to 180^o inside the lock-in region. At the same region, when using tripping wires, the phase shifted from 0^o to around 90^o at $6.5 \leq V_R \leq 8$, and for $V_R > 8$ it decreases gradually as the reduced velocity increases. These near 90^o phases means that lift forces are working near a pure excitation regime, meaning that the lift force efficiently excites the cylinder vibration when tripping wires are attached, what leads to large amplitudes of response.

(5.4a)

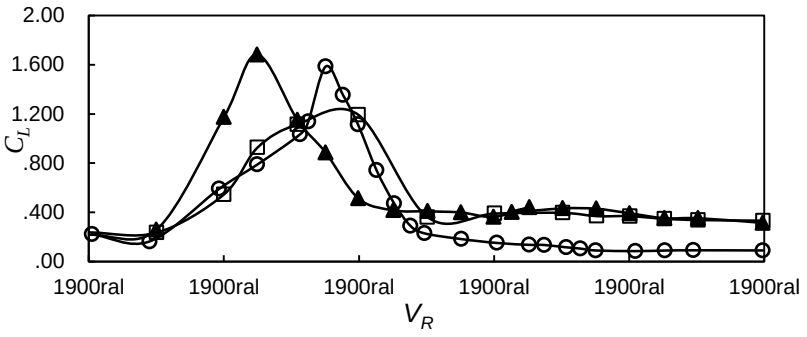

(5.4b)

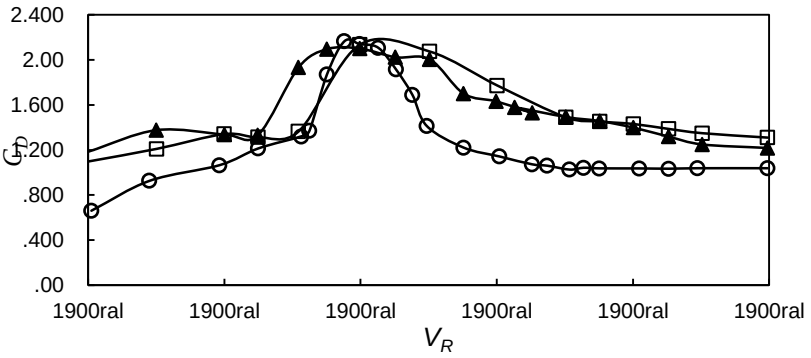

Figure 5.4: Lift and Drag coefficients for free-oscillating cylinder cases. ○: smooth cylinder, □: tripping wires at $\beta = 60^o$, ▲: tripping wires at $\beta = 75^o$.

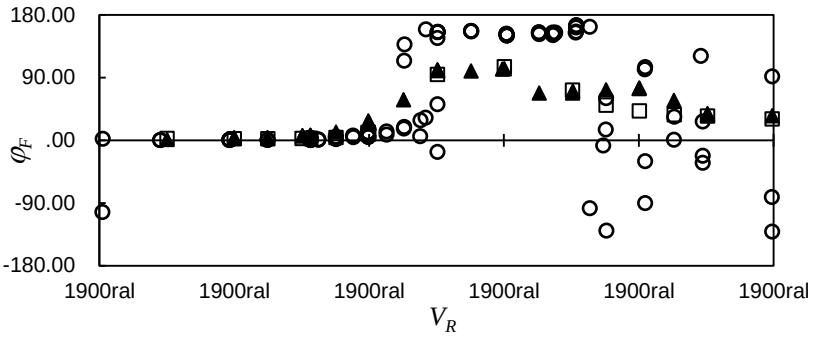

Figure 5.5: Difference of phase between position and lift force. ○: smooth cylinder, □: tripping wires at β = 60°, ▲: tripping wires at β = 75°.

5.2.3 VIV reduction and suppression: Tripping wires at 105° and 120°

The reduction of amplitude of oscillation of the cylinder was obtained when positioning the tripping wires behind the cylinder, at angles of 105° and 120°. The significant decrease in the amplitude is shown in figure 5.6. The two cases have very different responses between them. For β = 105° the around reduced velocity 6 are lower than the smooth cylinder case. A small increase is observed when $4 < V_R < 5$ because tripping wires shifted the start of the lock-in to smaller reduced velocities. The lift and drag coefficients, presented on figure 5.7, follow the same amplitude response behavior and are lower than those of the smooth cylinder case, except at the region where the amplitudes were higher.

(5.6a)

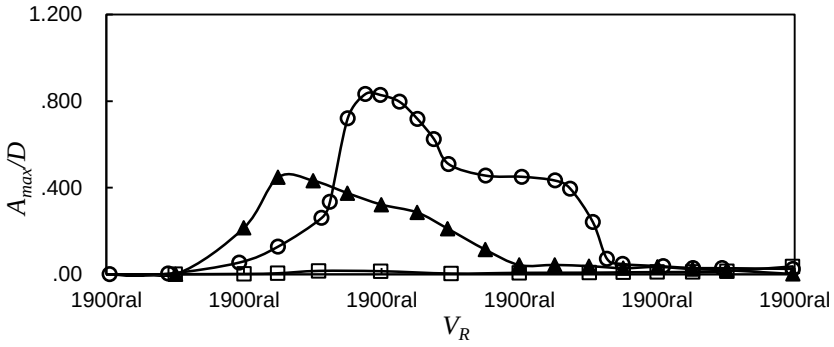

(5.6b)

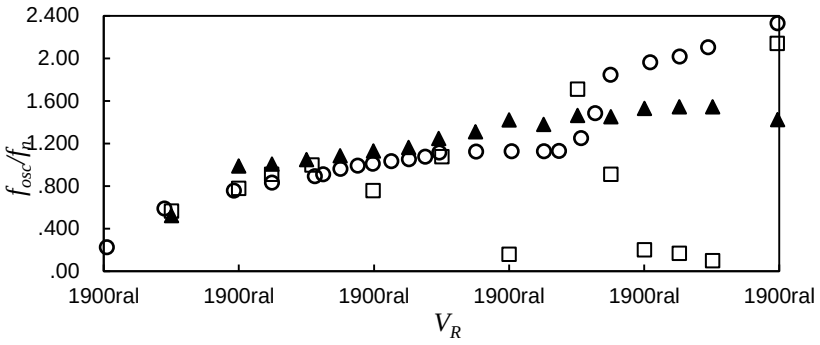

Figure 5.6: (a) Amplitude and (b) frequency responses. ○: smooth cylinder, □: tripping wires at β = 120º, ▲: tripping wires at β = 105º.

Almost a complete suppression of the VIV is obtained in the whole range of reduced velocities tested when $\beta = 120^o$. The amplitudes (Figure 5.6a) and lift coefficients (Figure 5.7a) are nearly zero. The drag coefficients are almost constant around 0.87, which is even lower than those for the stationary cylinder case. The reductions of the forces and amplitudes may come from the prevention of vortex formation behind the cylinder by the presence of the tripping wires.

Analyzing the phase differences shown on Figure 5.8 it is possible to see that the behavior with and without tripping wires is similar until reduced velocity 9. The three cases presented near zero phases at reduced velocities lower than 5, point where they started to shift to values around 170^o. These phase values presented means that the force is exciting the system, but with very low efficiency. This low efficiency allied to the lower lift coefficients presented is the reason of the reduction in the amplitude of oscillation present on figure 5.6a.

(5.7a)

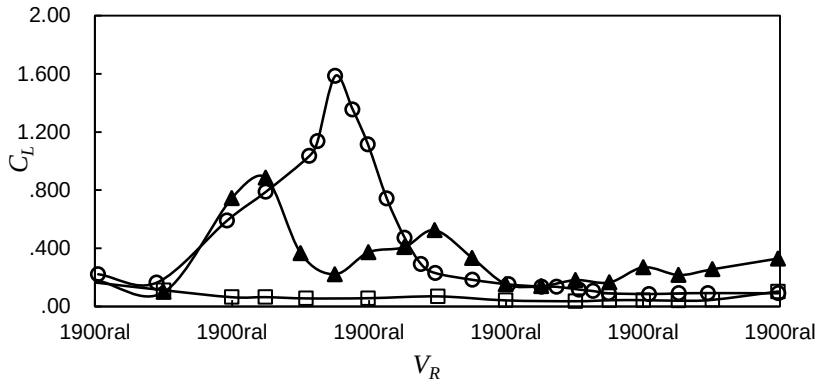

(5.7b)

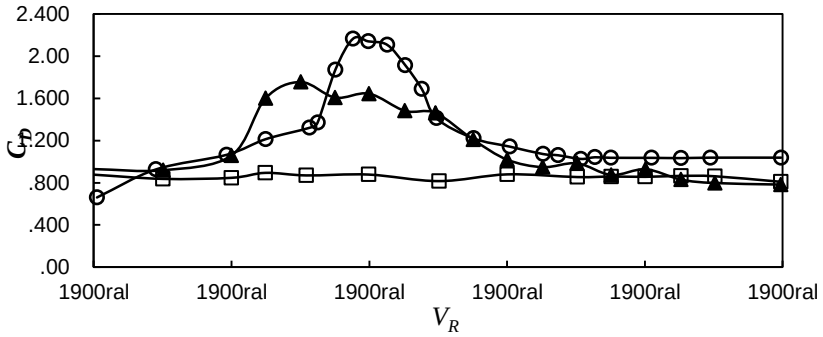

Figure 5.7: Lift and Drag coefficients for free-oscillating cylinder cases. ○: smooth cylinder, □: tripping wires at β = 120^o, ▲: tripping wires at β = 105^o.

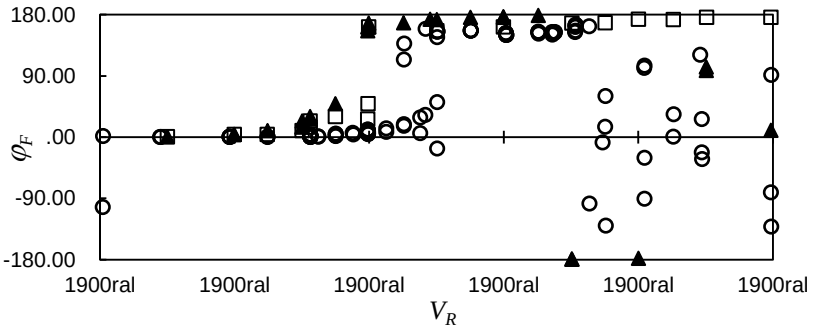

Figure 5.8: Difference of phase between position and lift force. ○: smooth cylinder, □: tripping wires at β = 120^o, ▲: tripping wires at β = 105^o.

5.3 Free-Oscillating Cylinder with generator

The results presented in this section were obtained with the electricity generator attached to the system. The experiments for this section were conducted with the tripping wires positioned at $\beta = 75^o$ and $\beta = 60^o$ because these two cases presented very high amplitudes of oscillation on the case without the generator. Figure 5.9 contains the VIV amplitude and frequency responses. Both cases with tripping wires present larger amplitudes and a wider lock-in region than smooth cylinder case. The maximum normalized amplitudes for $\beta = 75^o$ and $\beta = 60^o$ are, respectively, 0.63 and 0.74, however, for smooth cylinder case, it is only 0.23. The monotonically increase in amplitude related by Quadrante & Nishi[28] and presented in Figure 5.3a can be observed on Fig. 5.6, but it occurred only when $\beta = 60^o$ and $V_R \geq 10$ and, even then, not for all repetitions. For $V_R = 10$ and 11 it is possible to see distinct responses, with one of the test runs presenting large amplitudes and the other one a near zero value. The monotonically increase of amplitude is related to a transition from VIV to galloping phenomenon, which occurs at higher reduced velocities than VIV.

The lock-in range, characterized by $f_{osc}/f_n \approx 1$, also presents differences between the three cases. Smooth cylinder and $\beta = 75^o$ cases have a limited lock-in range while $\beta = 60^o$ lock-in range starts at $V_R = 6.0$ and extends until the maximum reduced velocity tested.

To understand the changes caused on amplitude and lock-in we analyzed the lift coefficients and the difference of phase between lift force and cylinder displacement (Equation 4.9), shown on Figure 5.10. To achieve large amplitude response a favorable combination of lift force and phase difference is necessary. A phase difference equal to 90^o means that the lift force acts in a purely excitation rule and as near it is to 90^o larger amplitudes are expected for a constant lift force.

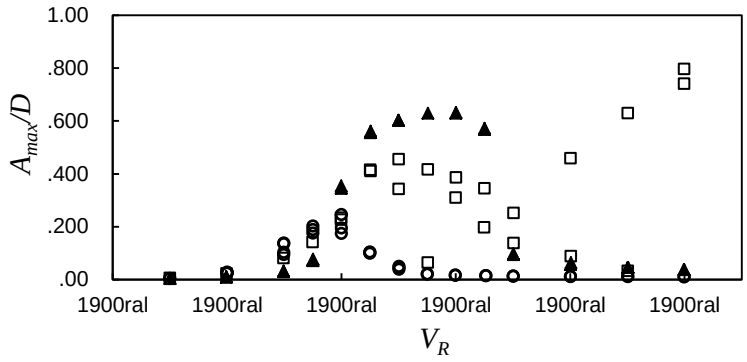

Figure 5.9: Amplitude and frequency response of VIV. ○: smooth cylinder, □: tripping wires at β = 60°, ▲: tripping wires at β = 75°.

Smooth cylinder case presents lower lift coefficients than tripping wires cases, except at the region between reduced velocities 4.0 and 5.5 within it achieved almost the same maximum coefficient than β = 75° case. However, even these large lift coefficients were not translated into high amplitudes because the phase difference is around 30°. β = 75° case presents a phase difference around 70° inside the lock-in region and shifts to near 180° after it ends. The same not happened when β = 60°, where the phase remained around 50° even at V_R > 9, fact that justifies the appearance of large amplitudes.

(5.10a)

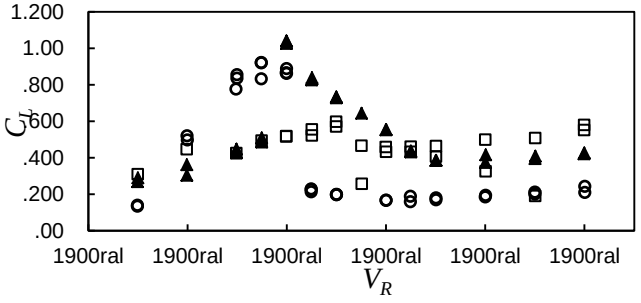

(5.10b)

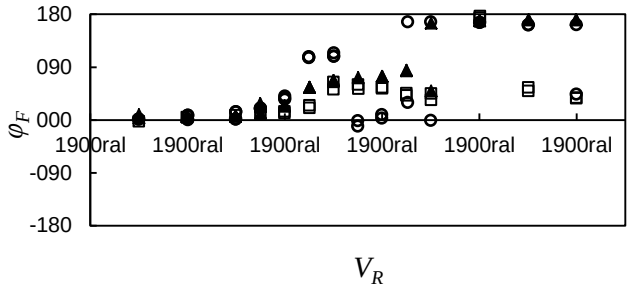

Figure 5.10: (a) Lift coefficients and (b) phase difference between lift force and cylinder vertical position. ○: smooth cylinder, □: tripping wires at β = 60^o, ▲: tripping wires at β = 75^o.

5.3.1 Generated power and conversion efficiency

The Generated power was calculated using the numerator of equation 4.7 and is shown on Figure 5.11. The maximum electric power generated was 57.8mW and occurred on β = 60^o case at V_R = 12. β = 75^o case also presented large electric power between reduced velocities 6.5 and 8.5, achieving up to 50.41mW. Smooth cylinder case had the lowest power generation, achieving a maximum of 4.86mW at V_R = 6.0.

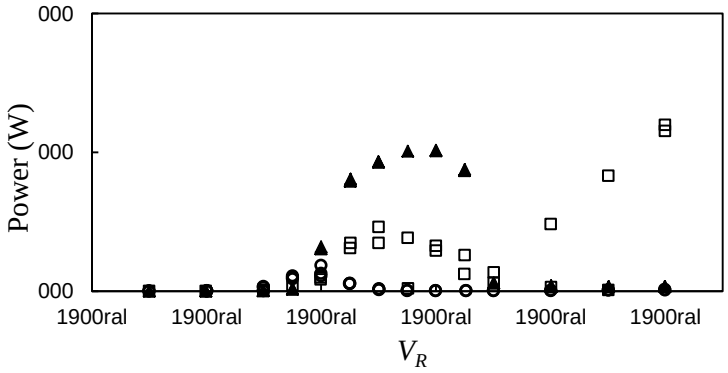

Figure 5.11: Electric power generated. ○: smooth cylinder, □: tripping wires at β = 60^o, ▲: tripping wires at β = 75^o.

Figure 5.12 shows the efficiency in function of reduced velocity. $\beta = 75^o$ case had the best performance, achieving a maximum efficiency η = 12.41% at V_R = 6.5, about 4 times the maximum efficiency obtained on smooth cylinder case. Although the maximum power generation occurred in $\beta = 60^o$ case its efficiency is very low because the high flow speed involved.

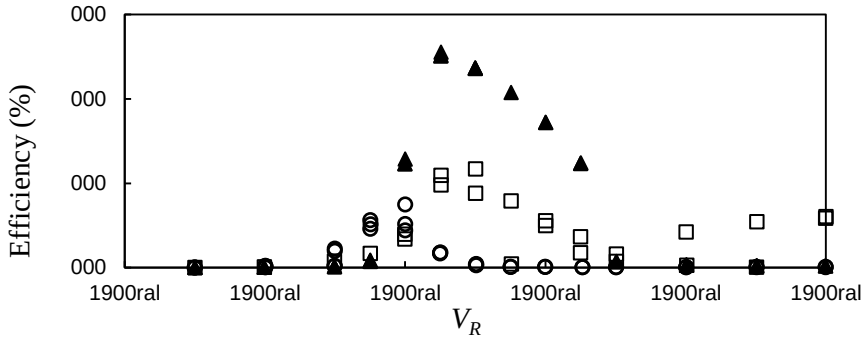

Figure 5.12: System conversion efficiency. ○: smooth cylinder, □: tripping wires at β = 60°, ▲: tripping wires at β = 75°.

5.3.2 Results summary

In this section the results obtained for the cases with the generator attached were summarized in Table 5.1. The maximum amplitude response and electric power generated occur when r_3/r_2 = 1.0 and $\beta = 60^o$, at V_R = 12, but this case presents a low efficiency because the power of the flow is high at this speed. Smooth cylinder cases presented very small amplitude response and, consequently, low electric power generation and efficiency at all tested configurations. The most efficient case was $\beta = 75^o$, presenting values between 10.71% and 12.47%, at reduced velocities between 6 and 8.

From Table 5.1 is also possible to realize that the presence of large lift forces acting on the cylinder do not guarantee a high amplitude response. The phase difference between lift force and

displacement also has an important influence since larger will be the force contribution to excite the system VIV as near it is to 90^o.

Table 5.1: Summary of results obtained for each r_2/r_3 configuration.

Test configuration		Natural frequency (Hz)	Mass and Damping ratios		Maximum A_{max}/D			Max. Lift Coefficient		Max. Electric Power (mW)		Max. Efficiency (%)	
r_3/r_2	case	f_n	m*	ζ	value	V_R	φ_F (^{o})	value	V_R	value	V_R	value	V_R
0.9	Smooth	2.44	9.88	0.041	0.35	6.0	41	0.84	5.5	15.21	6.0	2.48	6.0
	$\beta = 60^o$	2.42	10.08	0.050	0.44	7.0	34	0.55	7	26.19	7.0	6.08	7.0
	$\beta = 75^o$	2.42	10.08	0.045	0.61	8.0	72	0.96	6	55.07	8.0	10.71	7.0
1	Smooth	2.38	10.38	0.042	0.23	6.0	35	0.92	5.5	4.87	6.0	2.82	6.0
	$\beta = 60^o$	2.36	10.60	0.048	0.74	12.0	59	0.58	12	57.7	12.0	5.12	6.5
	$\beta = 75^o$	2.36	10.60	0.045	0.63	8.0	74	1.03	6	50.47	8.0	12.41	6.5
1.1	Smooth	2.30	10.10	0.058	0.15	5.5	13	0.75	5	0.45	5.5	2.21	5.5
	$\beta = 60^o$	2.29	11.13	0.053	0.67	12.0	31	0.59	12	50.28	12.0	5.96	6.5
	$\beta = 75^o$	2.28	11.28	0.052	0.55	7.5	69	0.86	6.5	46.99	7.5	12.47	6.5

5.3.3 Discussion of power generation

The efficiency of energy generation systems using vortex-induced vibrations has been studied in a few works[4,5]. The main characteristics and results of previous and current works are listed on Table 3. VIVACE[4] is the best system developed until the present moment, achieving a 22% conversion efficiency, value much larger than obtained by Nishi et. al.[5] and the current smooth cylinder experiment.

There are two main differences between the VIVACE[4] and the other two systems: the mass ratio and Reynolds number. Low mass ratio can increase the length of lock-in region, as discussed by Khalak and Williamson[24], but has small influence on amplitude response. On the other hand, variation of Reynolds number has large influence on response because the regime of vortex

generation changes[3] as it increases. Nishi et. al.[5] and the current experiment operates in lower Reynolds number, under TrSL2 regime, which is a subcritical regime characterized by the formation of transition vortices in free shear layer. VIVACE[4] operates on TrSL3 regime, which also is a subcritical regime, but has a fully turbulent shear layer that results in larger fluid forces and amplitude response.

Table 5.2: Characteristics and efficiency of known energy generation systems that uses VIV.

Experiment		Re	m*	ζ	η (%)
VIVACE		9.4×10^4	1.45	0.059	22.00
Nishi et. al.		$5\sim7\times10^3$	12.68	0.023	4.50
Current experiment	Smooth	$2.9\sim22\times10^3$	10.38	0.042	2.82
	$\beta = 60^o$		10.08	0.050	6.08
	$\beta = 75^o$		11.28	0.052	12.47

The attachment of tripping wires to our system increased the lock-in range and amplitudes of oscillation without necessity of change on Reynolds number. It probably induced a transition from TrSL2 to TrSL3 regime even at lower Reynolds number, but it is not possible to confirm without obtaining the vortex pattern behind the cylinder.

The system efficiency had a significant increase on efficiency when $\beta = 75^o$. Moreover, the amplitude of oscillation and, consequently, the power generated had almost stabilized values within the lock-in range ($6.0 \leq V_R \leq 8.5$). This characteristic is very important as it is expected that the current speed suffer fluctuations along time and, with a large lock-in range, it is possible to tune the system to deal with these fluctuations to minimize downtime.

By observing Table 5.3 it is clear that lots of new configurations can be studied to search for a more efficient system. It is not possible to predict what will happen if tripping wires are attached to VIVACE[4], or what will happen if the current experiment is conducted at higher

Reynolds numbers. Further research and experiments are necessary to clarify these questions and check the real potential of generating energy from a fluid flow using vortex-induced vibrations phenomenon.

6 Conclusions and recommendations of future works

The effects of the attachment of a pair of tripping wires on a circular cylinder were investigated experimentally with the objective of increasing the energy conversion efficiency from the fluid flow to electricity. The tripping wires were positioned parallel to the axis of the main cylinder at angular positions, symmetrically positioned in relation to the stagnation point. The experiments were divided in three parts: stationary cylinder experiments and free-oscillating cylinder experiments without generator attached and free-oscillating experiments with generator attached.

The stationary cylinder experiments confirmed the increase and decrease of the lift and drag coefficients observed by other researchers, like Igarashi[6], Nebres & Batil[2] and Alam et al.[3] when tripping wires are positioned at angles ranging from 0^o to 90^o. Furthermore, a new region within the hydrodynamic coefficients were reduced has been found. This new region comprehends the angles larger than 90^o, when the tripping wires are positioned behind the cylinder. The tripping wires positions $\beta = 60^o$ and $\beta = 75^o$ resulted in the maximum increase of hydrodynamic coefficients during the stationary cylinder.

The presence of tripping wires at $\beta = 60^o$ and $\beta = 75^o$ resulted in a large increase on the energy generated during the free oscillating experiments. At the best configuration, when $\beta = 75^o$, the system efficiency achieved $\eta = 12.47\%$, more than four times the efficiency obtained on smooth cylinder experiments, showing that the attachment of tripping wires has a great potential to be used to enhancement of vortex-induced vibrations, but some points needs further research.

The first point that needs to be investigated is related to the operational Reynolds number. The current experiments covered a Reynolds range from 2.9×10^3 to 2.2×10^4, represented by the green region in Figure 6.1. Inside this range the lift coefficients present lower values than when Reynolds number ranges from 3.0×10^4 to 1.0×10^5, represented by the orange region. The effects of tripping wires cannot be extrapolated to from the current results to higher Reynolds numbers and further experiments are necessary to check if it is possible to enhance the system efficiency using tripping wires inside the orange region.

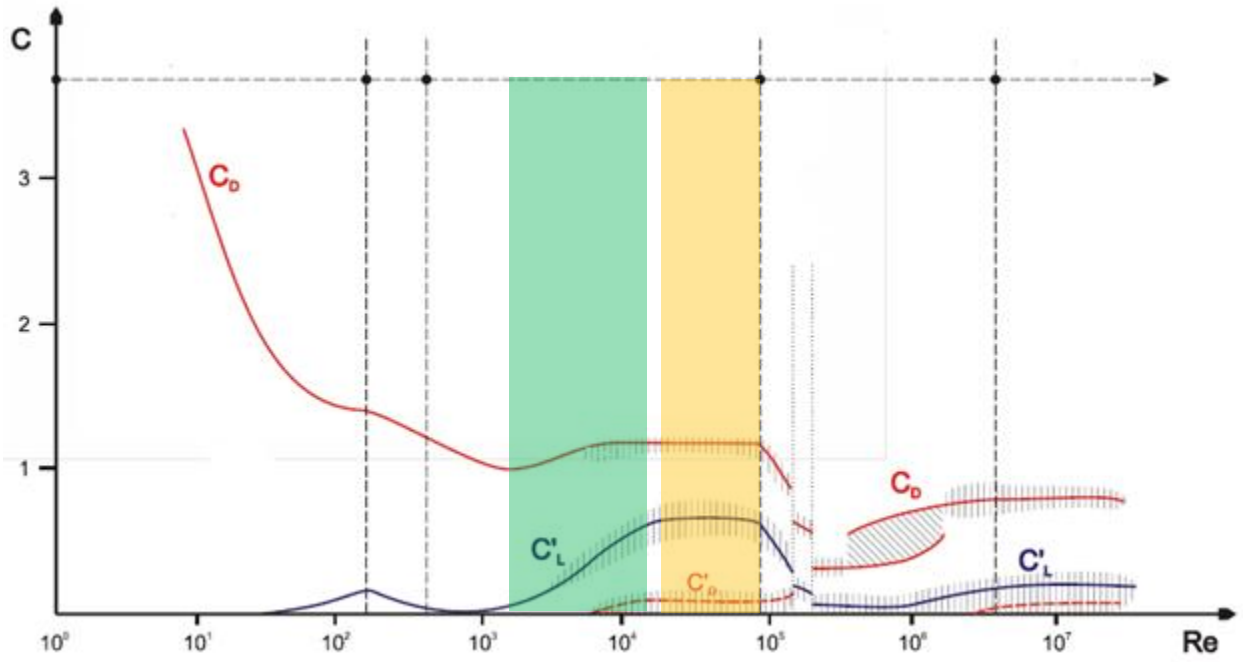

Figure 6.1: Comparison between the ranges of Reynolds number of the current experiment with VIVACE[4].

Another important point that needs further research is the optimization of the system mass ratio and mechanical damping to achieve the maximum efficiency. The system used in this research was not optimized and probably it is possible to increase fairly the system efficiency.

7 References

1. Zdravkovich MM., Review and classification of various aerodynamic and hydrodynamic means for suppressing vortex shedding. *Journal of Wind Engineering and Industrial Aerodynamics* (1981); 7: 145-189.

2. Nebres J., Batill S., Flow about a circular cylinder with a single large-scale surface perturbation. *Experiments in Fluids* 15 (1993), 369–379.

3. Alam M. M., Moriya M., Sakamoto H., Reduction of fluid forces acting on a single circular cylinder and two circular cylinders by using tripping rods. *Journal of Fluids and Structures 18* (2003), 347-366.

4. Bernitsas M.M., Raghavan K., Ben-Simon Y., Garcia E. M. H., "VIVACE (Vortex Induced Vibration Aquatic Clean Energy): A New Concept in Generation of Clean and Renewable Energy from Fluid Flow", OMAE 2006; and *Journal of Offshore Mechanics and Arctic Engineering, ASME Transactions,* (2008) Vol. 130, No. 4, pp. 041101-15.

5. Nishi Y., Ono K., Kokubun K., Development of a renewable energy system using vortex-induced vibration of a cylinder and principle of leverage aiming for application in deep sea, *Journal of Marine Science and Technology*, 17(3) (2012) 382-389.

6. Igarashi, T., Effect of tripping wires on the flow around a circular cylinder normal to an airstream. *Bulletin of the Japan Society of Mechanical Engineers.* (1986) 29, 2917–2924.

7. Hover, F.S., Tvedt, H., Triantafyllou, M.S., Vortex-induced vibrations of a cylinder with tripping wires. *Journal of Fluid Mechanics* (2001) 448, 175–195.

8. Raghavan, K., Bernitsas, M.M., Enhancement of high damping VIV through roughness distribution for energy harnessing at $8 \times 10^3 < \mathrm{Re} < 1.5 \times 10^5$. *Proceedings of the International Conference on Offshore Mechanics and Arctic Engineering (OMAE 2008)*, Lisbon.

9. Bernitsas, M.M., Raghavan, K., Duchene, G., Induced separation and vorticity using roughness in VIV of circular cylinders at $8\times10^3 < \mathrm{Re} < 1.5\times10^5$. *Proceedings of the International Conference on Offshore Mechanics and Arctic Engineering (OMAE 2008)*, Lisbon.

10. Nguyen, V.T., Nishi, Y., Numerical simulation of effect of tripping rod on increase in lift force acting on a cylinder using lattice Boltzmann method. *Journal of Fluid Science and Technology* (2012) 7, 304–314.

11. Bearman P.W., Vortex shedding from oscillating bluff bodies; *Annual Review of Fluid Mechanics*; (1984) 16, 195–222.

12. Van Dyke M.D.; An Album of Fluid Motion. Stanford, *CA: Parabolic Press* (1982).

13. Batchelor, G.K., An introduction to fluid dynamics; *Cambridge University Press*; Cambridge (1967).

14. Bernard, H. Formation periodique de centres de giration a larriere dun obstacle en mouvement, *C.R. Acad. Sci.*, (1908) 147, 839–842.

15. KÁRMÁN, T.; Rubach, H. (1912); Über den Mechanismus dees Flussigkeits und Luftwiderstandes.; Phys. Z; 13; 49-59.

16. Roshko, A., On the drag and shedding frequency of two-dimensional bluff bodies; *NACA TN* (1954) 3169.

17. Zdravkovich, M.M., Flow around circular cylinders: Vol. 1 Fundamentals; *Oxford University Press* (1997).

18. Perry, A.E.; Chong, M.S.; Lim, T.T. (1982); The vortex-shedding process behind two-dimensional bluff bodies; *Journal of Fluid Mechanics*; 116, 77-90.

19. Willimson, C.H.K.,Vortex dynamics in the cylinder wake; *Annual Review of Fluid Mechanics* (1996) 28, 477-539.

20. Williamson, C.H.K.; Roshko, A., Vortex formation in the wake of an oscillating cylinder; *Journal of Fluids and Structures* (1988) 2, 355-381.

21. Blevins, R.D. Flow-induced Vibrations; *Van Nostrand Reinhold*; New York (1990).

22. Wlliamson, C.H.K.; Govardhan, R.,Vortex-Induced Vibrations; *Annual Review of Fluid Mechanics* (2004) 36, 413-455.

23. Feng, C.C., The measurements of vortex-induced effects in flow past a stationary and oscillating circular and D-section cylinders; *MSc Thesis, University of British Columbia, Vancouver, Canada* (1968).

24. Khalak, A.; Williamson, C.H.K., Motions, forces and mode transitions in vortex-induced vibrations at low mass-damping; *Journal of Fluids and Structures* (1999) 13, 813-851.

25. Sarpkaya, T. Hydrodynamic damping, flow-induced vibrations, and biharmonic response; *ASME Journal of Offshore Mechanics and Arctic Engineering* (1995) 117, 232-238.

26. Griffin, O.M.; Ramberg, S.E., The vortex street wakes of vibrating cylinders. *Journal of Fluids Mechanics* (1974) 66, 553-576.

27. Quadrante L. A. R., Nishi Y., Effects of tripping rods on the flow around a cylinder and VIV amplification, Proccedings of *Hydroelasticity Conference* (2012), Tokyo, Japan.